Motor Integrated Variable Speed Drives

Singh, Yash Veer

Publication date:
2015

Document Version
Publisher's PDF, also known as Version of record

MOTOR INTEGRATED VARIABLE SPEED DRIVES

by

YASH VEER SINGH

AALBORG UNIVERSITY
DENMARK

Dissertation submitted
to the Faculty of Engineering and Science
in partial fulfilment of the requirements
for the degree of Doctor of Philosophy (Ph.D.)

Department of Energy Technology
Aalborg University
Aalborg, Denmark

Thesis title: Motor Integrated Variable Speed Drives

Name of PhD student: Yash Veer Singh

Name and title of supervisor: Peter Omand Rasmussen, Associate Professor

Name and title of Co-supervisor: Torben Ole Andersen, Professor

List of published papers:

- Paper 1: Yash Veer Singh, Peter Omand Rasmussen, Torben Ole Andersen: " Three-phase electric drive with modified electronic smoothing inductor". Energy Conversion Congress and Exposition (ECCE), 2010 IEEE , vol., no., pp.4199,4203, 12-16 Sept. 2010.
- Paper 2: Yash Veer Singh, Peter Omand Rasmussen, Torben Ole Andersen, Hamid Shaker: "Modeling and control of three phase rectifier with electronic smoothing inductor,". IECON 2011 - 37th Annual Conference on IEEE Industrial Electronics Society, vol., no., pp.1450,1455, 7-10 Nov. 2011.
- Paper 3: Yash Veer Singh, Peter Omand Rasmussen, Torben Ole Andersen: "Performance improvement of three phase rectifier by employing electronic smoothing inductor,". IECON 2014 - 40th Annual Conference of the IEEE Industrial Electronics Society, vol., no., pp.1713-1719, Oct. 29 2014-Nov. 1 2014.
- Paper 4: Yash Veer Singh, Peter Omand Rasmussen, Torben Ole Andersen: "Robust and reliable rectifier based on electronic inductor with improved performance,". Power Electronics, Drives and Energy Systems (PEDES), 2014 IEEE International Conference on , vol., no., pp.1-5, 16-19 Dec. 2014.

"This present report combined with the above listed scientific papers has been submitted for assessment in partial fulfilment of the PhD degree. The scientific papers are not included in this version due to copyright issues. Detailed publication information is provided above and the interested reader is referred to the original published papers. As part of the assessment, co-author statements have been made available to the assessment committee and are also available at the Faculty of Engineering and Science, Aalborg University."

ENGLISH SUMMARY

A new trend in the variable speed drives (VSDs) is to develop fully integrated systems, which lead to low-cost products with shorter design cycles. Motor Integrated design of VSDs will reduce cable length to connect drive with machine windings and installation time for end user. The electric drives are expected to have minimum effect on grid and motor connected to it, i.e. currents drawn from grid should be within specified limits and currents injecting in to machine should not overheat the machine windings to avoid insulation failure due to harmonics. It is also necessary that electric drives should not disturb other loads connected to the point of common coupling (PCC). Diode rectifier followed by a voltage source inverter (VSI) is well accepted by the industry, and it has low losses and high reliability, but it requires big and bulky passive elements to ensure total harmonic distortions (THDs) in input currents to be within specified limits of present standards. Improving the quality of input currents of a three-phase-fed VSD is a requirement that needs cheap and competitive solutions for implementation.

High efficiency, small volume and low cost are nowadays basically the first three aspects mentioned when it comes to the development of any kind of power converter topology for power electronic applications. Concerning the use of a power converter in motor integrated VSDs, the first two mentioned aspects receive an even greater importance. Power converter design for integrated drives poses a host of significant challenges that originate both from the limitations on available space and the need to adapt the power converter to the thermal, vibration, and electromagnetic field stresses inside the motor housing. Losses in the motor can heat up the motor environment to a significant temperature above ambient. The high operating temperature of the power electronics in integrated drives seriously limits the power they can dissipate, which decreases the power handling capability of the converter. In motor integrated VSDs, the main challenge, as mentioned above, is to reduce the power converter losses and its size so it can fit inside the motor housing.

Weight and volume of a filter inductor has to come down drastically to make it a suitable power converter for motor integrated variable speed drives. Introduction of active power electronic switches can ensure very high performance and small size of such an inductor. Such an arrangement is usually referred to as “Electronic Smoothing” techniques. The electronic smoothing inductor (ESI) based converter is easy to integrate in the existing power circuit of a VSD and does not demand too many changes either in the power circuit or in the control. Volume and weight of these drives with ESI are smaller and it is very much suitable for integration with an electrical motor.

Converter topologies with reduced size of passive components will provide a compact power converter for integrated drives. In research, efforts have been made to replace the traditional limited-lifetime electrolytic capacitors with film capacitors. The voltage

source inverter (VSI) with a small dc-link capacitor is getting more and more attention from the research community and industry.

Impact on the utility of VSI with smaller DC link filter and standard three phase diode bridge rectifier at the front end is presented in this thesis and requirements of a buffer stage in the form of ESI is explained in detail. An equivalent circuit and linear model are developed to give the transfer function and control of the ESI based three-phase rectifier. In this thesis a power converter with ESI is designed and tested with standard induction motor to verify functionality of a working drive.

One modified version of the ESI based converter has also been looked into to reduce losses of converter, but because of difficulties in reducing the bus-bar inductance in that design, further investigation was not carried out. The ESI based converter successfully brought down total harmonic distortions (THDs) in grid current to 31% level and improved power factor to 0.95 by employing a small converter with estimated losses of 23W for a 4kW system. Hence, there is a significant improvement in the performance of the drive.

DANSK RESUME

En ny tendens for frekvensomformer-styrede motordrev er at udvikle fuldt integrerede løsninger som giver billigere produkter og "hurtige" design. Ved fysisk at integrere motor og frekvensomformer reduceres både kabellængde mellem motor og omformer samt installationstiden for slutbrugeren. De integrerede elektriske drev forventes at have minimal indvirkning på såvel forsyningsnettet som på motoren. Dvs. strøm trukket fra forsyningsnettet skal være inden for specificerede grænser og motorstrømmene skal have et lavt harmonisk indhold således motoren ikke overophedes hvormed viklingsisolationen ødelægges. Ligeledes er det også nødvendigt, at elektrisk drev ikke forstyrrer andre belastninger, der er forbundet til det samme knudepunkt i forsyningsnettet. En diode-ensretter efterfulgt af en spændingsstyret vekselretter er en klassisk løsning for frekvensomformere som giver lave effekttab og en høj pålidelighed. Omvendt så kræver denne løsning volumenmæssige store passive elementer (kondensatorer og spoler) for at sikre at den samlede harmoniske forvrængning i net-strømmene er inden for de specificerede grænser i nuværende standarder. For at forbedre kvaliteten af net-strømmene for frekvensomformere er det et krav at løsningerne er konkurrencedygtige og nemme at implementere.

Høj virkningsgrad, lille volumen og lave omkostninger er typisk de tre første parametre der nævnes når det kommer til udviklingen af enhver form for effektelektronisk omformer. Når det gælder motorer med integreret frekvensomformer er det de to første parametre der er de vigtigste. Design af motorintegrerede frekvensomformere giver betydelige udfordringer mht. plads, temperatur, vibrationer og elektromagnetisk stråling. Effekttab i motoren giver anledning til betydelige temperaturstigninger som gør at effektelektronikken der integreres sammen med motoren kommer til at arbejde i et varmere miljø. Et varmere miljø vil reducere den effektelektronikkens arbejdsområde, hvorved hovedudfordringerne, som nævnt ovenfor, er at reducere omformerens effekttab samt størrelse.

Vægt og volumen af omformerens filter-spole skal reduceres kraftigt for at lave et brugbart motorintegreret drev med variabel hastighed. Ved anvendelse af effektelektronik kan spolen laves meget mere kompakt og ydeevnen af drevet forbedres. En sådan løsning omtales normalt som en "elektronisk induktor-konverter" (eng. Electronic Smoothing Inductor ESI). Den elektroniske induktor-konverter kræver ikke ret mange ændringer i effektkredsen og styringen og er således nem at integrere i eksisterende frekvensomformere. Da volumen og vægt af den elektroniske induktor-konverter også er mindre er denne løsning derfor velegnet til et motorintegreret frekvensomformer-drev.

Frekvensomformer-topologier med en lille DC-kondensator har fået opmærksomhed fra såvel forskning som industri. Idéen er at udskifte de levetidsbegrænsede elektrolyt-

kondensatorer med filmkondensatorer hvorved størrelsen af omformeren kan reduceres. En sådan løsning med en mindre omformer er derfor velegnet til motorintegrerede drev.
Resultaterne for en frekvensomformer med en standard tre-faset ensretterbro og et mindre DC mellemkredsfilter er præsenteret i denne afhandling og kravene til den elektroniske induktor- konverter er gennemgået i detaljer. Ækvivalente kredsløbsmodeller og lineariserede modeller er udviklet for at kunne opstille en overføringsfunktion og designe en styring af ensrettertrinet i den elektroniske induktor-konverter. En frekvensomformer med den elektroniske induktor- konverter er ligeledes designet og testet sammen med en asynkronmotor for at verificere funktionaliteten.
For yderlige reduktion af effekttabene er en modificeret elektronisk induktor-konverter blevet undersøgt. Pga. vanskeligheder med at reducere bus-bar induktansen kunne den eksperimentelle del dog ikke udføres. Endeligt kan det konkluderes, at en lille elektronisk induktor konverter med et estimeret tab på 23W i et 4 kW drev med succes har nedbragt forsyningsnettets totale harmoniske forvrængning til 31 % og forbedret effektfaktoren på indgangen til 0.95. Dette er en signifikant forbedring af drevet.

ACKNOWLEDGEMENTS

I would like to thank my supervisor Peter Omand Rasmussen and my co-supervisor Torben Ole Andersen for their valuable guidance, suggestions, comments, inspiration, support, and continuous encouragement. I would also like to thank my steering group committee (Niels Gade, Jesper Roshlom Riber and Hornsleth Steen) from Danfoss for their guidance and support. I would also like to thank Hamid Reja Shaker for his technical help and expertise related to control.

This PhD project was financially supported by Danish Government and Danfoss Drives. I would like to thank both of them for support and financial assistance.

I would also like to thank my friends and colleagues from Aalborg University with whom I was associated in academic and/or non-academic activities.

I would like to thank my parents and my family for their continuous unconditional love and encouragement.

Table of Contents

List of Figures

List of Tables

Chapter 1. Introduction

The research documented in this thesis examines aspects of integration of power converter and electrical machines for variable speed drives (VSDs) used in different applications such as pump and compressor. Integration of power converter and electrical machine has been an interesting research area in academics and as well as in industry for last two and half decades. It is a very challenging task as it involves multi-disciplinary engineering work to overcome several issues like vibrations and thermal problems along with electrical issues associated in the motor integrated variable speed drives.

In particular this research is focused mainly on modelling and control of a compact power converter, which is based on electronic smoothing technique. The electronic smoothing inductor based power converter offers reduced size of passive components usage in drive and it paves a way for high performance and compact variable speed drive solution for motor integrated variable speed drives applications.

This chapter includes motivation and background, objective and structure of the thesis.

1.1 Motivation and background

1.1.1 Three phase electric drive

Power electronics and electric motor drives are the two enabling technologies crucial for industrial competitiveness in the world market place in the present situation. One of the most valuable achievements in power electronics is to introduce variable voltage and variable frequency from the fixed voltage and fixed frequency of the generated electrical power supplies. Now a days over 60 percent of the total generated energy globally is consumed by different kind of

electric motors [1]. The loads in which the use of speed controls in by variable speed electric drives can bring the largest energy savings are mainly the fluid handling applications (pumps, compressors and fans) with variable flow requirements. Other applications that can also benefit from the application of the VSDs include conveyors, machine tools, lifts, centrifugal machines, etc. [2].

Variable speed drive (VSD), which regulates the speed of the motor by controlling the stator terminal voltage and its frequency applied to electrical machine windings, can significantly reduce the energy consumption. High energy prices and limited resources to generate the required electrical energy in the current scenario are the major concerns in front of the world these days, and therefore, improvements in efficiency of the drive systems are one of the most effective measures to reduce the primary energy consumption [1].

1.1.2 Essential and desired features of drives

Electric drives are expected to operate from a fixed voltage and fixed frequency grid (source) to feed electric motor with variable voltage and variable frequency to produce desired torque and speed for a given application. In most of the applications, it is highly desirable to operate these motors in wide range of speed and torque without loss of much energy in the energy conversion unit (power converter). The electric drives are expected to have minimum effect on grid and motor connected to it, i.e. currents drawn from grid should be within specified limits and currents injecting in to machine should not overheat the machine windings to avoid insulation failure of the machine.

It is also necessary that electric drive should not disturb other loads connected to the point of common coupling (PCC). These electric drives should require minimal maintenance and service after the commissioning of the system as it involves resources to allocate for this purpose [2].

The globally accepted and widely used prominent speed control technology - electronic VSDs coupled with alternated current (AC) 3-phase motors (mostly

squirrel cage induction motors) - have practically replaced other technological solutions: mechanical, hydraulic as well as direct current (DC) motors. The speed of the rotating electrical field created by the induction or synchronous motor stator windings is directly linked with the frequency of the supply applied to the stator windings. Electronically powered VSDs can produce variable frequency, variable voltage waveforms which can be utilized to control the motor speed and torque at the shaft.

The adjustment of the motor speed through the use of VSDs can lead to better process control, less wear in the mechanical equipment, less acoustical noise, and importantly significant energy savings. However, VSDs can have some disadvantages such as electromagnetic interference (EMI) generation, current harmonics introduction into the supply and the possible reduction of efficiency and lifetime of motors [3].

1.1.3 Integration of power converter with electrical motor

There are increasing demands for compactness and high power density of power converter used in industry. In industry and commercial applications, integrated motor drives are becoming very popular in textile drives, motive mining machinery, spindles of machine tools, hermetic pumps, and motion controls in the power range of fractional kW to 25 kW. Also, in today's hybrid or all-electrical vehicle and more-electrical aircraft applications, the integrated motor drive is an interesting technology for achieving compactness and reduced-weight design to meet more stringent requirements of on-board power and actuator control systems.

Machines with high torque density are required for many applications, including automotive and aerospace, and a high electric loading is often employed to increase the torque density [4]. For a particular application designer can design the most suitable drive system from all the possible choice. In this thesis com-

pressor application is one of the targeted applications for a motor integrated VSD.

Development of high-speed electrical drive systems is needed for new emerging applications, such as generators/starters for micro gas turbines, turbo-compressor systems, drills for medical applications, and spindles for machining. Typically, the power ratings of these applications range from a few watts to kilowatts, and the speeds from a few tens of thousands rpm up to a million rpm [5]. Recently, high-speed centrifugal turbo-compressors have been under intensive research and development [6]. Since, compared to conventional compressors, high-speed centrifugal compressors have numerous qualities such as simple structure, light weight, small size, and high efficiency.

The advantages of variable speed electrically driven HVAC compressor include the followings:

1) Efficient operation as the compressor speed is independent of the engine speed unlike conventional belt driven units;
2) Improved packaging as the location is not restricted to the accessory drive side of the engine;
3) Elimination of the rotating seals reduces the leakage of the refrigerant into atmosphere [6].

Integration of electric motor and of load has been already done and resulted energy efficient operation of overall system in HVAC compressors. Motor integrated VSD will be one step further and will improve overall performance of total system in these applications.

Motor integrated VSD offers many desirable features, such as high compactness, reduced material cost, reduced engineering time for installation or integration, lower system losses, more effective cooling arrangement and better protection against short circuiting and over-voltage due to dv/dt induced voltage reflection waves [4].

The major technological obstacle for the elevated temperature high power density power converter for motor integrated VSD is the unavailability of high temperature power components, such as high power semiconductor switching devices, large value of dc-link capacitors, as well as control electronics devices and passive components. Consequently, challenges presented to the designers for the next level of innovations include alternative power devices, total optimization of circuit topology and whole system (machine + frequency converter), thermal management and cost-effective design.

1.2 Objective of the thesis

1.2.1 Problem statement

It is possible to make a high performance motor integrated variable speed drive utilizing new advanced compact power converter topologies that are very efficient and small in size combined with optimized designed motors with or without permanent magnet operating at relatively higher efficiency and good thermal stress handling capabilities. Using the advanced control method it is also possible to improve and optimize performance of the motor integrated VSD system in all aspects compared to a traditional VSD system powering up the electrical machines.

1.2.2 State of the art for motor integrated variable speed drive

Power converter of a typical VSD comprises two stage of power conversion, first AC to DC by a rectifier and then DC to AC by an inverter. Many rectifier topologies have been developed so far by various researchers from different part of the world. Active rectifiers are one of the solutions to reduce harmonics and volume of the passive components of the power converter, i.e. current can be actively controlled and bulky passive components are not necessary with the help of power semiconductors. A purely sinusoidal current can be provided with the help of the active rectifiers. However, in many applications, a high

input current quality is not required [7]. For instance, rectifiers drawing rectangular or quasi square wave currents are widely applied in motor drive applications in various industries. In case of the active rectifiers, a high switching frequency (around 10kHz) is also required in order to obtain a pure sinusoidal input current, i.e. unity power factor at input and to reduce the volume of passive components (filter inductor and dc-link capacitor), which ultimately reduces the system efficiency by 2% to 3% because of high switching losses of the power converter [8].

Cost and kVA rating of power electronic devices in the active rectifier is also relatively higher. The practical realization of the active rectifiers is also high because the control and EMI filter designs are relatively complicated and costly. The other advantages of the active rectifiers of the front end include bidirectional power flow and controlled dc-link voltage, which allow regeneration of energy from a load to the mains power source. Although it is a very good feature, but regeneration is not needed/required in many applications. Passive rectifier fed electric drive can be useful in some, if not many areas of electrically driven loads.

Quasi square wave input currents may be a compromise in order to improve the quality of the input current while keeping drives cost low and, therefore, may constitute an intermediary development stage from the uncontrolled diode-rectifier towards fully controlled sinusoidal input current drives. VSD topologies with an auxiliary power converter inserted between the output of the diode bridge and the dc-link capacitor can provide continuous conduction of the current into the dc-link capacitor and to obtain a square-wave shape of the input currents [9].

This kind of VSD offers the following benefits: the input current THD decreases to a new level of about 30%, the VSD becomes more robust to unbalanced voltage supply (up to 10%), and it is possible to decrease the physical size of the inductors than used previously for passive filtering.

To decrease physical size of DC inductor, an intermediate electronic stage is required. Such arrangement generally referred as Electronic smoothing inductor (ESI) performs the function of an inductor that has controlled variable impedance. The ESI can control output current of a three phase diode bridge to a dc value and makes it possible to reduce not only mains current harmonics but also reduces the output voltage ripple [10]. The ESI consists of a high frequency dc inductor, two power MOSFETs, two fast switching power diodes, and a DC-link capacitor. This arrangement can be compared to a passive smoothing inductor which is having infinite inductance, if its losses are neglected, also behaves like a pure energy storage element.

The ESI realizes the energy storage characteristic required for smoothing by the dc-link capacitor of the switch-mode power stage instead of only by employing an inductor alone. Electrolytic capacitors, however, being usually applied for this reason show a very high specific energy storage density as compared to the magnetic energy storage capability of an inductor. Output capacitor of the rectifier is film capacitor with high lifetime and very good reliability.

A new power converter topology utilizing electronic smoothing concept where power circuit is slightly modified from standard ESI has been presented but not evaluated in past [8]. This modified electronic smoothing inductor (MESI) is also able to control a diode bridge output current and makes it possible to reduce not only mains current harmonics but also output voltage ripple [8]. The MESI is connected to the output capacitor in series. In this case average load current will not flow through active switches. In order to charge and discharge the DC-link capacitor, the bidirectional current must be controlled. Therefore, four switches are employed.

MESI based power converter is an emerging and promising converter topology which may be able to deliver a compact and robust power converter for integrated VSDs. Although it has advantages of lower losses, but there is a challenge in the circuit layout as inductance associated with the connection of MESI

converter with the main inverter of the drive can cause flow of high frequency current with high amplitude in the system.

Different types of machines including induction machine, reluctance machine and permanent magnet machine have been studied to find suitability for motor integration purpose. Detailed study of the state of the art of the machine types and converter topologies is given in next chapter.

1.2.3 Research areas

This thesis is focused on three phase motor integrated variable speed drives. Several types of machines and different circuit topologies related to power converter of the electric drives are studied during this research and documented in this thesis.

The thesis deals with modeling and control of ESI based power converter topology for electric drive which will enable easy integration of power converter in electrical machine.

This research also deals with power converter with reduced size of passive components used in electric drive for VSDs applications.

1.2.4 Limitations

This research is mainly focused on medium power range of 1kW to 10 kW. Three phase input power supply is being utilized in circuit topologies discussed in the thesis. The thesis considers several assumptions and limitations that simplify the analysis and design.

The variable speed drive for motor integrated system is modelled as a front-end three phase diode bridge rectifier followed by voltage source inverter. This assumption is fair enough as most of the drives in low power to medium power range use traditionally this type of circuit topology in various industrial applications.

Three phase line to line voltage of 400V and 50 Hz is considered as input supply and referred as mains in this thesis. This voltage can have +10% and -15%

variations on either single phase or all the phases. Although other voltage ranges and frequencies (like 60 Hz) have not studied or considered in this thesis but they can be used with some modifications.

1.3 Structure of the thesis

This thesis is divided in three different parts. First part presents the background and different ways and means to design motor integrated variable speed drives. This part includes chapter one and chapter two. In second chapters state of the art for the power converter suitable for motor integrated VSDs is discussed in detail. In this chapter work done by other researchers has been reviewed in context of the integration of motor and power converter.

Second part is focused about electronic smoothing inductor based three phase rectifier for motor integrated variable speed drive. This section ranges from chapter three to chapter seven. In this section third chapter is dedicated for different filter schemes and response of three phase rectifier operating with different type of loads connected at the output of the rectifier. Need of electronic smoothing technique instead of passive filter is established in this chapter. In next three chapters, electronic smoothing inductor (ESI) and its linear and non-linear modelling, different transfer functions and control schemes of the ESI based converter are discussed in detail.

Last part of thesis includes chapter 8 and chapter 9. Chapter 8 is about a modified topology of ESI and advantages of this topology. This chapter also includes some practical issues related its implementation in three phase electric drive for motion control applications. This part also includes conclusion and contribution of this thesis in last chapter of the thesis.

Chapter 2. Motor integrated variable speed drives

2.1 Background

Electric motors are found in practically every branch of industry for all sorts of applications. They are cheap to manufacture, reliable and require little or no maintenance in operation. However when electric motor is powered from fixed frequency, some limitation arises about change in speed of the shaft. Frequency converter i.e. inverter allows the frequency of stator current and therefore shaft speed of the motor to be adjusted, allowing the drive system to operate in wide speed range. In Figure 1., block representation of an electric drive system is presented. Although grid and loads are out of the scope of this study, but impact of drive on the system performance has been studied in this thesis.

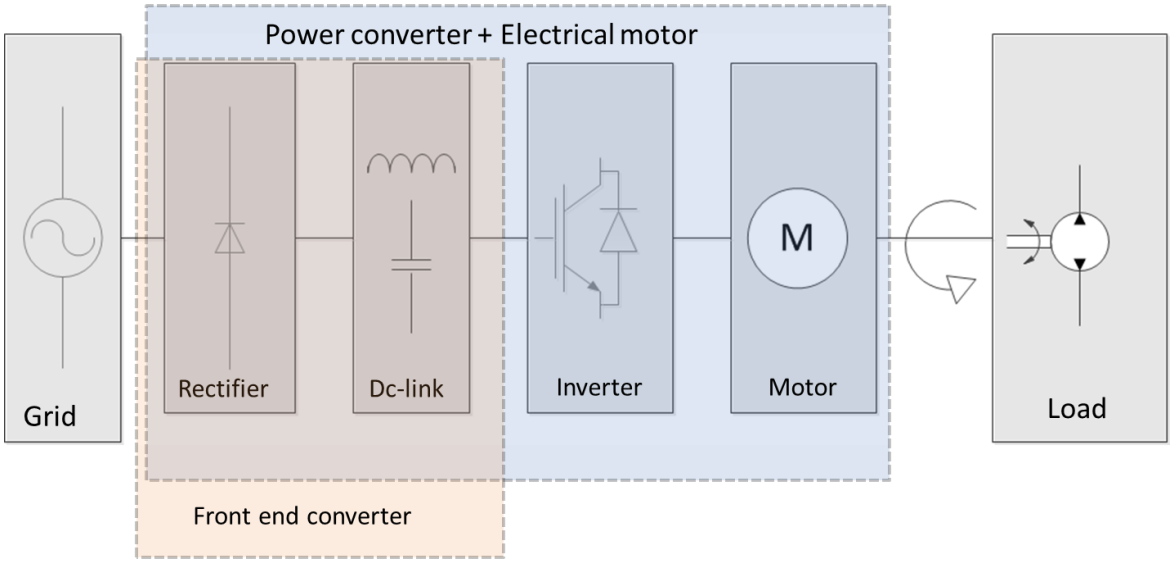

Figure 1. Block representation on an electric drive system.

Power flow takes place from grid to load via electric motor with the help of a power converter. Intermediate dc link essentially is a filter comprising passive components. These types of drive require knowledge of both the motor and the converter performance to the user. The motor integrated VSDs will come into one package and will eliminate such a need.

This chapter is a review on the different attempts of motor integration with power converter, study of different type of loads in which VSDs can bring significant energy saving, sate of the art for converter topology and machine type suitable for integration purpose. In this chapter, discussion on advantages associated with motor integration and concerns associated with reliable operation of the VSDs has been included.

2.2 Previous work in the direction of integration of electric drive and electrical machine

Research on integration of electrical motors and power converter was carried out in the laboratories even before the 1990's, and pump manufacturing company *Grundfos* in Denmark combined an induction motor and an inverter for their pumps already in 1991 [11]. However, the plastic module producer *Franz Morat KG* in Germany was probably one of the first to produce integrated motors commercially for industrial use in 1993 [11].

These days many different integrated electrical motors are available in the market. Various electrical machine manufacturers like *GE, Siemens, VEM Motors, Bosch Rexroth, Rockwell Automation* etc. have integrated motors on their product list, and research on the integration of power electronics and motor to one package is very much in focus in industrial and academic world. The current research area in motor integrated VSDs covers both the induction motors, as well as the permanent magnet motors [11]. The main focus of research in motor integration has been for low power applications. The integrated motors conceptualized by several researchers in the past had output powers below 2.2 kW.

The integrated drive for induction motors is commercially available and normally they have an output power below 7.5 kW (i.e. about 10 hp). This is not the absolute power limit for integration of induction machine but around this power the thermal problems start increasing, according to some manufacturers [11].

Rockwell Automation claimed that thermal problems arise already at 3.7 kW (5 hp), while *Siemens* saw a possible increase to 15 kW before the end of 2001. One exception is *VEM Motors*, which already offers integral motors up to 22 kW. Their smaller integral motors are equipped with drives from *Danfoss* in Denmark, while the larger sizes use drives from *Emotron* in Sweden.

Integration of higher powers motors needs more complex designs regarding e.g. the heat sink(s) and thermal management. Also the amount of copper and the iron quality of the motor, and the amount of silicon in the converter have to be increased. This leads to more expensive motor integrated products [12].

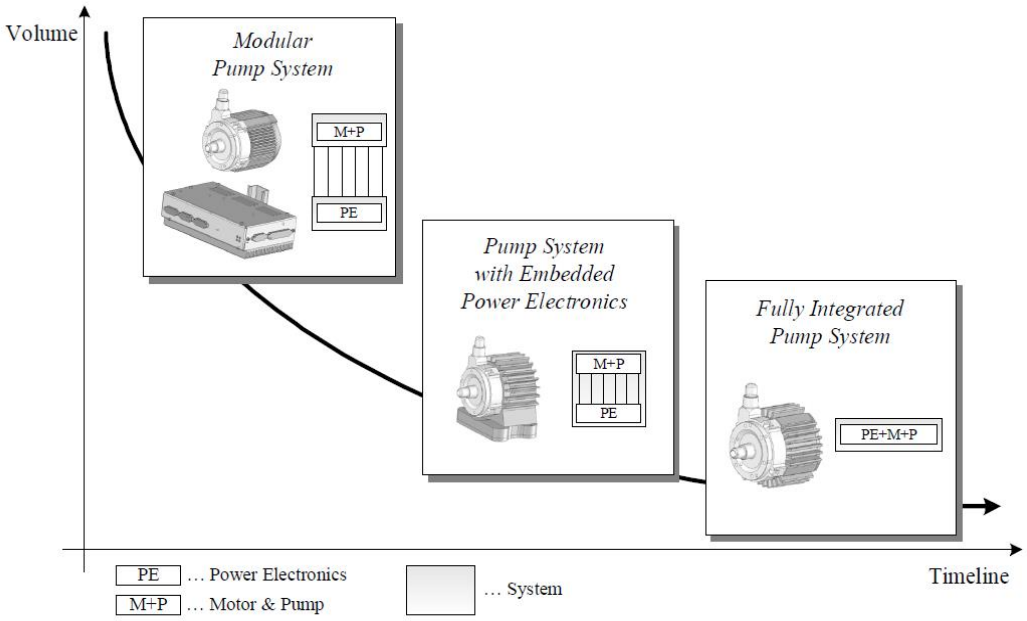

Figure 2. Levels of integration of the magnetically levitated pump system [13].

A level of integration of the magnetically levitated pump system is schematically depicted along with timeline in Figure 2. The integration of the power electronics (signal processor and power inverter unit) and the motor and pump

as separate working units into one casing with compact design and minimized cabling distances brings several advantages. By doing so, the space inside the case can be used more efficiently and the cabling effort is reduced significantly. However, in this integration, the power electronics and the motor and pump are still separate modules of the system. In one another attempt, Wisconsin Electric Machines and Power Electronics Consortium (*WEMPEC*) presented an Integrated Modular Motor Drive (IMMD) [14] as shown in Figure 3., which comprises of five stator coils and a six-pole surface permanent magnet rotor.

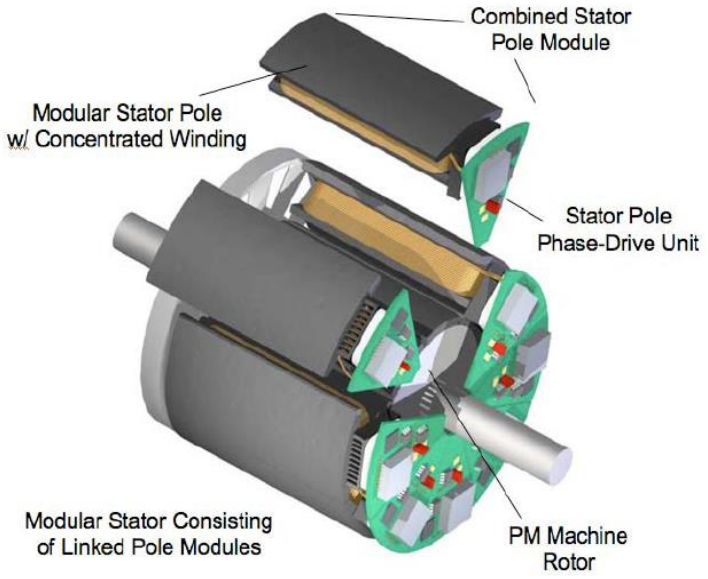

Figure 3. Illustration of integrated modular motor drive [14].

The IMMD concept is based on the adoption of a modular motor phase-drive unit for the stator assembly that includes the following key components:

1. A segmented stator pole piece fabricated from either conventional magnetic steel laminations or soft magnetic composite (SMC) material;
2. A concentrated coil winding on the stator pole;
3. An autonomous power converter dedicated to the motor pole that includes the required power electronics and controller to excite the pole winding in a coordinated fashion with the other stator phase-drive units.

The trend towards more-electric aircraft creates a need and challenge for power electronic modules, converters, and motor drives that can operate in environments that are different from conventional industrial applications. In many aerospace applications, such as electric actuation systems and aircraft power conversion and conditioning systems, it is desirable to have a new grade of power modules and converters that can operate safely in an elevated temperature environment, with reduced weight and size [15].

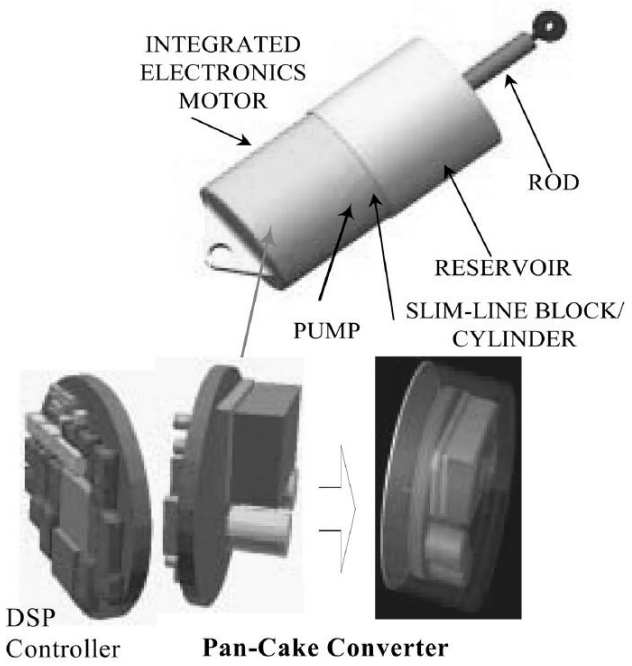

Figure 4. Illustration of compact integrated electronics connected inside the motor for slim-line actuator [15].

An illustrative example of employing a compact integrated electronics motor for slim-line actuator is given in Figure 4. As shown in Figure 4., the actuation application calls for a very compact and low-weight power converter. On the other hand, the temperature of a hydraulic system used in aircraft can be at a level of 85 deg C to 90 deg C, which makes it difficult to use the available liquid flow for cooling the power electronics devices and converters that are based on a conventional design, thus requiring additional cooling mechanism with a penalty of added size and weight of the cooling unit [15].

The evolving markets of industrial integrated motor and drive also present similar design challenges because the power converter circuit must be joined with the motor in an increasingly compact package, and is often located in a hot housing or compartment. This is because the maximum allowable p-n junction temperature of today's silicon based solid-state power devices is limited to 175 deg C and gives insufficient margin over the local operating ambient temperatures. Although, employing an advanced silicon carbide (SiC) power device can improve the capability of high temperatures, it unfortunately brings a significant penalty of high cost of fabrication of power module and other auxiliary circuit requirement such as gate drive circuit.

The SiC devices are very useful when converter is operating at high voltage (more than 1.2kV) and high frequency (more than 20 kHz) as compare to Si power devices, and another big advantage in SiC based converter is smaller filter size. In VSDs switching frequency is around 5 to 10 kHz and output filters are normally not used as stator windings have sufficient inductance for filter purpose. In these scenarios SiC based converter does not provide major advantages, but still if high temperature operation is required then it is necessary to go for SiC based converter.

Motor efficiency upgrades can achieve potential savings of about 19.8 billion kWh per year. Improved methods of rewinding failed motors can contribute an additional 4.8 billion kWh. Energy savings from system efficiency improvements are potentially much larger: 37 to 79 billion kWh per year as studied in year of 2005 [2].

2.3 Potential of energy saving in different applications utilizing variable speed drive

Different types of electric motors are used to provide mechanical motive power for a wide range of end users for different applications in domestic and industrial world. Most of these electric motors are designed to run at 50% to 100% of

rated load during their normal operation. Maximum efficiency of the motor used for these purpose is generally achieved near 75% of rated load. If the operation uses equipment with motors that operate for an extended periods under 50% of rated load, modifications in the governing system (control) will improve the total energy consumption of the system. Sometimes these electrical motors are designed as overrated because they must accommodate peak conditions, such as when a pumping system must satisfy occasionally high demands by the users.

Different available options for the end user to meet variable loads include two-speed motors, variable speed drives, and load management strategies that maintain loads within an acceptable range are provided by the different industrial manufacturers.

Variable speed drives (VSDs) are typically considered or perceived as an extra component to 'common' systems or machines. They are typically acquired either directly by the end-user from the VSD supplier or through intermediate parties such as OEM and installers. A relatively small number of the potential end-users are willing to actively search for a VSD related solutions for their system [15]. These end-users typically are early market clients. VSDs have to move further with a greater pace to main market clients. The distribution of electrical energy usage for different types of loads is shown in Figure 5.

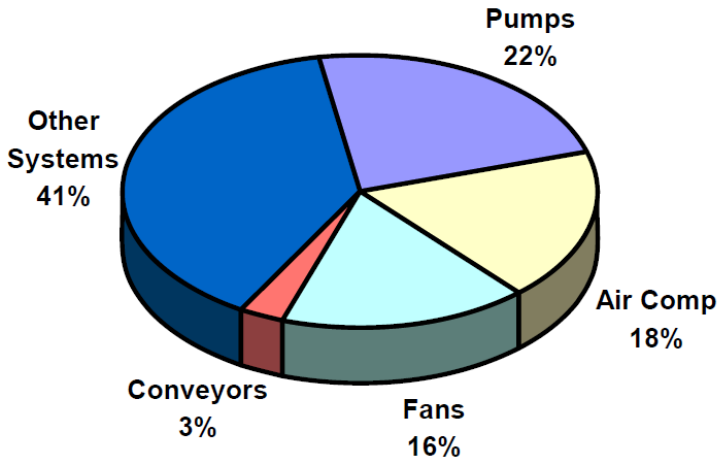

Figure 5. Motor Electricity Consumption for different applications [15].

Variable speed drives are being applied to a wide range of loads of different applications. Examples of the different types of loads in which significant energy savings can be achieved by adding VSD are described as follows:

2.3.1 Single pumps

In comparison with a traditional throttling valve to control the flow rate of the pump, the variable-speed driven pump can result in significant energy conservation where reduced flow rates are required for long periods of time as described in [2]. The centrifugal pumps without lift (e.g. closed loop circuit), respect the cube power law, i.e., the consumed power is proportional to the cube of the speed, as shown in Figure 6.

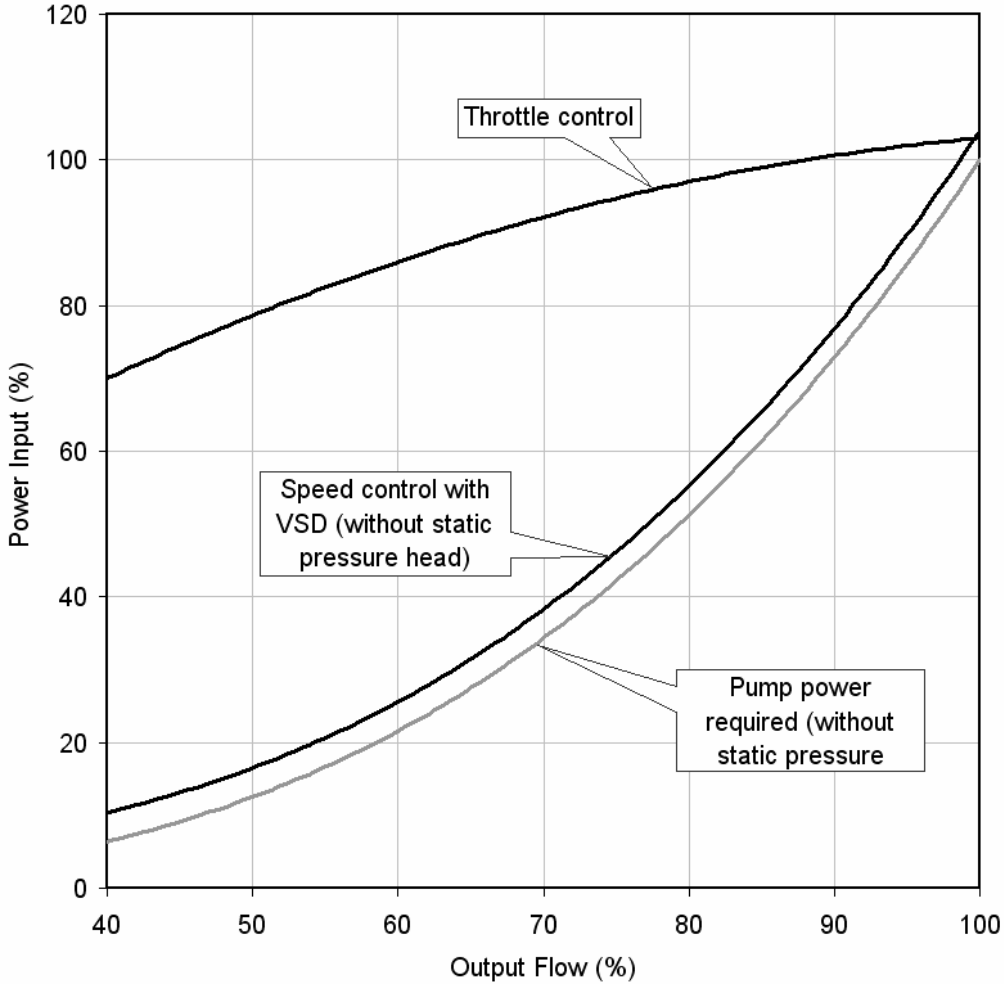

Figure 6. Input power for different flow control methods of a centrifugal pump [2].

The overall efficiency of the pumping system depends on the efficiency of the different components of the system. For the same output flow, the inefficient system absorbs more than twice the power absorbed by the optimized system, showing the importance of integrated motor systems design.

2.3.2 Staged pumping plants

In many pumping applications several pumps are used in parallel to produce the required flow. Operating all pumps at reduced speed rather than cycling the pumps on/off according to the demand, significant energy savings can be reached [2]. Water hammer has the potential to rupture valves, pipes, and fittings. It is easy to control this effect by controlled acceleration/deceleration using VSDs. Use of VSDs can make the operation easy to control and will have smooth transition along with the significant energy saving.

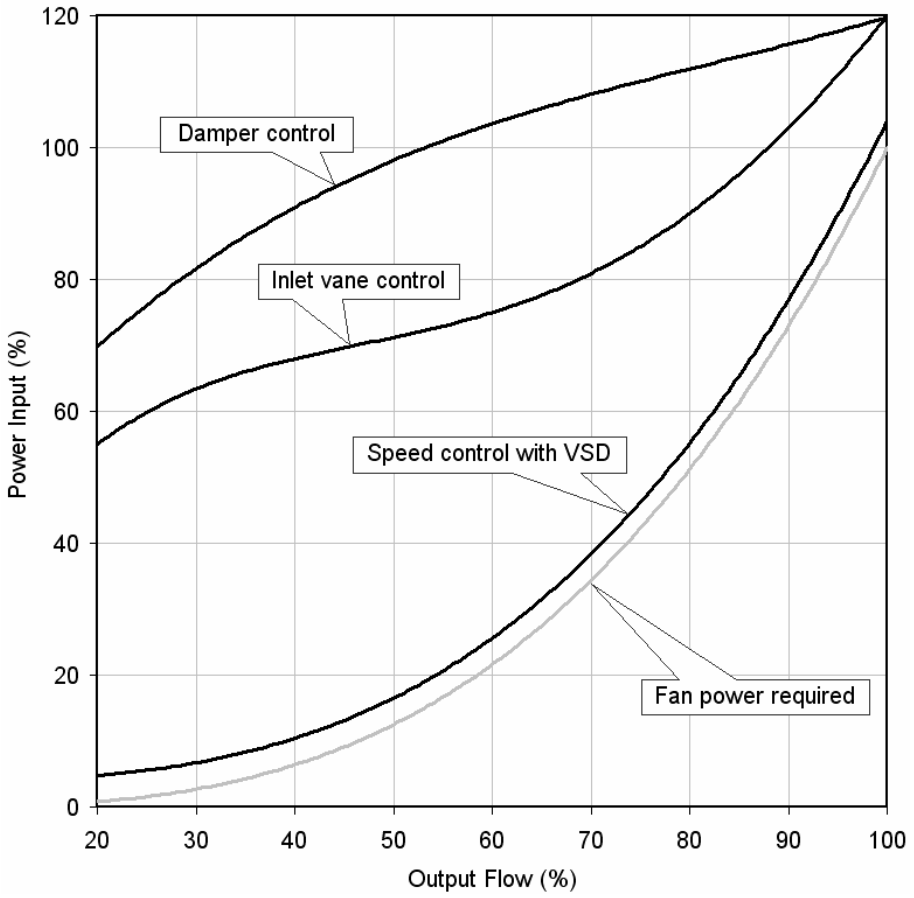

Figure 7. Input power for different flow control methods of a centrifugal fan [2].

2.3.3 Fans

Energy savings from adding variable speed control to fans can be significant. The illustration of the energy savings potential with a VSD versus common throttling methods is shown in Figure 7. High amounts of energy are wasted by throttling the air flow versus using adjustable speed [2]. The worst method is outlet dampers, followed by inlet vane control. The energy consumption in these loads is so sensitive to the speed that the user can achieve large savings with even modest speed adjustments. Compared with an on/off cycling control, is a more stable temperature in the controlled space and more efficient operation, by typically decreasing the fan energy in the range 25-50%.

2.3.4 Compressors

Rotary screw and piston air compressors are essentially constant torque loads which can also benefit from the application of variable speed control. The energy savings related to the use of variable speed control are dependent on the control system that is being replaced by VSDs. The energy savings achieved by fitting a VSD to a rotary screw compressed air unit, compared to other methods of flow control at partial load, can be seen in Figure 8.

Energy savings in constant torque loads is typically considerably less than with centrifugal pumps or fans, which obey the power cube law, and so to retrofit a VSD to a compressor it is less likely to be economic on the grounds of energy savings alone. Additionally, care needs to be taken to ensure adequate lubrication at reduced speeds. However, the introduction of screw compressors with integrated motor and speed control has enabled the additional price of variable speed control to be significantly reduced, will lead to typical energy savings of 15-20% as compared to previous solution. The use of VSD for temperature control (floating head operation) in the refrigeration pumps/compressors can eliminate the on/off cycling losses and decrease the temperature difference between the condenser and the evaporator, with large energy savings.

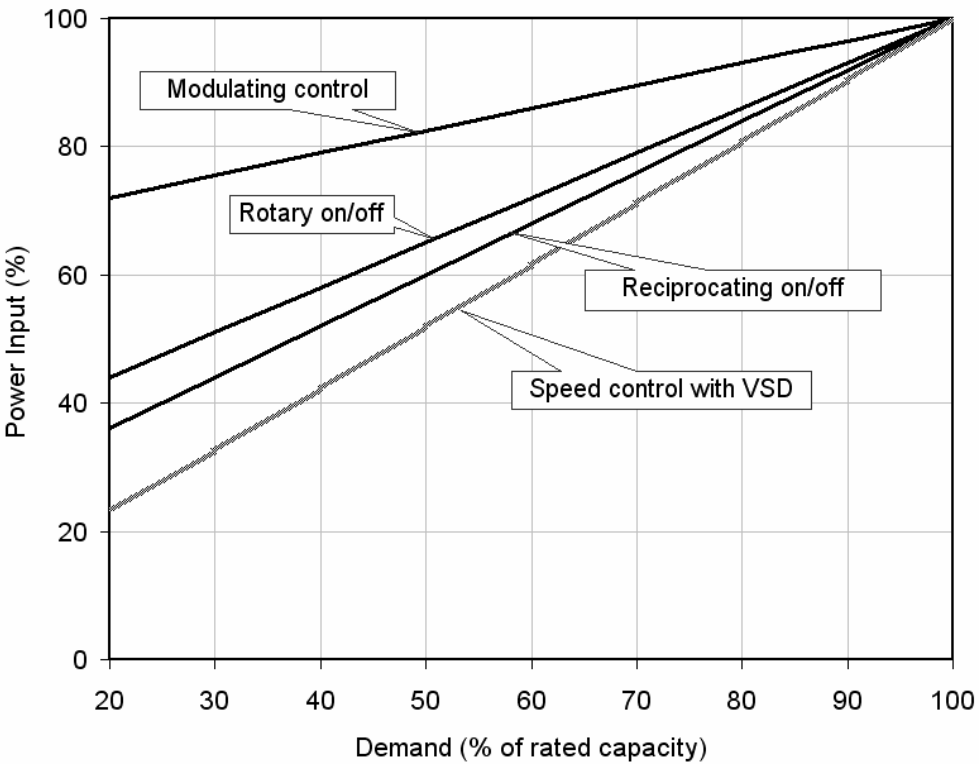

Figure 8. Energy saved by using a VSD on a rotary screw air compressor [2].

2.3.5 Lifts

New VSD topologies (active front end) allow the braking energy to be injected back to the source/grid – VSDs with regenerative capability. This feature can be a way of saving a significant amount of energy in applications with frequent braking operations, namely, lifts. This is only possible if the motor mechanical transmission allows this mode of operation. When the lift is going down, and the load weight (people inside) is larger than the counterweight, then the motor torque is in opposite direction to the speed, i.e., the motor is braking. In the same way, when the lift is going up unloaded, energy savings can be reached if the motor is controlled with a regenerative VSD. By using VSD in lifts lots of different functionality can be incorporated.

2.3.6 Centrifugal machines and machine-tools

In high inertia loads (e.g. machine-tools) or/and high speed loads (e.g. centrifugal machines), with frequent accelerating/braking operation, it is possible to

save significant amounts of energy. When running, this type of loads has a large amount of kinetic energy, which in a braking process, can be regenerated back to the grid, if a regenerating VSD is used [2]. A more efficient acceleration technique uses a VSD that will significantly reduce the energy consumption, comparatively to the other mentioned techniques. Such machines are normally operated with intermittent duty as nature of the work, and there is huge potential to save electrical energy utilized in centrifugal machines and machine-tools.

2.3.7 Conveyors

In the constant torque device, the required torque is approximately independent of the transported load (is only friction dependent). Typically, the materials handling output of a conveyor is controlled through the regulation of input quantity, and the torque and speed are roughly constant [2]. But, if the materials input to the conveyor is changed, it is possible to reduce the speed (the torque is the same) with the help of a VSD, and, significant energy savings will be reached, proportional to the speed reduction.

2.4 Motor selection for integrated drive

Interest has grown significantly in the development of electrically-powered accessories to replace conventional hydraulic and mechanically-powered equipment during last two decades in different industrial applications. This trend has been motivated by opportunities for energy savings and customer friendly features. Nearly all accessory systems present in today's industrial equipment are candidates for electrical conversion. These include a variety of pumps, blowers, and actuators that can benefit from the introduction of variable-speed motor drives. However, key barriers impeding the widespread introduction of such electric accessories include cost and reliability of the electrical equipment. Challenges include the harsh environment where temperatures can reach as high as 150 degC [16-18]. However, cost remains the overriding

challenge facing the developers of such type of electrical accessory equipment. The principle of operation of any rotating electric motor is derived from Lorenz force. A current carrying conductor placed in a magnetic field is acted upon by a force by way of the *Lorenz force BLI* rule.

To minimize the total thermal losses and reduce the requirement for heat dissipation, a high efficient motor is very desirable for the integrated motors. Reducing the dc-link capacitors needs to minimize the reactive load current circulating between the motor magnetizing inductor and the dc-link capacitor. This can be achieved by using an optimally designed electrical motor operating at high power factor.

In this section different types of electrical motors are investigated to find their suitability for motor integration with VSDs.

2.4.1 Induction motor

The induction motor is by far the most widely used choice for development application in industry as compared to other type of motors. Being both rugged and reliable, it is also a preferred choice for the variable-speed drive applications. Low cost, high reliability, fairly high efficiency, coupled with its ease of manufacture, makes it readily available for development application in any location of the globe. The cage-rotor induction motor requires minimal maintenance when commissioned in the system. When operating at the normal utility ac supply, the motor speed is essentially constant, and for fixed-speed applications, the cage-rotor induction motor has become the industry workhorse. Rotor of an induction machine is very simple, squirrel-cage rotor consists of copper or aluminium bars placed in the slots and short circuited at the endrings. These bars are normally skewed to prevent torque ripple and to reduce noise.

Balanced supply with sinusoidal distributed stator winding produces a sinusoidal magnetomotive force (MMF) rotating at synchronous speed, which is proportional to the frequency of supply and inversely proportional to the num-

ber of stator poles. This MMF results in rotating magnetic field at the synchronous speed. This rotating flux wave sweeps past the conducting rotor bars, and generates an EMF in them which causes current flowing in the short-circuited rotor bars.

These induced rotor currents interact with the airgap field to produce a torque which causes the rotor to rotate in the same direction as the rotating airgap field. Rotor speed is slightly less than the synchronous speed of the rotating magnetic field. Because of the low resistance of the shorted rotor bars, only a small relative speed difference between the rotating flux wave and the rotor bars is required to produce the necessary rotor EMF and current. Normally, the rotor rotates at a speed N_r rpm, which is slightly lower than the synchronous speed N_s.

The fractional slip s is defined as:

$$s = \frac{(N_s - N_r)}{N_s} \qquad \textbf{2-1}$$

If the load is increased, rotor speed will fall, which means slip will increase, the stator magnetic field cuts through the rotor bars at an increased rate. This induced greater voltage and current in the rotor bars at a higher frequency. The current in the rotor bars creates a magnetic field in the rotor that rotates synchronously with the stator magnetic field, but at an angular displacement to it. The magnitude of each magnetic field, along with the angular displacement between the stator and rotor, produces torque that resists the slowing down of the rotor.

When this torque equals that of the load, steady state is reached. In short, current in the rotor in the rotor bars changes in magnitude and frequency (along with slip) as necessary to produce the required load torque. The slip is equal to the rotor copper losses divided by the power across the air gap, P_{Cu}/P_{gap}, so as a result, for a given output power, slip is proportional to P_{Cu}. For a given design, slip is also proportional to output power, but P_{Cu} as I^2R losses will vary as the

square of the load current. Therefore, the greater the rotor-bar resistance, the greater the slip required to produce rated load. Subsequently, the temperature rise will be higher and the efficiency will be lower.

The wound-rotor has a polyphase winding similar to the stator winding with the same number of poles. The winding are connected to slip rings in order to connect external impedance, limiting starting currents, improving power factor and controlling speed. Traditionally, the squirrel-cage rotor induction motor has been regarded as constant-speed motor when operating on the normal utility ac supply. However, modern developments in power electronics and microelectronics enable the induction motors to compete with dc motors in torque/speed regulation required field. In induction machine, there are significant losses occurs in rotor, and it is relatively difficult to remove losses from rotor as compared to stator and therefore for motor integrated VSDs application, induction machine with lower losses on rotor side will be a preferred choice. This can be achieved either by reducing airgap between stator and rotor by introducing another converter to control rotor side losses. By adding converter to rotor side will make it doubly fed machine and will not be a cost effective solution for low and medium power level.

2.4.2 Switched reluctance motor

The structure of the switched reluctance motor is simple, robust and very reliable in operation. The machine has a salient pole stator with concentrated windings and a salient pole rotor with no winding (electric conductors) or permanent magnets [19]. Recently, developments of the Switched Reluctance Motors (SRMs) have been active in the world for various applications. Due to the impact of enabling technology of power electronics, variable speed drivers based on SRMs have become affordable. There are several advantages in SRMs such as rotor robustness, low cost and possible operation in high temperatures or high rotational speeds. Cooling is easy because most of the heat generation

occurs in the stator. Salient rotor structure provides an opportunity higher torque/inertia ratio. Thus, fast acceleration and deceleration can be realized with low load inertia. These motors have been in mass-production in the application of oil pressure pumps and vacuum cleaners.

It is recognized that efficiency of SRM is rather low, in general, compared with the permanent magnet machines. Improving the motor efficiency is an important goal for machine designers for promoting applications of SRMs [20]. It can be noticed that efficiency is high in high power motors. In a few kW motors efficiency is generally less than 85%. However, the efficiency of IPM machines in a range of 0.7kW-2kW is quite high, i.e., about 95% [20]. These machines are used in air-conditioners and general purpose drives. Realizing these efficiencies by SRM is still challenging. Many test machines have been built and tested in a power range of 1-4kW since 1990. Efficiency improvement is achieved by some techniques such as a contribution of low iron loss materials, machine design, increased winding slot fill factor and optimized voltage waveforms, etc. The efficiency of SRM has been improved about 95.6%as it is reported by some authors [20].

2.4.3 Permanent magnet motor

Permanent Magnet (PM) Motors have a stator winding configuration which is similar to a three phase induction motors, but these machines use permanent magnets in the rotor instead a squirrel cage rotor or a wound rotor as it is used in induction machine. The permanent magnet rotor tracks with synchronism the stator rotating field, and therefore, the rotor speed is equal to the synchronously rotating magnetic field produced by the stator.

The advancements of permanent magnet materials, power electronic based converter and microelectronics based control have contributed to energy efficient, high performance electric drives which use modern PM brushless motors utilizing rare-earth permanent magnets. These rare earth permanent magnet

based motors are advantageous compared to induction motors concerning the performance and cost with benefits of increased efficiency, reduced time constant, higher power volume/weight ratio, and cost effective production.

There are several disadvantages as well, for instance requirement for position sensors for low speed, cost of rare earth magnets and its mounting constraints and so on. The majority of PM machines employ an interior rotor, the permanent magnets (PMs) being surface-mounted on the rotor. The magnets usually need to be protected from the centrifugal force by employing a retaining sleeve, which is made of either stainless steel or non-metallic fiber. The rotor temperature rise may create a problem due to poor thermal dissipation, which may lead to irreversible demagnetization of the magnets and ultimately limit the power density of the permanent magnet machine.

Recent developments in PM machines technology include availability of improved PM material, varying construction for motor and generators such as axial field, radial field, two phase, three phase, higher phases with different rotor geometries, hybrid configuration, rectangular fed motor, sinusoidal fed motor, improved sensor technology, fast semiconductor modules, low cost high performance microelectronics devices. New control approaches have been proven to use these machines suitable for position control in machine tools, robotics and high precision servos, speed control and torque control in various industrial drives and process control applications. In spite of being most promising nature of these machines they have faced many hurdles to come to their present stage in terms of cost, torque ripple, noise, vibration, reduce reliability due to large number of components, operational constraints such as temperature rise [21-23].

Permanent magnet synchronous motors with concentrated windings have many advantages. The motor size can be reduced because of the short end-windings. In addition, not only the copper loss but also the copper cost can be reduced [19]. However, the rotor losses, which are the rotor core loss and magnet eddy

current loss, may increase because of the harmonic magnetic field due to the wide stator slot pitch. The thermal demagnetization of the magnet by the eddy current loss is one of the biggest problems in the motor. It can be seen that the magnet eddy currents in the concentrated winding motor is much larger than the distributed winding motor. The rotor core loss also increases. On the other hand, the stator core loss and the torque decrease.

To understand these characteristics, the losses are decomposed into harmonic components and classified due to their origins. The stator core loss can be decomposed into the losses caused by the fundamental rotational field, harmonic magnetomotive forces of the permanent magnet, and carrier harmonics of the PWM inverter. On the other hand, the rotor core and magnet loss can be decomposed into the losses caused by the stator slot harmonics and carrier harmonics. These different losses are listed below [24]:

1. The stator core losses caused by the fundamental field: In both motors (distributed or concentrated windings). The loss of the distributed winding motor is larger. It is for the same reason why the toque is larger.
2. The stator core losses caused by the harmonic magnetomotive forces of the permanent magnet: The loss of the distributed winding motor is several times larger than the loss of the concentrated winding motor
3. The rotor losses caused by the slot harmonics: The loss of the concentrated winding motor is several times larger than the loss of the distributed winding motor. Especially, the magnet eddy current loss is more than 10 times larger, even though the rotors are identical.
4. The carrier harmonic losses of the stator and rotor: The difference of the losses between the concentrated and distributed winding motor is slight.
5. In case of the distributed winding motor, the stator core loss caused by the harmonic magnetomotive forces of the permanent magnet is relatively large. On the other hand, in the case of the concentrated winding

motor, the rotor losses caused by the slot harmonics, especially the magnet eddy current loss, are significant.

In low-speed high-torque applications, a multipole PM motor is an attractive solution. The advantage is a low iron mass per rated torque due to rather low flux per pole. A high pole number in conventional distributed winding motors leads to a high slot number, which increases costs and, in the worst cases, leads to a low copper fill factor. The fractional-slot concentrated-winding solution does not require many slots although the pole number is high, which reduces both the iron and copper mass in the motor.

The fractional-slot winding allows a longer stator stack in the same frame length than conventional windings, since the axial length of end winding is typically smaller. As the stator yoke can be manufactured very thin, the larger airgap diameter in a certain limited stator outer diameter is possible. These lead a remarkable potential to increase the torque density. Therefore, the multipole PM motor with fractional-slot concentrated windings is selected as the direct-drive motor. Interior permanent magnet (IPM) synchronous motors possessed special features for adjustable speed operation which distinguished them from other classes of ac machines. They were robust high power density machines capable of operating at high motor and inverter efficiencies over wide speed ranges, including considerable range of constant power operation.

2.4.4 Flux switching permanent magnet motor

Flux-switching permanent magnet (FSPM) machines have been a popular research topic due to high power density and robust rotor structure similar to SRM [25]. With both PMs and armature windings on the stator and a robust single piece rotor similar to the switched reluctance machine, the FSPM machines are well suited to high speed applications. Cross-section of a FSPM is shown in Figure 9. The use of high energy PMs on the stator and the flux focusing effect of the 'U'-core modular stator topology result in high airgap flux

density, together with bi-polar winding flux-linkage, which is desirable in torque dense machines. The operation principle of the FSPM machine is be explained in Figure 10.

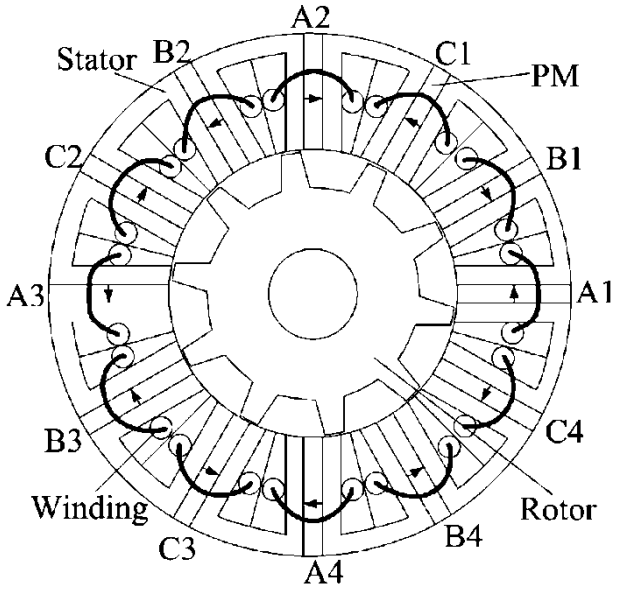

Figure 9. Cross-section of three phase, 12/10 FSPM [25].

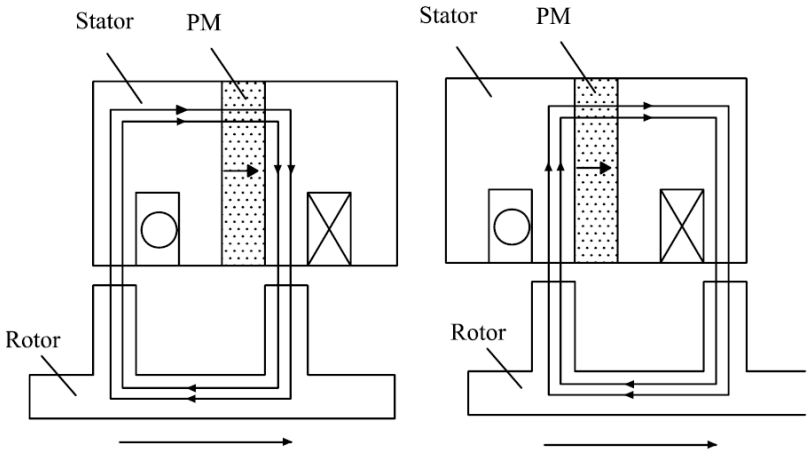

Figure 10. Operating principle of FSPM [25].

At the position in left half of Figure 10., the PM flux which is linked in the coil goes out of the coil and into the rotor tooth. When the rotor moves forward to the direction in right half of Figure 10., the PM flux goes out of the rotor tooth and into the stator tooth, keeping the same amount of flux-linkage whilst reversing the polarity, i.e., realizing the "flux-switching".

Consequently, as the rotor moves, the flux-linkage in the windings will change periodically, and back-EMF will be induced. Both the PM flux-linkage and back-EMF can be sinusoidal versus the rotor position as long as the machine is properly designed, thus it can be driven in the blushless ac (BLAC) mode. The FSPM machine is supplied with an inverter. When the machine is operated in the constant torque region under the current limit of the inverter, the inverter is able to supply a sufficiently high voltage to the machine. In contrast, when the machine is operated above the base speed, as the back-EMF rises, the inverter voltage will be lower than back-EMF, thus energy cannot be into the machine, namely entering constant power region. Then, the machine is operated under flux-weakening control to reach higher speed.

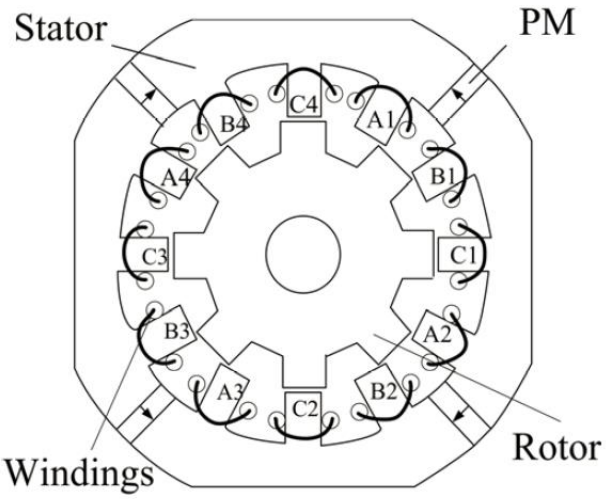

Figure 11. Cross-section of three phase, 12/8 DSPM [26].

Other doubly-salient machine types having permanent magnet include doubly-salient PM machines (DSPM), is shown in Figure 11., and flux-reversal PM machine (FRPM) is shown in Figure 12. The operation principle of DSPM machines can be simply described by assuming that the fringing is negligible and the permeability of the core is infinite, therefore a linear variation of flux-linkage with rotor position and consequently a trapezoidal back-emf is induced in the stator windings on no-load in these type of machines.

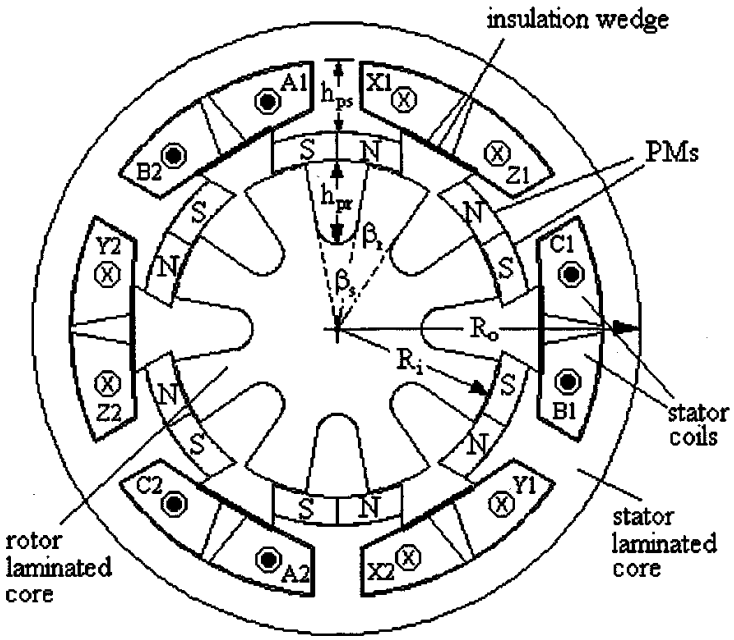

Figure 12. Cross-section of three phase, 6/8 FRPM [28].

This indicates that the DSPM machine is also suitable for brushless DC operation. Due to the existence of the PMs, a very high reluctance path for the armature reaction flux and thus the inductance of phase winding is small at both aligned and unaligned positions. Consequently, unidirectional torque can be achieved by applying a positive current when the PM flux is increasing and a negative current when the PM flux is decreasing to the corresponding winding. The torque is dominated by the permanent magnet excited torque, and the resultant reluctance torque as well as cogging torque are negligible. They share the traits of FSPM machines, in that they have a salient pole rotor without any coil or PM, and a salient stator containing the PMs and armature windings. The electromagnetic performance of FSPM and DSPM machines has been compared in past by some researchers [27]. It shows that the FSPM machine can have significant higher torque density than that of the DSPM machine in which the flux-linkage is uni-polar.

The operating principles of the FRPM and FSPM are very similar in that each stator pole has a “north” and a “south” that provides a bipolar flux linkage in a

concentrated coil. Although they operate on the same principles, existing FSPM and FRPM machines have different stator to rotor pole combinations, e.g. Ns/Nr =12/10 for FSPM and Ns/Nr =12/16 for FRPM for 3-phase topologies according to the design guidelines set out in [26]. The FRPM machine can be compared on a like to like basis of a 12/16 and 12/10 machines. From the design of both topologies it can clearly be seen that the FSPM machine will have the advantage of flux focusing. Flux linkage and back-EMF constant of FSPM are higher as compare to the FRPM machine, therefore a higher torque density for the FSPM machine is possible. However the FRPM machine has the advantage of being able to reduce its electrical frequency by halving the number of stator and rotor poles to 6/8 providing a reduced fundamental frequency, which is not possible with the FSPM 12/10 machine without introducing the unbalanced rotor force in the 6/5 FSPM machine. However, as both machines operate on the same principles, an increase in rotor pole number of the FSPM machine from 10 to 16 so that 6/8 FSPM can be realized without any inherent unbalanced magnetic force.

In terms of FSPM machine, both the value and polarity of the PM flux linkage in a coil vary with the rotor position. The rotor pole aligns with one of two stator teeth over which a coil is wound and the PM flux which is linked with the coil goes out of the coil and into the rotor tooth. When the rotor moves forward to align with the other stator tooth belong to the same coil, the PM flux linked goes out of the rotor tooth and into the stator tooth. Consequently, as the rotor moves, the flux linkage in the windings will change periodically. Hence, when the alternating currents are applied to the windings in accordance with the PM flux linkage, the motoring torque will be produced. Because the waveforms of the flux-linkage and thus the back-emf are essentially sinusoidal, it makes the FSPM machine an excellent candidate for brushless AC drive operation.

In addition, since a high per-unit winding inductance can readily be achieved, such machines are eminently suitable for constant power operation over a wide

speed range. Since the armature reaction flux in a FSPM machine does not pass through the magnets, the irreversible demagnetization withstand capability of the magnets is high, which makes it particularly suitable for flux weakening operation. In addition, flux focusing can be utilized and low cost magnets, such as ferrites, may be employed. In the case of adopting high energy magnet materials, such as samarium cobalt (SmCo) and neodymium-iron-boron (NdFeB), the ideal sinusoidal PM flux-linkage and back-emf may be distorted due to magnetic saturation. Using Ferrite (Fe) magnets, instead of NdFeB magnets, may reduce the total cost of the PM motor. Ferrites have lower remanent flux density than NdFeB. Reduced flux density will cause a decrease in efficiency, prolong the pay-off time and decrease future monetary savings. The flux switching motor offers improved performance and lower power electronic cost than an equivalent switched reluctance drive. The flux switching motor had a lower peak to peak value of radial force than the switched reluctance motor. The total change in radial force is therefore less in the flux switching motor. The flux switching motor allows a smoother transition of the magnetic flux from one set of stator poles to the next [29].

Lesser no. of rotor poles allow the consideration of three-phase FSPM topology in high speed applications with regards to lower losses without the torque ripple penalties of using single or two-phase FSPM topologies. With the 6/8 FSPM topology an improved torque output can be achieved while maintaining the high torque density of the 3-phase FSPM topology [30].

2.4.5 Multiphase electric machines

VSDs are nowadays invariably supplied from power electronic converters. Since the converter can be viewed as an interface that decouples three-phase mains from the machine, the number of machine's phases is not limited to three any more. Nevertheless, three-phase machines are customarily adopted for variable speed applications due to the wide off-the-shelf availability of both machines

and converters. Such a situation is expected to persist in the future and multiphase variable speed drive utilization is always likely to remain restricted to specialized niche applications where for one reason or the other, a three-phase drive does not satisfy the specification or is not available off-the-shelf either.

Due to the sixstep mode of three-phase inverter operation, one particular problem at the time was the low frequency torque ripple. Since the lowest frequency torque ripple harmonic in an n-phase machine is caused by the time harmonics of the supply of the order 2n±1 (its frequency is 2n times higher than the supply frequency), an increase in the number of phases of the machine appeared as the best solution to the problem. Hence, significant efforts have been put into the development of fivephase and six-phase variable-speed drives supplied from both voltage source and current source inverters.

This is an advantage of multiphase machines that is nowadays somewhat less important since pulsewidth modulation (PWM) of voltagesource inverters (VSIs) enables control of the inverter output voltage harmonic content. The other main historical reasons for early developments of multiphase drives, better fault tolerance and the possibility of splitting the motor power (current) across a higher number of phases and thus reducing the per-phase (per switch) converter rating, are nowadays still as relevant as they were in the early days.

The types of multiphasemachines for variable-speed applications are in principle the same as their three-phase counterparts. There are induction and synchronous multiphase machines, where a synchronous machine may be with permanent magnet excitation, with field winding, or of reluctance type. Three-phase machines are normally designed with a distributed stator winding that gives near-sinusoidal MMF distribution and is supplied with sinusoidal currents (the exception is the permanent magnet synchronous machine with trapezoidal flux distribution and rectangular stator current supply, known as brushless dc

machine, or simply BLDC). Nevertheless, spatial MMF distribution is never perfectly sinusoidal and some spatial harmonics are inevitably present.

2.4.6 Challenges in motor design suitable for integration

One of the most important physical constraints that limit the minimum size of each machine is its ability to dissipate its thermal losses without overheating. This thermal constraint is represented in the machine design optimization programs by setting a maximum limit on the stator winding current density. More specifically, most of the machines are sized using the same limiting value of stator current density ($7A/mm^2$) appropriate for machine cooling using hot pressurized water as the coolant (110 degC). Higher current density values would normally be used for water-cooled machines. Thermal management is one of the necessary areas to increase the operating life and to reduce the risk of failure. Lower losses in electrical machine will be enabler for motor integration with power converter.

2.5 Power converter topologies for integrated drives

High efficiency, small volume and low cost are nowadays basically the first three aspects mentioned when it comes to the development of any kind of converter topology. Concerning the use of a converter in a motor with integrated electronics, the first two mentioned aspects receive an even greater importance. The trend to an increased integration level of the power electronics and the motor leads first of all to the demand of very compact converter solutions simply because the available space is quite limited [31].

A problem in this respect is the DC link capacitor in an AC/AC converter. Today's mostly used electrolytic capacitors are large, expensive and have a short expected life time in comparison to the semiconductor devices. Decreasing the capacitor size would lead to an increase of the ripple current per unit volume. This implies higher loss density and it may cause a breakdown of the capacitor.

Most promising for this purpose is the metalized polypropylene capacitor. It was shown that the use of such a capacitor can reduce the DC bus capacitor size significantly [32].

The new trend in variable speed drives (VSD) is to integrate the inverter and the motor into a single unit in order to reduce the production cost, the commissioning time, and the physical size of the equipment. In the new generation of integrated motor drives, the lifetime of the converter as well as the improved interaction with the grid (lower THD of the current, more robust to voltage unbalance) will be very important [9]. In the last twenty years, several industry attempted to design a VSD topology (the integrated frequency converter motor) to reduce the production and commissioning costs and also to improve the EMC compatibility of the whole package.

The application area for motor integrated variable speed drives is limited to the low-power range due to the problems that appear in the high-power range such as vibrations and the difficulties of dissipating a higher amount of energy in dusty environments.

In research, efforts have been made to replace the traditional limited-lifetime electrolytic capacitors with film capacitors. Also, new frequency converter topologies are currently being investigated: the voltage source inverter (VSI) with a small dc-link capacitor or the matrix converter (MC), which has the advantage of the bidirectional power flow [32].

Improving the quality of input currents of a three-phase-fed VSD is a requirement that needs cheap and competitive solutions for implementation. Sinusoidal input current is desired, but the cost is still prohibitive. Square-wave input current may be a compromise in order to improve the quality of the input current while keeping its cost low and, therefore, may constitute an intermediary development stage from the uncontrolled diode-rectifier towards fully controlled sinusoidal input current drives. Additionally, the robustness to unbalanced voltage supply may be increased and, optionally, boosting and

regulation capability of the dc-link voltage to fully decouple the functionality of the inversion stage from the rectification stage may be achieved [33].

The drive reliability depends on the operating conditions and on the requirements for the used components. However, because the diode bridge offers the most reliable solution for interaction with the power grid and because voltage sensors are needed on the grid side for the matrix converter or active front end converter, this solution is not able to compete with the classical diode-bridge VSI solution regarding the reliability.

2.5.1 Converter topology of VSD drawing sinusoidal current from grid

The best situation for utility or power distributor is when the VSD is able to provide sinusoidal input currents, and this may be considered as one of the important feature of the VSD, but it is more expensive as compare to square wave input current topologies. Currently, there are no compulsory regulations to force the manufacturers to produce sine wave input current drives. In this category, input side has to be modified. For three-phase ac–ac converters, such as industrial motor drives, the two-level pulse width modulated (PWM) voltage source inverter (VSI) with six-pulse diode front-end rectifier has become the topology of choice, due to its simplicity and relatively low cost. One drawback of the diode front-end topology is the low-order, low-frequency harmonics on the dc link and ac input line, which, consequently, requires a bulky dc-link capacitor and inductor (ac or dc) filters. In order to improve converter performance and achieve higher power density, many topologies for three-phase ac–ac converters or motor drives with active front-end rectifiers have been proposed and studied in past.

2.5.1.1 VSD converter topologies DCM boost converter

In VSD, by using a Discontinuous Conduction-Mode (DCM) boost converter [34] in the dc-link of a diode-bridge VSI, the input currents (low THD) and dc-link voltage level (boost capability) are controlled. The DCM provides continu-

ous utilization of all the three line currents, which provides better waveform than square wave. Due to a higher current ripple higher ratings for the semiconductor devices and for the magnetic are necessary. The converter circuit topology is shown in Figure 13.

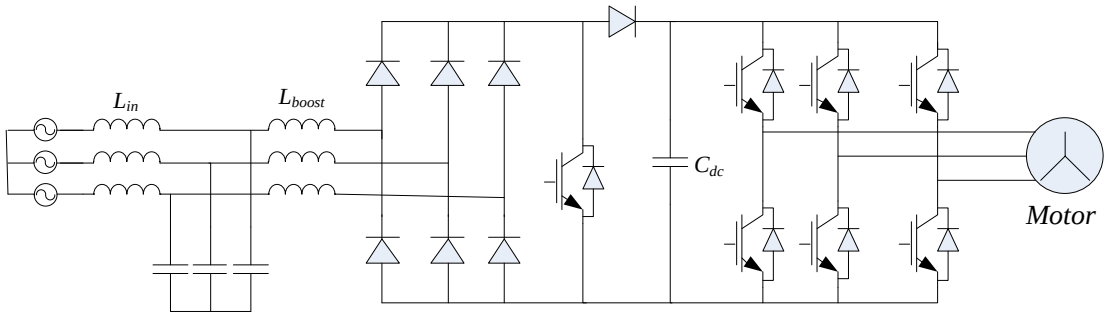

Figure 13. VSD converter topologies DCM boost converter [34].

It has one extra active switch and one power diode as compared to traditional drive. In order to achieve DCM, the inner inductors L_{boost} have a smaller value compared to a continuous conduction mode (CCM) boost converter. Turn-on of the IGBT is soft and soft reverse recovery for the boost diode takes place for this circuit topology. This compensates somehow for the IGBT increased turn-off switching losses caused by switching a much higher current than in a CCM boost converter. In order to provide lower input current THD, the magnitude of the input current vector is controlled instead of the dc-link current. Also, a higher transfer ratio of the boost converter is needed, which reflects in a higher dc-link voltage reference (near 700 V). This type of converter offers unity power factor at the mains.

2.5.1.2 A Vienna rectifier based VSD

A Vienna rectifier [34], which is shown in Figure 14., needs only three IGBTs to control the input currents derived from the three phase grid. The boost inductances are usually smaller, and the semiconductor devices have a lower voltage rating compared to a standard two-level PWM rectifier since they switch only a half of the dc-link voltage.

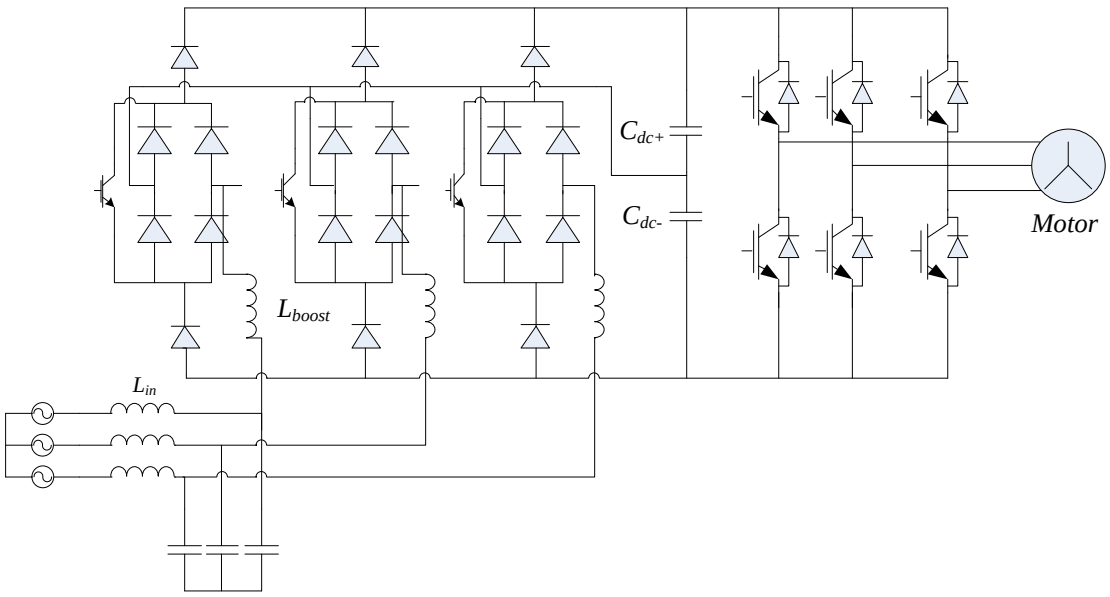

Figure 14. VSD topology with a Vienna rectifier [34].

The conduction losses are high because the current path on each input line consists of two diodes or two diodes and an IGBT. Independent control on each input-phase current is possible by providing the proper switching to its corresponding IGBT on and off.

The input currents of this circuit topology are sinusoidal with a lower THD at rated power. Because of full control of the active front-side stage, it is possible to fully compensate the influence of unbalanced voltage supply in the input-current quality, but this will cause a 100-Hz ripple in the dc-link voltage. However, this imposes a restriction on the size of the two dc-link capacitors that have to maintain the voltage ripple within safe operation limits.

2.5.1.3 A three-level PWM rectifier with bidirectional switches build with reverse blocking (RB) IGBTs

This requires lower consumption of semiconductors as compare to Vienna rectifier: only six fast recovery diodes (FRDs) and six RB-IGBTs with half-voltage ratings. Circuit topology of a three-level PWM rectifier with bidirectional switches build with reverse blocking (RB) IGBTs based VSD is shown in

Figure 15. Functionality and performance of this drive are similar to the previous case, but as the conduction path for the currents consist only of a FRD or a RB-IGBT, therefore it will cause lower conduction losses. Switching losses will not change because the intrinsic diode of the RB-IGBT is not experiencing reverse recovery [35]. The input currents are sinusoidal with a lower THD at rated power. Because of full control of the active front-side stage, it is possible to fully compensate the influence of unbalanced voltage supply in the input-current quality, but this will cause a 100-Hz ripple in the dc-link voltage.

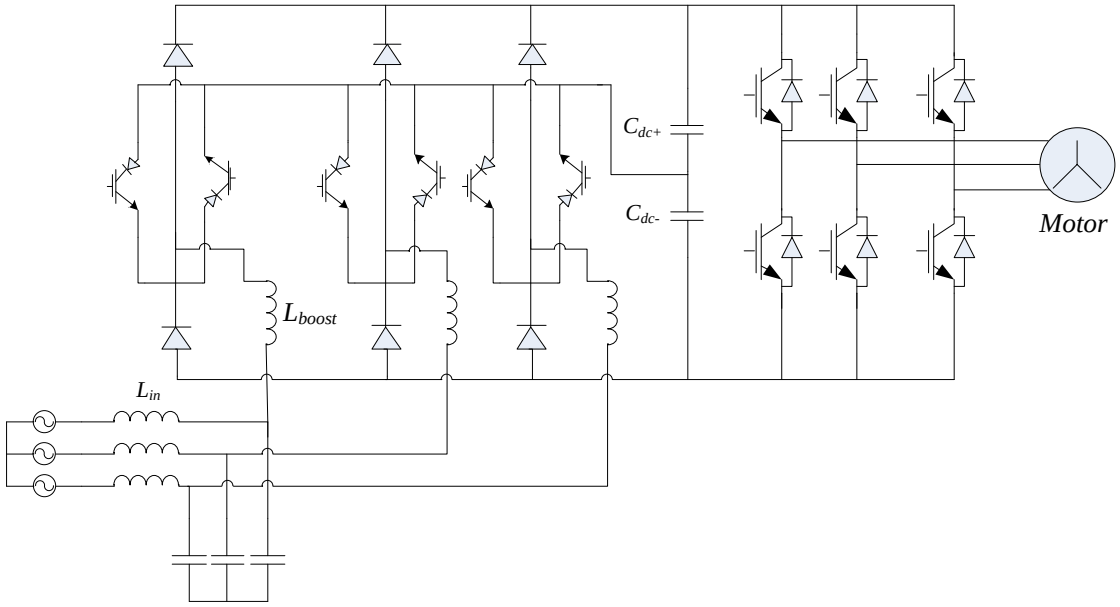

Figure 15. Three-level PWM rectifier with bidirectional switches build with reverse blocking (RB) IGBTs [35].

2.5.1.4 Three-phase Buck Converter Rectification Stage Directly Connected to VSI

This topology [36] is shown in Figure 16., and it consists of a three-phase buck converter as a rectification stage directly connected to and a standard B6-VSI. An LC input filter is necessary to reduce the input current ripple. The rectification stage has to apply at any instant an input line-to-line voltage with the right polarity to the dc-link, which is then inverted by the VSI to produce the desired

output PWM voltages. In order to obtain the proper sharing of the constant output power on the input currents in order to provide sinusoidal waveform, at two line-to-line voltages have to be mixed into the dc-link with the proper duty-cycle during the switching period. Even though the consumption of diodes is smaller compared to the topology of Vienna rectifier, three film capacitors with high pulse current capability are needed in the input filter, compared to two in the previous case.

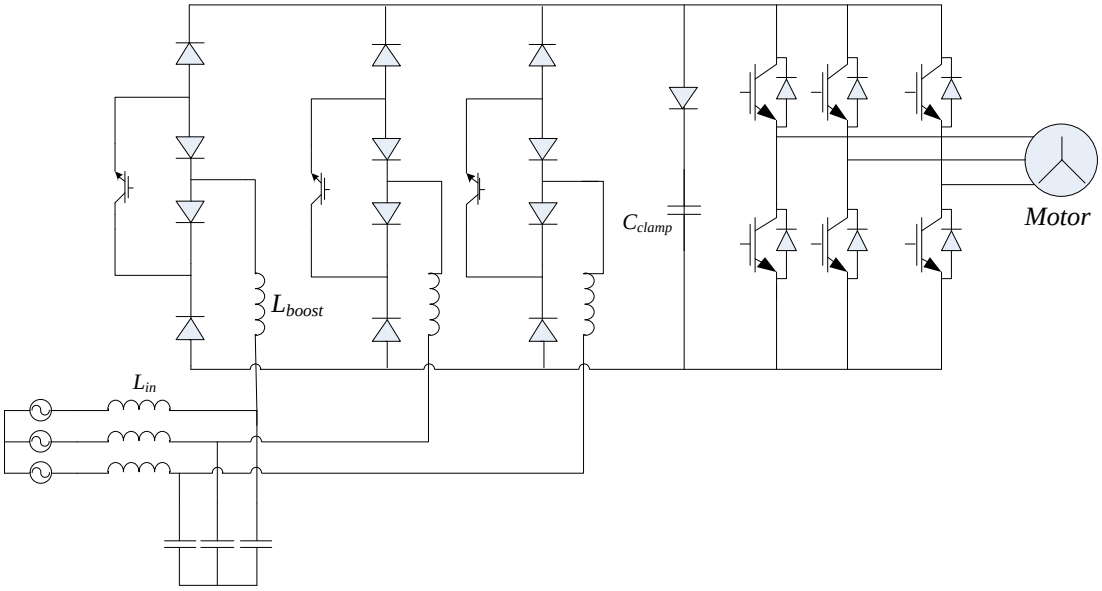

Figure 16. Three-phase buck converter [36].

A clamp circuit consisting of a diode and a capacitor provides a freewheeling path for the inductive load currents in case the converter is turned off. Regenerative operation, as well as operation with highly inductive load which causes negative dc-currents is not possible. The voltage transfer ratio is limited to 0.86 as in any direct power converter that allows for sine-wave-in sine-wave-out operation [48]. The input currents are sinusoidal with a lower THD at rated power. Because of full control of the active front-side stage, it is possible to fully compensate the influence of unbalanced voltage supply in the input-current quality, but this will cause a 100-Hz ripple in the dc-link voltage. Multilevel converters when used as rectifiers have the advantage to provide a low switch-

ing voltage ripple across the boost inductance that allows for smaller size of the input filter and lower voltage ratings of the switching devices. A three level rectifier will therefore halve the size of the boost inductance compared to a two-level rectifier. As it may use switching devices rated at half the voltage compared to a two level rectifier, it may be able to switch faster and losses associated to switching will also be lesser.

2.5.1.5 Three-phase Back to back voltage source converter

This circuit topology is shown in Figure 17., and it consists of a three-phase boost converter as a rectification stage directly connected to and a standard B6-VSI through an intermediate dc link. An LC input filter is necessary to reduce the input current ripple.

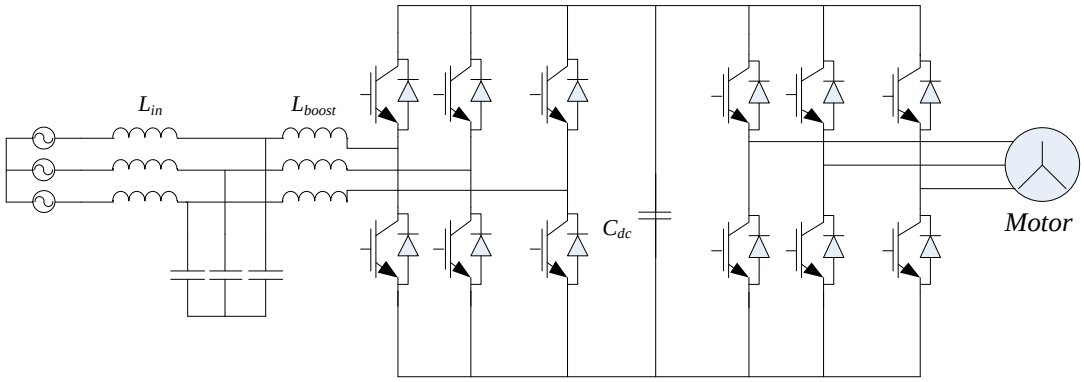

Figure 17. Back to back voltage source converter.

Efficiency of this topology is poor but it can ensure unity power factor at input and bidirectional power flow, which can be used in braking and improving dynamic response of overall drive. Requirement of input filter makes drive bulky which does not fit for motor integrated VSD application. Lower efficiency will result higher losses and therefore heat removal from integrated system will add difficulty in overall system design.

2.5.2 Converter topology of VSD drawing rectangular current from grid

This category of circuit topologies consists of VSD topologies that are based on the front end diode-rectifier followed by VSI topologies but have an auxiliary converter inserted between the diode bridge and the dc-link capacitor in order to provide continuous conduction of the current into the intermediate dc-link capacitor and to obtain a square-wave shape of the input currents. This category offers the input current THD decreases to about 30%, and the ASD becomes more robust to unbalanced voltage supply (up to 10%). Problem of unbalanced input voltage is very common and it is reflected in the intermediate dc link voltage and in low voltage condition it force VSI to operate in over-modulation.
The trend to an increased integration level leads to the demand for very compact inverter solutions. The aim is to design the converter in such a way, that it can be integrated into the motor (integral motor).
Several topologies presented in this thesis are dedicated only for general purpose integrated motor drives, only unidirectional power flow drives will be analyzed seven candidate topologies are shown. During comparison between candidates for VSDs the following assumptions have been taken.

1. Constant current ripple magnitude in the boost inductor:

$$L_{boost} \cdot \frac{f_{SW}}{V_{ripple}} = const. \qquad \textbf{2-2}$$

2. Constant switching losses in the semiconductors:

$$N_{IGBT} \cdot f_{SW} \cdot V_{ripple} \cdot I_{\max\_sw} = const. \qquad \textbf{2-3}$$

Where L_{boost} is the boost inductance value in front end rectifier circuit, f_{sw} is the switching frequency, V_{ripple} is the switching voltage ripple equal also to the forward voltage the switching device should withstand, N_{IGBT} is the number of IGBTs that switches in a switching period and I_{sw} is the average current that is handled by the switches at rated power. In the following, the four candidates will be briefly introduced with highlight on their advantages and drawbacks.

2.5.2.1 Diode rectifier and an electronic dc-link inductor with a small dc-link capacitor connected to VSI

This circuit topology [37] is shown in Figure 18. By using a low-kVA asymmetrical H-bridge inverter in the dc-link between the diode-bridge and the dc-link capacitor it is possible to achieve continuous conduction of the dc-link current with the effect on improving the shape of the input currents.

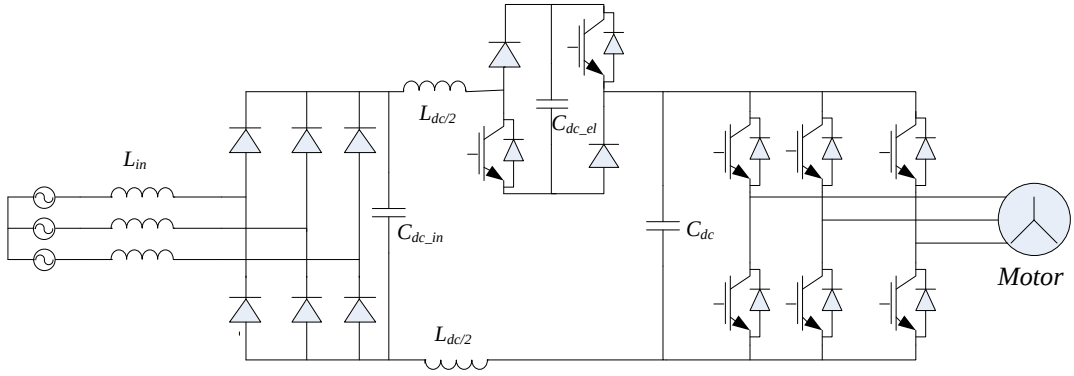

Figure 18. VSD converter topology with electronic inductor in dc-link [37].

The asymmetric H-bridge inverter and the series inductors form a controlled current source which has functionality similar to the dc-link inductor in a standard drive, but since it is controlled, it may achieve high and constant attenuation of the low-frequency ripple in the dc-link current with a bandwidth going up to kilohertz range. As the voltage in the H-bridge dc-link is small (40-60V), fast components as MOSFETs and Schottky diodes that allow operation above 100 kHz with low losses may be used. The higher switching frequency in conjunction with the lower switching voltage across the boost inductance will allow the reduction of the size of the passive components L_{in}, $C_{dc\text{-}in}$ and L_{dc} which have to limit only the switching ripple. Grid voltage unbalance may be successfully compensated. 31% at rated power and remain almost unchanged under 5% unbalance [33], proving that this topology is more robust.

In this circuit topology, a disadvantage is that the average dc-link voltage decreases to 490 V, which means that the voltage transfer ratio is around 0.9. As in

an integrated motor drive the converter and the motor are designed as a single unit, winding the motor for a smaller rated voltage may overcome this drawback. This problem can be addressed by better control of DC link voltage and also with some modification in topology.

2.5.2.2 Diode rectifier and a CCM boost converter with a small dc-link capacitor connected to VSI

The circuit topology of diode rectifier and a CCM boost converter [38] is shown in Figure 19. This circuit topology consists of a Continuous Conduction-Mode (CCM) operating boost converter connected between at the output of the three phase diode-bridge rectifier and the dc-link capacitor. This controls the dc-current (rectangular input current shape) and the dc-link voltage (boost up capability).

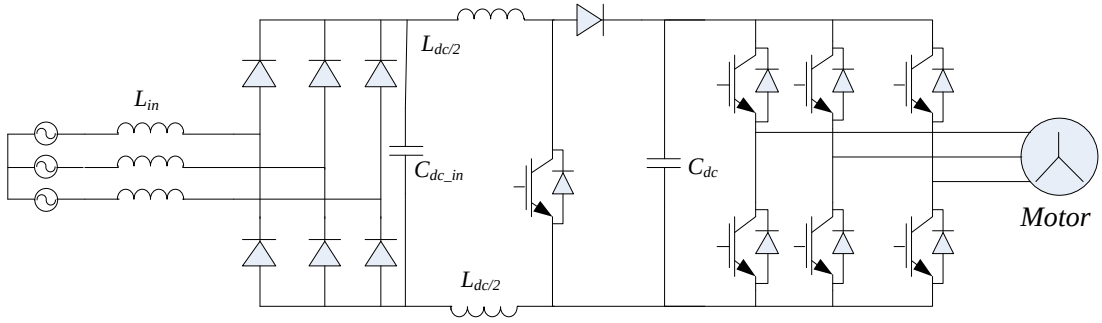

Figure 19. VSD converter topology with CCM boost converter [38].

This is already industrially implemented as a PFC stage providing sinusoidal input current and regulation of the dc-link voltage, but a large dc-link capacitor is needed for this purpose.

Only one active device is needed, but the voltage stress of this active device is equal to the full dc-link voltage and the current stress is equal to the peak value of the dc-link current, which means it has to switch the rated power of the VSD. As the voltage ripple across the inner filter inductors is equal to the dc-link voltage and the switching frequency is smaller previously, a larger boost in-

ductance is needed that will experience higher core losses. Two control loops, a slow one for the dc-link voltage and another one faster for the dc-link current, are needed. Measurements of the dc-link voltage and of the current through the boost inductor are needed. The input current THD will be around 34 % at the rated power.

2.5.2.3 Diode-Rectifier and two interleaved CCM Boost Converters with a Small dc-link Capacitor Connected to VSI

This circuit topology [39] is shown in Figure 20., and it is another solution to decrease the size of the magnetic by using two interleaved the boost converters. Each inductor will carry only half of the total dc-link current while its switching voltage is the full dc-link voltage. Even though the current ripple through the boost inductors is higher, it partially cancels when they sum while the equivalent frequency of the switching ripple doubles. This decreases the size of the input filter compared to the previous topology. The input current THD will be around 35 % at the rated power.

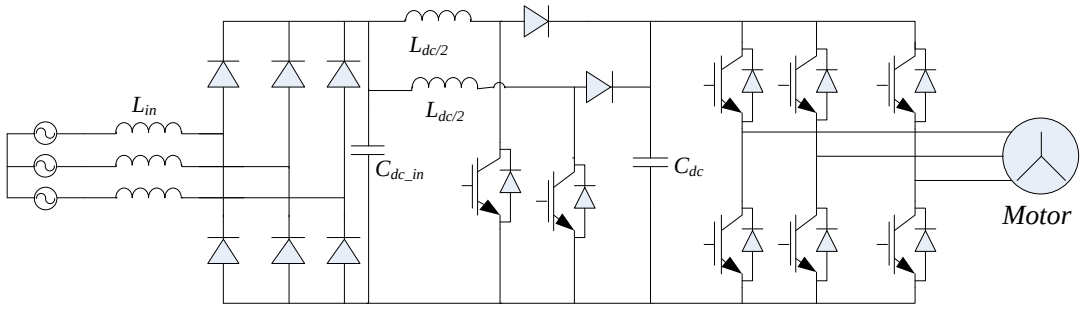

Figure 20. ASD converter topology of interleaved CCM parallel boost converter [38].

2.5.2.4 A three-level CCM boost converter

This circuit topology [38] is shown in Figure 21. The lower switching stress due to the three-level approach allows the increase of the switching frequency by a

factor of two, which in conjunction with halving the voltage ripple across is an important size reduction factor for the boost inductor.

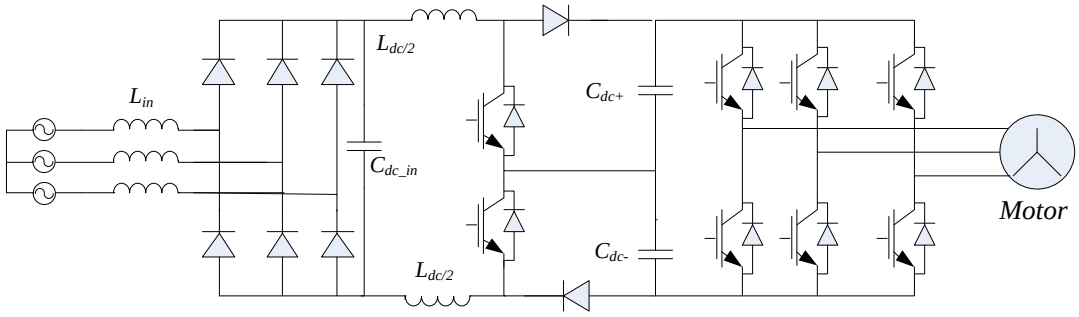

Figure 21. VSD converter topologies three-level CCM boost converter [38].

A split dc-link capacitor and two CCM boost converters mounted between each dc-link terminal and its middle point. Even though there are two transistors in the boost stage, the installed power is similar to the previous case. Only one transistor is working at a time depending on the potential of the split capacitor middle point. Conduction losses are higher, since an extra diode appears in the conduction path compared to the previous case. Since the semiconductors are chosen to withstand only a half of the dc-link voltage, faster devices may be used.

An extra voltage sensor is needed, and an extra dc-link capacitor, even the though energy is similar. Additionally, the voltage unbalance of the two dc-link capacitors has to be controlled. The grid side behavior is typically same for all the CCM boost topologies, under normal and 5% unbalanced voltage supply [33]. The input current quality is preserved, while the unbalanced supply reflects in the 100-Hz ripple of the dc-link voltage, which is not critical, as its level can be boosted up.

2.5.3 Slim DC-link drive for VSD

Small dc-link capacitances have been applied in ac drives equipped with active rectifiers, where both the rectifier and the inverter can be used to control the

power balance of the dc link. These capacitors are MKP type film capacitor having low ESR and increased operating lifetime.

Commercial drives equipped with a diode rectifier and a small dc-link capacitance, are available, a small capacitance is advertised by manufacturer to reduce the mains harmonics, while the dynamic performance of the drive has not been used as an argument. In research publications, the concept of a diode rectifier and a small dc-link capacitance has not received a lot of attention, with the exception of very few recent studies: pulse-width modulation (PWM) was studied in [40], and control issues relating to 2.2-kW and 37-kW drives were studied in [44].

Three phase AC-drives for HVAC applications (Heating, Ventilation & Air-Conditioning) are designed to meet moderate demands on shaft-torque dynamics and high demands on acoustic noise, efficiency and harmonic distortion at the line-side. Also, compatibility with long motor cables is a typical requirement. Traditional AC drives employing diode rectifiers, chokes and electrolytic capacitors have been used for decades. Recently, commercial HVAC drives have emerged, where all traditional DC-link components are replaced with a "small" film capacitor. These are referred to as slim DC-link AC-drives by several authors in literature. The aim of these studies [39-47] was to analyse consequences, if going for a slim DC-link AC-drive over traditional types.

Typical fields of usage of slim dc-link based drive can be found in applications such as closed-loop speed control of fans for ventilation and extraction, as well as in circulation pumps for heating and cooling systems and pumps for boosting the pressure and control levels [48].

The slim dc-link drive employs an integrated RFI-filter at the line-side, a diode bridge for converting three line voltages (50Hz or 60 Hz) to a pulsating DC-link voltage and a film capacitor bank (C_{dc}) to attenuate the 300Hz pulsations in order for the inverter to give ideal PWM output voltages. C_{dc} is large enough to provide enough storage energy for the internal switched-mode power supply

(SMPS), ensuring a proper shutdown of the control circuitry in case of a mains failure. The power circuit of the slim DC-link AC-drive is shown in Figure 22.

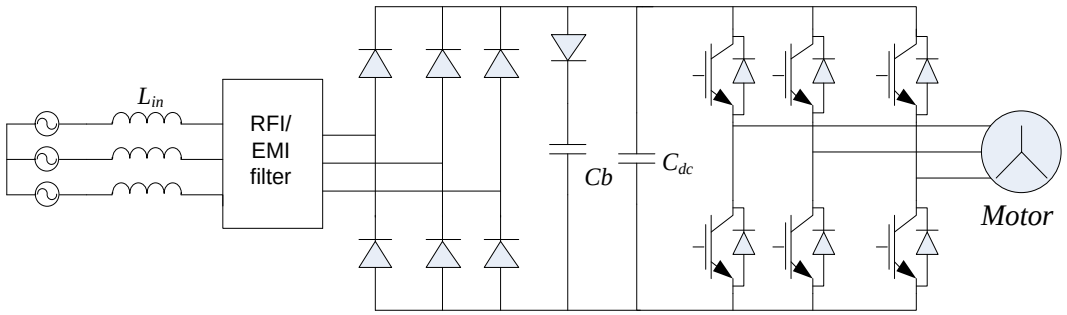

Figure 22. Circuit topology of slim dc-link drive.

This drive offers a compact and low-cost approach towards low line-side harmonics. This drive is similar to the traditional types, except for the intermediate DC-link. A MKP type film-capacitor bank can be used, which in rough figures exhibits the same physical size as the capacitor bank in traditional drive, while giving a much smaller C_{dc} value and a much better life time. MKP capacitors intended for slim dc-link drives are available on the market. The small C_{dc} enables the drive to obtain a rated THD_i around 30-35% at the line-side [40].

The drive also includes a secondary electrolytic DC-link capacitor bank C_b to ensure a sufficient hold-up time of the SMPS during a mains failure. Also, the SMPS-supply branch may improve the robustness against line transients as defined by EN61000-4-4/5 and provide sufficient damping support for the main capacitor bank, which is an issue on soft lines.

Benefits of a slim DC-link AC-drive relative to traditional AC-drives are a low-cost and compact design giving a low THD in phase currents at the line-side along with a good life time of the DC-link storage element. Else, the topology suffers from a reduced performance level in general. The drive is claimed to exhibit friendliness towards the grid in terms of reduced low-frequency current harmonics, but IEC1000-3-12(2) compliance requires installation of external AC-inductors. This emulates a soft line, giving potential stability problems of the

drive. If the technology penetrates the market substantially, one may predict increasing grid problems in the switching-frequency range. Especially, large slim DC-link AC-drives may impact significantly on small high-capacitance electronic equipment, if installed at the same PCC via a low impedance link.

In terms of smooth operation of the motor load, the slim DC-link AC drive exhibits a substantially larger 300Hz torque ripple, which is less desirable for some applications. Also, spurious tripping due to under/over voltages will be more frequent compared to traditional drives, regardless of what modern control algorithms can achieve. Instability of the dc link may occur in conventional drives (having a low dc-link natural frequency), if the inductance of a choke is large relative to the dc-link capacitance. The dc link can be stabilized by manipulating the reference of the torque-producing current component [45].

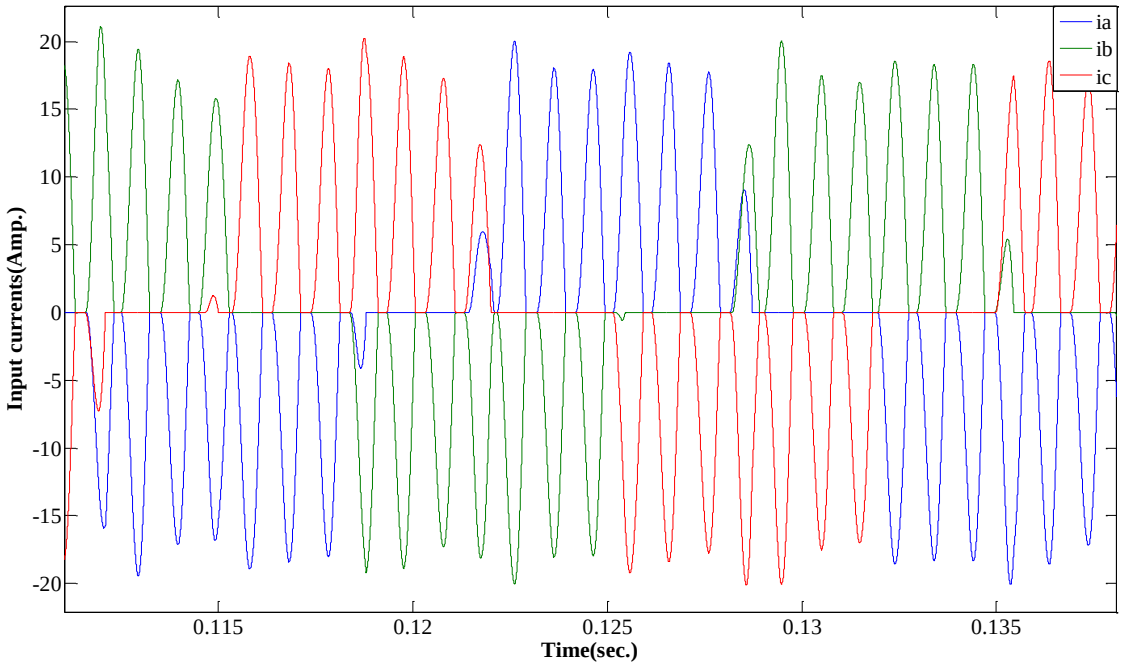

Figure 23. Input currents in steady state at nominal load for slim dc-link drives in simulation.

If a small dc-link capacitance without an additional choke is used, the dc-link natural frequency becomes high and dependent on the mains inductance. Especially in large-power drives, the mains inductance relative to the dc-link

capacitance may be large enough to cause instability in the dc link, while the dc-link natural frequency is above the bandwidth of the current-control loop. Mains current in simulation are shown in Figure 23. Hence, conventional stabilization methods relying on the current controller cannot be used. It becomes neccesary to stablize dc-link through active control of PWM inverter.

2.5.4 Modifications in VSI design for electric motor

Some modifications in inverter design can help to reduce the losses associated with inverter and will have big impact in the integration process of power converter and the electrical machine. Two possible changes in inverter design are discussed in this section.

2.5.4.1 SiC or Hybrid IGBTs (Si+SiC) based inverter

Silicon Carbide (SiC) has significant advantages over Silicon (Si) in power applications requiring low losses, high frequency switching, and/or high temperature environment conditions because of their lower switching losses. Powerex/Mitsubishi offers a full line of Silicon Carbide (SiC) modules to serve a wide range of applications. SiC hybrid modules (Si IGBT + SiC Schottky diode) and full SiC modules (SiC MOSFET + SiC Schottky diode) are available in market for high efficiency designs or to achieve significant loss reduction in existing designs [49].

A 45% decrease in inverter losses result from this modified design by using SiC hybrid module, whereas if Full SiC module will be used, it can result around 70% loss reduction as shown in Figure 24. All components and interconnects are isolated from the heat sinking baseplate, offering simplified system assembly and thermal management. SiC diodes have no effect on IGBT E_{off} but reduce IGBT E_{on} And E_{rr}.

A lower R_g reduced IGBT E_{on} by up to 85% but will excited a turn-on oscillation problem due to possible faster dv/dt and lower energy damping loss at turn-on attributed to V_{CE}-I_C power loss.

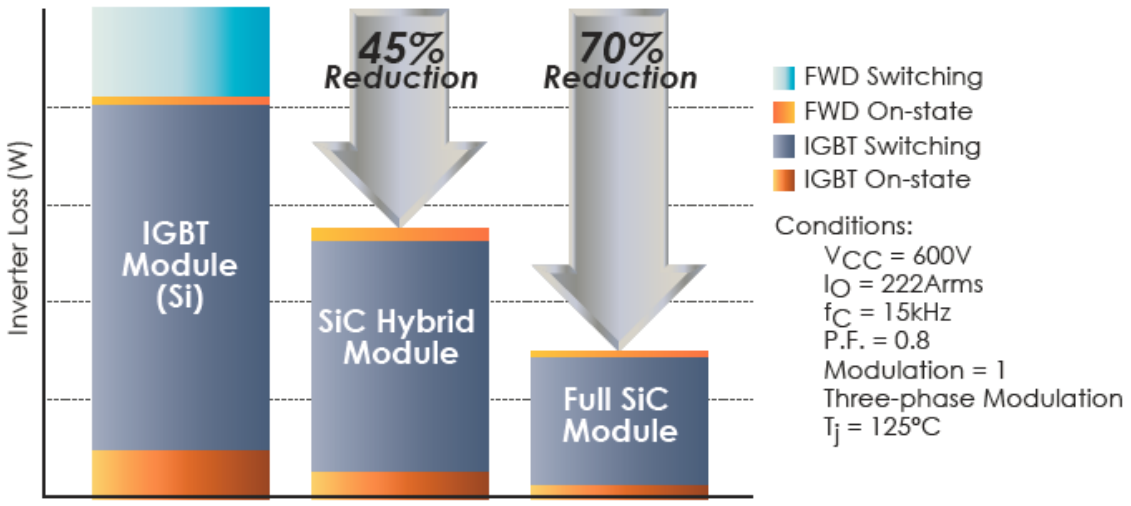

Figure 24. Comparison of inverter losses in Si module with SiC hybrid and Full SiC module [50].

2.5.4.2 Multi-level Inverter for VSD

Three or higher level inverters have been used in drive applications. These inverters offer many advantage over traditional two-level VSI, such as less common mode voltage and lower bearing currents. These converters require higher no. of power semiconductor and gate drive circuitries and therefore may not be suitable for low voltage VSDs. For medium voltage drive applications, such converters are suitable as one has to connect several devices to achieve that much voltage capability.

2.5.5 Challenges in power converter topology suitable for integration

Power converter design for integrated drives poses a host of significant challenges that originate both from the limitations on available space and the need to adapt the power converter to the thermal, vibration, and electromagnetic field stresses inside the motor housing. Continued advances in power electronics component and packaging technologies, including the development of high-temperature power semiconductor materials such as silicon carbide and gallium nitride, will help make it possible for the power converter to meet these environmental demands. There are many options for the front-end converter that

offer advantages for the integrated drives, but they each come with the price of added converter complexity, size, and cost [13]. For example, an active front-end power converter stage offers the opportunity to absorb the current ripple from the inverter stage by coordinating the dc link input current with the output current.

Research in past has shown that this approach can be used to minimize the required dc bus capacitance value. Control schemes can also be introduced to cope with the reduced dc bus capacitance, although they generally limit the fractional percentage of the dc bus voltage that can be used to excite the motor. There are also significant issues surrounding machine-drive dynamics with reduced dc link capacitance. Design of the control strategies for the front-end and motor must be carefully performed to avoid potential instabilities or destructive dc link voltage transients. These issues suggest that the entire motor drive must be designed as an integrated system to insure that reductions in the dc link capacitor volume are not offset by increased passive component requirements elsewhere in the converter.

Many of today's existing integrated motor products are restrained in a mechanical repackaging, where the power inverter is physically mounted onto or inside the motor housing frame. The concerns arise primarily from new power converter design constraints, including elevated ambient temperature inside the motor housing, more confined space volume, and geometric dimensions.

2.6 Advantages with integration of power converter into electrical machine

There are several advantages of motor integrated of variable speed drives, some of them are mentioned as follows:

1. Lower installed system cost (wiring, installation, and control panel space savings);

2. Short motor leads eliminate standing wave dv/dt failures and reflected voltage spikes;
3. Possibility of built-in prevention of voltage peaks at the motor terminals;
4. Optimum motor-inverter match;
5. No design problems with motor-inverter rating, filters or power cable length;
6. Guaranteed electromagnetic compatibility by the manufacturer;
7. Compact design and more efficient operation.

2.7 Reliability issues of VSD fed motors

The Three-Phase Induction Motors fed by VSDs based on Voltage Source Inverters with Pulse Width Modulation (VSI-PWM) may have to support three main additional stress factors that are described next, namely, internal temperature increase, partial discharges and breakdown of the stator windings insulation system and bearing currents

2.7.1 Internal temperature increase of the electric machine

The internal temperature increase of the electric machine is mainly due to the harmonics increase which leads to an increase of iron and copper losses and, therefore, the overall losses will increase typically between 15% and 35% with load factors higher than 60%. Based on the Arrhenius law, a 10ºC increase in the operating temperate will lead to a 50% and 35% decrease for the insulations and lubricants lifetime, respectively [2]. It is very important to properly size the motor for loads requiring speeds lower than nominal. For low speeds (below 70% of the nominal speed) an external cooling arrangement may be required to avoid motor overheating.

2.7.2 Partial discharges and breakdown of the insulation system

If the voltage transient exceeds the insulation dielectric strength, short-circuit can occur with/without the partial discharge effect. Because of the temperature increase, partial discharge and voltage stress, the insulation system of older motors (in particular) with long cable runs may have a significant shortened lifetime when fed by VSI-PWM VSDs.

2.7.3 Bearing currents

Because of the induction motor parasitic capacitances between the windings and frame, windings and rotor, rotor and frame, and inside the bearings, high frequency currents can circulate in the bearings of motors fed by VSI-PWM VSDs. The currents have two main different modes, but the same primary cause which is the common mode voltages generated in the VSD output due to the unbalance of the three output PWM voltage waveforms. The first current mode is a consequence of the generated voltage between the shaft and the ground due to the referred parasitic capacitances. The presence of a shaft-ground high frequency voltage leads to the circulation of capacitive and resistive high frequency currents through both bearings. The second high frequency current mode is a consequence of the voltage between the shaft ends, induced by the circulation of a high frequency common mode current in the windings and between them and the frame. These bearing currents can significantly decrease the lubricant and bearing lifetime.

2.7.4 Harmonics and electromagnetic interference

Current harmonics in the VSD input stage can also feed back into the power bus grid, and can disrupt other types of equipment in the premises. Harmonics can also cause supplementary losses and temperature-rise of all the elements in the supply system (rotating machines, transformers, cables, capacitors banks). In the case of three-phase diode rectifiers being used in the input stage, the negative sequence harmonics (5th and 11th) are particularly worrying in terms of increase

of the losses. Harmonics can also produce electromagnetic interference (EMI) both as high frequency airborne radiated interference mostly in the inverter to motor cable, as well as the conducted noise in the supply cables.

2.7.5 Mitigation strategies

Manufacturers should specify the maximum transient voltage and dV/dt, which the motor windings can withstand. To mitigate the described undesirable problems, common mode and high frequency filters and special shielded cables (acting as a distributed filter), can be used between the VSD and the motor, keeping the link between as short as possible. Common mode voltage cancellation electronic devices connected between the VSD and the motor can be also a good solution. Also, proper grounding and shielding should be made. Several alterations can be made in the motor to increase its reliability. For example, use of magnetic wire with reinforced insulation, use of impregnation techniques that minimize the air cavities in the insulation system, use of insulated bearings in both sides (e.g. with external insulation coating or ceramic balls), connection of the shaft to the ground using a contact brush and install an electrostatic shield in the stator slot openings connected to the ground.

2.8 Total harmonic distortions

Harmonics are voltage and current frequencies in an electrical system those are multiples of the fundamental frequency (50 or 60 Hz). The harmonics are associated with non-linear loads such as magnetic ballasts, saturated transformers and power electronics [51-62]. The most common sources of power electronics harmonic distortion are found in computers, office equipment, electronic equipment using switch-mode power supplies, VSDs, arc furnaces and high-efficiency electronic light ballasts. Harmonics often come, too, from poor-quality line power - an increasingly important issue for many utilities. Harmonics can

affect the equipment performance and are both caused by and can interfere with the function of VSDs.

Harmonics increase equipment losses and have also raised concerns about excessive currents and heating in transformers and neutral conductors. Harmonic waveforms are characterised by their amplitude and harmonic number. All power electronic converters used in different types of electronic systems can increase harmonic disturbances by injecting harmonic currents directly into the grid. When harmonic currents flow through the impedances of the power system they cause corresponding voltage drops and introduce harmonics onto the voltage waveform. This causes the system voltage waveform to become distorted and since this voltage is distributed to other users on the power system it causes harmonic currents to flow through otherwise linear loads.

A non-sinusoidal periodic function *f(t)* in an interval of time T could be represented by the sum of a fundamental and a series of higher orders of harmonic components at frequencies which are integral multiples of the fundamental component. The series establishes a relationship between the function in time and frequency domains. This expression is called Fourier series representation. A distorted waveform can be analyzed using Fourier series representation given as the following equation:

$$f(t) = F_0 + \sum_{h=1}^{\infty} f_h(t) = \frac{1}{2}a_0 + \sum_{h=1}^{\infty}\{a_h \cos(hwt) + b_h \sin(hwt)\} \qquad \textbf{2-4}$$

The harmonic current on the three phases power distribution system is defined as frequency components which is an integer multiple of the fundamental frequency. A pure sine wave does not contain harmonic. When a wave becomes distorted, it means harmonics current are present in this distorted waveform. The harmonics current generated by three phase converter in three phases three wires power distribution system are 5-th, 7-th, 11-th, 13-th, 19-th and so on.

2.9 Filter for improving current quality drawn from mains

The harmonics of a voltage source AC drive can be significantly reduced by connecting a large enough inductor in its AC input or DC bus. The trend has been to reduce size of converter while the inductor size has been also reduced, or in several cases it has been omitted totally. Filters can be classified broadly in three different category namely passive, active and hybrid filter. These different filter arrangements are discussed in following section.

2.9.1 Passive filter

The passive filter consists of two components: a coupled inductor and a capacitor. These are energy storage element and provide smoothing to voltage and current. Together, they form a ripple cancellation circuit. The structure of the passive filter is shown in Figure 25. To understand this filter topology, a coupled inductor and a method commonly referred to as the "zero ripple," "ripple cancellation," or "ripple steering" are addressed.

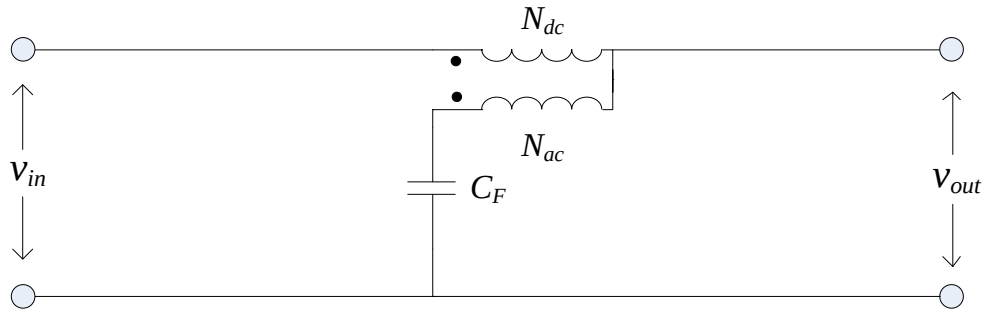

Figure 25. Illustration of a coupled inductor based passive filter.

This method, known and used in different applications for many years, employs a coupled inductor as the main filtering component. The general structure of a coupled inductor is shown in Figure 25.

The use of inductors in frequency converters is a known practice often used to smooth the high inrush currents and reduce the harmonics. Manufacturers may include dc-link coils in frequency converters to reduce harmonic currents or for

smoothing the dc current but this can be done only during the frequency converter's manufacture. Once the frequency converter is installed in the field it is impossible to add or remove the dc-link coil. The simplest, fastest and non-invasive solution is to install ac-coils in front of the drive. The biggest advantage of the ac-coil is the simplicity. As the ac-coil is a passive harmonic solution, there is no need of special setup when commissioning, and the downtime at installation is relatively short.

For the first 25 harmonic components the theoretical THD minimum is 29%. That value is practically reached when the inductance is 100 *mH* divided by the motor kW or 10 *mH* for a 10 kW motor (415 V, 50 Hz). Practically sensible is about 25 *mH* divided by motor kW, which gives a THD of about 45%. This is 2.5 *mH* for a 10 kW motor. The voltage distortion with certain current distortion depends on the Short Circuit Ratio (*Rsc*) of the supply, which is defined by ratio of maximum short circuit current (I_{SC}) and the maximum demand load current (I_L) at the point of common coupling (*PCC*). The higher the ratio, the lower will be the distortion in voltage at PCC.

Sometime Passive filters are connected to the parallel to drives at PCC. These filters are tuned to particular frequency and termed as selective harmonic filter. They supply harmonic current for particular harmonic. 5^{th} and 7^{th} order harmonic filter are very common to use in 6 pulse diode rectifier based drive in order to meet the standard of EN 61000-3-12.

Passive filters consisting of a *LC* bank of tuned filters and/or a high-pass filter have been broadly used to suppress harmonics because of low initial costs and high efficiency. However, passive filters have the following drawbacks:

1) Filtering characteristics are strongly affected by the source impedance.
2) Amplification of currents on the source side at specific frequencies can appear due to the parallel resonance between the source and the passive filter.

3) Excessive harmonic currents flow into the passive filter due to the voltage distortion caused by the possible series resonance with the source.

2.9.2 Active filter

The task of the active filter is to improve attenuation in the low-frequency range, where the attenuation provided by the passive filter is insufficient. To allow suitable voltage control, the active filter should be capable to receive or release a sufficient amount of energy to preserve the capacitor voltage constant irrespective of low-frequency load current fluctuations. The filter energy storage components can thus be considered as one of the most affecting parts of the active filter. Different topologies can be used to achieve the desired energy storage capability.

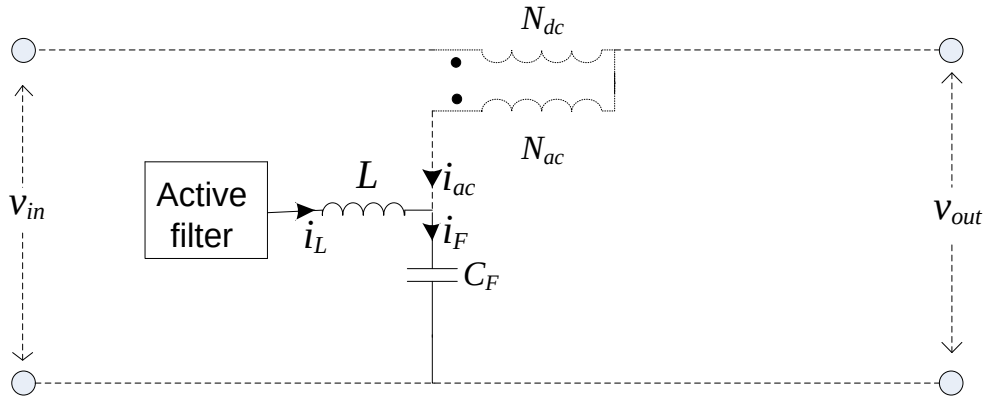

Figure 26. Illustration of an active filter.

A filter with its own energy storage enables its independence, although additional components are needed in such case, commonly resulting in weight and/or cost increase of the application. Usually, an inductor, capacitor, or additional source (battery) is selected as an energy storage element. If only passive components are used, connection to the main power grid is required. Such connection is symbolized with a dotted line.

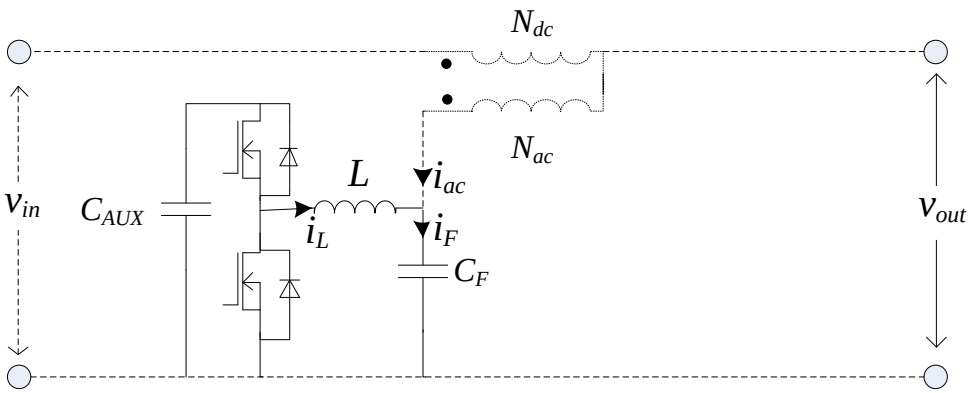

Figure 27. Active filter connected in dc link.

In a steady state situation, the active filter has to provide a current which is opposite to the current flowing through coupled inductor i_{ac}, and therefore;

$$i_F = i_{ac} + i_L = 0 \qquad \textbf{2-5}$$

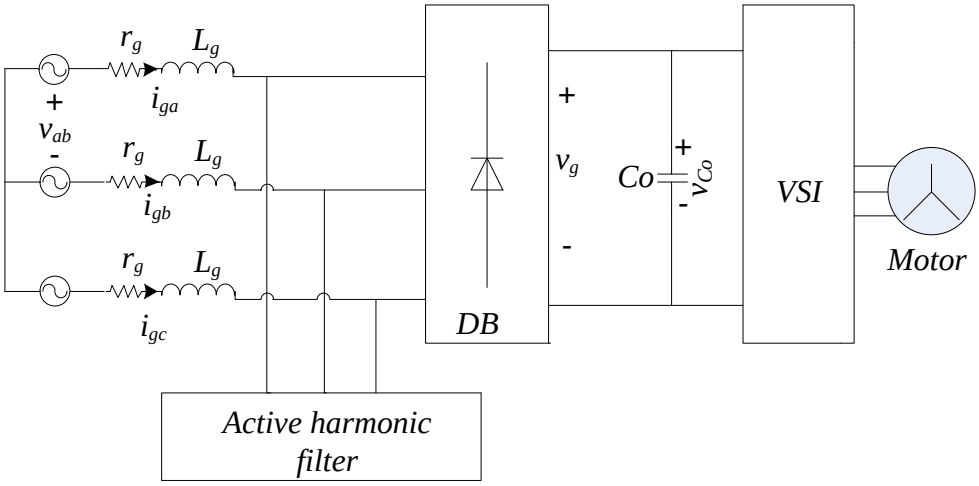

Figure 28. Three phase electric drive with active harmonic filter rectifier.

With such a measure, the excessive change in the capacitor voltage is compensated. Active filter can be installed at the point of common coupling, where drive is connected to grid. In this case such active filter will provide only the harmonics currents other than fundamental. Sometime these filters are referred as active harmonic filter in literature and circuit topology grid side connected *AHF* is shown in Figure 28. Grid sees a resistive kind of load connected to it and

gives power at unity power factor. Such active filter requires power electronic devices and energy storage passive components and control strategy and circuitry to provide harmonic currents to drive.

2.9.3 Hybrid filter

Hybrid filter are those topology where behaviour of large passive component is achieved by combination of small passive components and electronic devices. With control of these electronic devices, current coming out from the grid is controlled and only limited magnitude of harmonic current is allowed to go through it. Such topology can limit low order harmonic to certain level. To meet the standard of EN 61000-3-12, one may need some filter at the input of drive, but filter size is reduced now as compare to passive solution. This type of hybrid circuit topology is termed as electronic smoothing inductor and studied quite a few times by different researchers in past.

2.10 Summery and conclusion

Nowadays, VSDs are considered as one of the most important tools for *Motor Management* and *Energy Saving*. Most motor efficiency upgrades can be achieved fairly easily by selecting the most efficient available motor for the application available in the market at hand. Diode rectifier followed by VSI is well accepted by the industry, and it has low losses and high reliability, but it requires big and bulky passive elements to ensure current THD within specified limit of present standards. Improving the quality of input currents of a three-phase-fed VSD is a requirement that needs cheap and competitive solutions for implementation.

The trend to an increased integration level of the power electronics and the motor leads first of all to the demand of very compact converter solutions simply because the available space is quite limited. A problem in this respect is the size power converter which is large due to requirement of big passive components in a power converter utilized in motor integrated drive.

In Future we may see constraints to have sinusoidal current at the utility end with unity power factor, and then active front end topologies and direct power conversion scheme will come into real existence, but as of now traditional drive with uncontrolled rectifier is in big demand.

Many applications do not require bidirectional power flow or four quadrant operation of VSD. In such cases, Vienna rectifier or three-level PWM rectifier with no dc link capacitor (Sparse Matrix converter) can be useful topology. Many times VSD does not operate at full load condition, in such cases these topologies provides efficient performances of power processing unit.

In motor integrated VSD, care need to be taken in selection of power converter and machine both and one need to optimize both for specific application. Integration of passive elements is possible in stator core of machine and value of passive components can be optimized. Diode bridge based front end converter is elected for the motor integrated VSDs for having lower losses, performance of this front end converter is analyzed in next chapter and much needed modifications to improve the grid side performance has also been studied.

Chapter 3. Three phase diode bridge rectifier: Operation and performance evaluation

3.1 Background

Three-phase standard rectifiers are widely used as front end converter in most of the industrial drives for variable speed applications as discussed in previous chapter. These drives equipped with standard rectifier suffer with low quality of input currents in terms of harmonic contents and poor power factor at the grid. High reliability and a low EMI/EMC solution as well as cost saving are the main advantages of these drives. High efficiency, small volume and low cost are nowadays basically the first three aspects mentioned when it comes to the development of any kind of power converter topology for power electronic application. Concerning the use of a power converter in a motor with integrated electronics, the first two mentioned aspects receive an even greater importance.

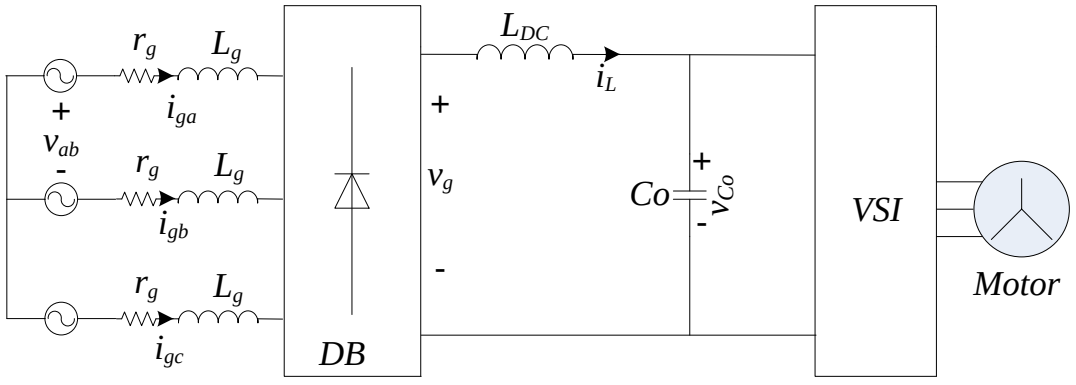

Figure 29. Three phase electric drive with standard passive rectifier.

A typical three phase electric drive is shown in Figure 29. It contains standard diode-bridge six-pulse rectifier (DB), an intermediate DC-link filter and a volt-

age source inverter (VSI). Main purpose of having intermediate DC-link capacitor is to support high frequency current ripple originating from the switching of VSI and also to have reasonable stable voltage in front of the VSI. DC-link filter comprises one inductor and one electrolytic capacitor. Weight and volume of such filter is roughly 10% of total drive [10].

These electric drives have very poor performance on the mains side. With change in load their current qualities drawn from the grid become worse. Power factor and total harmonic distortions on the mains side is a major concerns for these electric drives.

3.2 Operation of a three phase standard diode rectifier

Three phase diode bridge rectifier is most commonly used front end topology of many industrial drives. There are different type of loads are connected at the intermediate dc-link of these industrial drives either directly or indirectly through a voltage source inverter. Some of the common types of loads are discussed in this chapter later on.

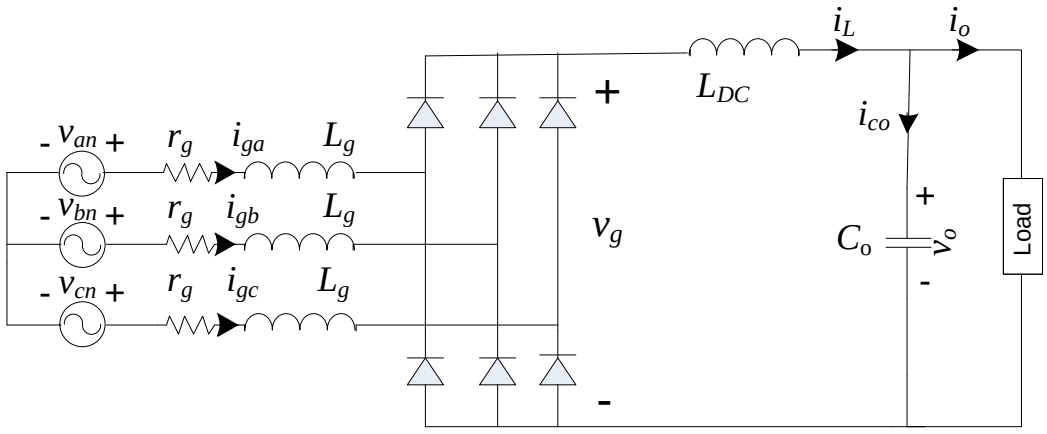

Figure 30. A mains connected three phase diode bridge rectifier.

Circuit schematic of a mains connected three phase diode bridge rectifier is shown in Figure 30. This figure shows a three-phase model of the mains, the diode rectifier, and the dc link. The mains resistance and inductance are denoted

by r_g and L_g, respectively, and the dc-link inductance and capacitance are L_{DC} and C_o, respectively. The phase-to-neutral mains voltages are v_{an}, v_{bn}, and v_{cn}, having the angular frequency w. The current at the output of the rectifier is i_L, while the current and voltage at the output are i_o and v_o, respectively.

The circuit model of three-phase rectifier is approximated by an extremely simplified model of an equivalent circuit as shown in Figure 31. In order to prepare this simplified linear model, two legs diode bridge is considered as out of three phases only two phases conducts at a given time if commutation is neglected, and output voltage of the diode bridge rectifier is represented by a voltage source which is combination of a dc and an ac voltage. Grid inductance is transferred to DC side. Total impedance of the conduction path is represented by equivalent impedance Z_{eq}. Load connected to the intermediate dc bus is represented by a current source. Simplification and parameter details are discussed in modelling section of Chapter 5 in detail.

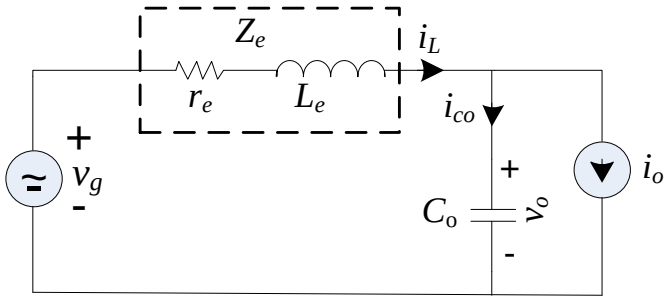

Figure 31. Equivalent circuit of three phase diode bridge rectifier.

The source voltage v_g is constructed from a function which gives maximum of absolute value of three phase line to line voltages i.e. six-pulse voltage of the diode bridge and having frequency of six times of the mains frequency. The ideal rectified voltage v_g is given by the following expression:

$$v_g = \max(v_{an}, v_{bn}, v_{cn}) - \min(v_{an}, v_{bn}, v_{cn}) \qquad \textbf{3-1}$$

In the equivalent circuit of the three phase diode bridge rectifier as shown in Figure 31., r_e and L_e are equivalent resistance and inductance of the current

conduction path respectively. The differential equation of the simplified linear model can be written as:

$$L_e \frac{di_L}{dt} = v_g - i_L r_e - v_o$$
$$C_o \frac{dv_o}{dt} = i_L - i_o \qquad \textbf{3-2}$$

Assuming the output power is P_o and then expression of output current i_o in terms of output voltage and power can be written as:

$$i_o = \frac{P_o}{v_o} = \frac{P_o}{\bar{v}_o + \tilde{v}_o} \approx \frac{P_o}{\bar{v}_o}\left(1 - \frac{\tilde{v}_o}{\bar{v}_o}\right) \qquad \textbf{3-3}$$

In above expression $\tilde{v}_o$ is the deviation of dc link voltage from its mean value $\bar{v}_o$. For a small $\tilde{v}_o$ approximation in the form of a first-order MacLaurin series expansion will hold [44].

Substituting expression of output current i_o in eq. (3-2), the following characteristic polynomial in the Laplace variable (s) can be obtained:

$$s^2 + \left(\frac{r_e}{L_e} - \frac{P_o}{C_o \bar{v}_o^2}\right)s + \frac{1}{L_e C_o}\left(1 - \frac{r_e P_o}{\bar{v}_o^2}\right) \qquad \textbf{3-4}$$

For stable operation of this circuit all the coefficient of the above expression should be positive and therefore two necessary conditions derived from the above expression are as follow:

$$P_o \le \frac{r_e C_o \bar{v}_o^2}{L_e} \qquad \textbf{3-5}$$

$$P_o \le \frac{\bar{v}_o^2}{r_e} \qquad \textbf{3-6}$$

The equivalent resistance of the conduction path is normally very small. Therefore second condition is normally true as output power is much lower than $\frac{\bar{v}_o^2}{r_e}$,

whereas first condition is met by careful design of filter components. For a small value of the equivalent resistance r_e of the circuit, characteristic equation (3-4) can also be written as:

$$s^2 + \left(\frac{r_e}{L_e} - \frac{P_o}{C_o \bar{v}_o^2} \right) s + \frac{1}{L_e C_o} \qquad \textbf{3-7}$$

From the above differential equation undamped natural frequency and the damping ratio of the dc link are given by:

$$w = \frac{1}{\sqrt{L_e C_o}}$$
$$\varsigma = \frac{1}{2w} \left(\frac{r_e}{L_e} - \frac{P_o}{C_o \bar{v}_o^2} \right) \qquad \textbf{3-8}$$

From the eq. (3-8), it is clear that damping ratio depends on several factors including the load power. Steady state and transient performance is influenced heavily from these factors and in next section evaluation of power factor and total harmonic distortions at grid side is given.

3.3 Performance evaluation of a three phase diode rectifier

Grid side performance of a three phase diode bridge rectifier is evaluated by total harmonic distortions of grid current and power factor at the grid. These are the two main important factors.

Power factor is calculated by ratio of the rectifier input power (power contribution from fundamental component) and rectifier apparent power (Power from rms). Power factor can also be obtained by ratio of rms value of fundamental component and rms value of input phase current.

$$PF = \frac{P_{in}}{S_{in}} = \frac{I_{1rms}}{I_{rms}} \cdot \cos\varphi \qquad \textbf{3-9}$$

The THDs of input current is defined as the root mean square (RMS) value of the total harmonics of the input current, divided by the RMS value of its fundamental component of the input phase current [62]. Expression of the THDs of the input phase current is defined as:

$$THD = \frac{I_H}{I_F} \qquad \textbf{3-10}$$

Where $I_H = \sqrt{\sum I_h^2} = \sqrt{I_{rms}^2 - I_{1rms}^2}$

I_h = RMS value of the harmonic h

I_F = RMS value of the fundamental current.

Grid side performance of a VSD is judged by the quality of currents it draws from the grid and how it behaves towards the disturbances on the grid. It is very important to see what happens to the mains current during steady state and transient operation of the drive at different operating points. In order to improve performance on the grid side of these drives, it is necessary to see how this standard rectifier performs in different situations and loading patterns. As we have seen equivalent inductance L_e and output capacitor C_o are two main components in this circuit, and therefore an analysis of power factor and THDs by varying one of these two components while keeping another one to fix value for three different type of load situation is carried out. Three different load patterns are resistive load, constant current type and constant power type load connected to the output of the rectifier. Average load power is fixed to 4 kW as only low to medium power drives have been studied in this thesis.

Resistive load of 73 Ω and constant current load of 7.4A is considered in the simulation study. Line resistance (r_g) and line inductance (L_g) have been assumed to be resistance of 0.01 Ω and inductance of 1 mH. Fixed value of 1 mH of the DC side inductor L_{DC} has been used in the simulation. Winding resistance of

DC side inductor is not considered in this simulation. Output capacitance is varied from 10 μF to 10 mF and power factor and total harmonic disturbances are compared at different output capacitor values for three different types of load. Power factor at the grid and THDs of input current for different types of load connected to output of the rectifier with the variation in output capacitor connected to the diode bridge rectifier are given in Table 1.

Table 1. Power factor and THDi for different types of load connected to the output of the rectifier with variation in the output capacitor.

Parameters / Output capacitor	Resistive load		Constant current Type load		Constant power Type load	
	PF	THDi	PF	THDi	PF	THDi
10 μF	0.949	33.03	0.898	48.83	0.678	108.38
20 μF	0.908	45.97	0.882	53.37	0.697	102.91
50 μF	0.8039	73.97	0.789	78.17	0.638	120.78
100 μF	0.7293	93.81	0.721	96.01	0.715	97.79
1 mF	0.8145	71.21	0.816	70.77	0.818	70.297
10 mF	0.8328	66.46	0.8344	66.05	0.8361	65.603

Power factor and total harmonic disturbances are also shown in Figure 32., at different output capacitor values of the three phase diode bridge rectifier for all the three different type of load.

When the output capacitor value is large enough to filter the low frequency components, all the three different type of load behave pretty much in a similar way. The power factor is close to 0.83 and THDs level is 65% when a high value of output capacitor is used. To achieve this level of performance the size of filter components is significantly large. Almost similar behaviour is observed when DC side inductance value varied while keeping output capacitance to a fix value of 10 μF.

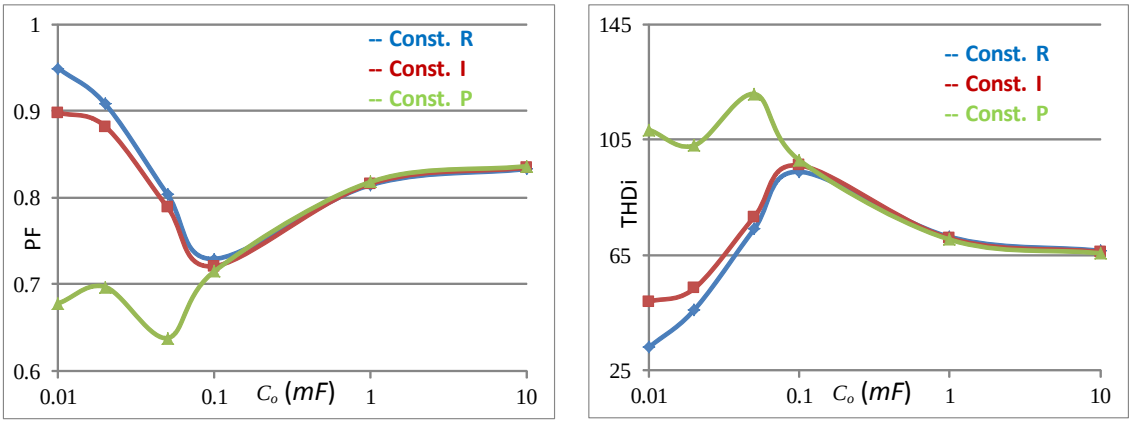

Figure 32. Power factor and THDs for different types of load.

In order to improve performance of the front end converter of a VSD, it is necessary to increase the power factor and bring down the THDs level to a comfortable range. If the load current can be modified in such a way that some of the harmonic content can go to load without affecting the average power flowing to the load, then it is possible to improve performance of the front end converter.

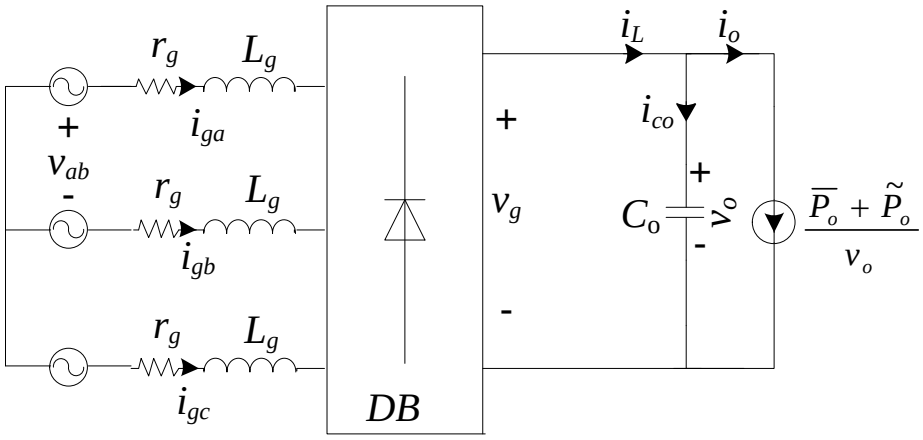

Figure 33. Three phase rectifier without the DC side inductor and operating with the load current modification to achieve stable output voltage.

Circuit schematic is shown in Figure 33. When the load current is modified in such a way that high frequency ripples are allowed to pass to the load through active control, output power contains some high frequency oscillations, which

reflects in output voltage if an inverter is connected at the output of the rectifier. This modification in load current is possible when an active power converter is connected to rectifier as load. In low performance type VSDs, there have been some circuit topologies called as slim dc-link drive. In these drives the DC link filter is completely removed and the electrolytic capacitor is exchanged with MKP type film capacitor of a relatively smaller value.

Power factor improves significantly and THDi levels also falls within the comfortable limit in slim dc-link type drive. Power factor and total harmonic disturbances for different values of the line side inductor with constant power load with load current modification are given in Table 2.

Table 2. Power factor and THDi of a three phase rectifier for constant average power load with the load current modification to achieve stable output voltage.

Parameters / Line side inductor	Power factor	THDi
100 μH	0.86	60.4
200 μH	0.95	32.5
500 μH	0.95	32.0
1 mH	0.93	38.4
1.5 mH	0.93	38.9

When line side inductor is 100 μH, power factor is low and THDi is not good, but as this inductance value increase significant improvement is observed. Earlier when line side inductance reaches close to 3 mH, output voltage was becoming unstable and a very high current flow from the mains.

A comparison is done for the output voltage without and with load current modification and is shown in Figure 34. This is the worst case and line side inductor was 1.5 mH. Peak to peak ripple was almost 500V and by employing active balancing of DC voltage this ripple value comes to comfortable level of

150V. This voltage ripple is still very high and put extra stress on the power semiconductor connected to the intermediate dc-link of the VSD.

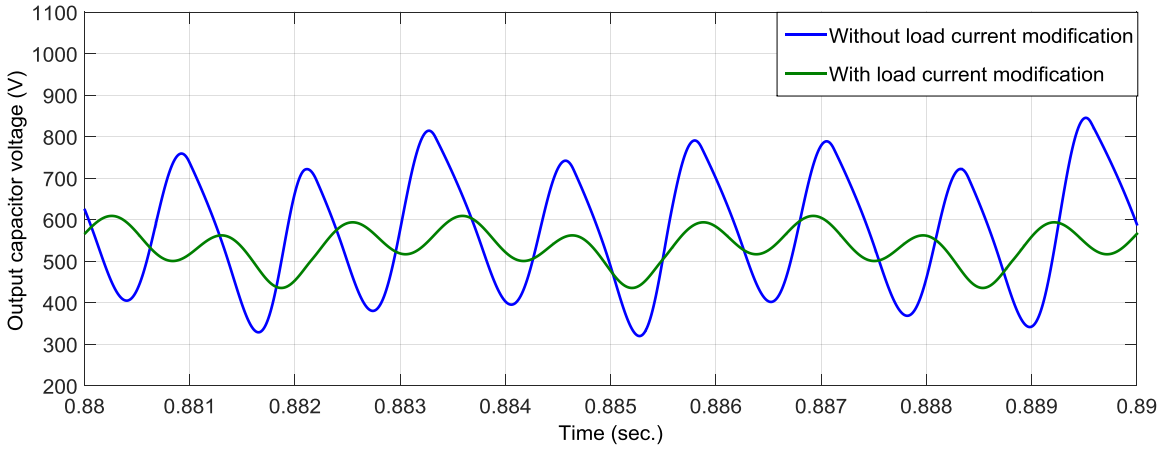

Figure 34. Comparison of the output voltage with and without modification in load current at line inductance of 1.5 *mH*.

Similar comparison was done for the mains current of phase 'a'. The current waveforms from both the situations are shown in Figure 35. Earlier peak value of the phase current was touching 23A, and with load current modification the peak value of phase current is now less than 11A.

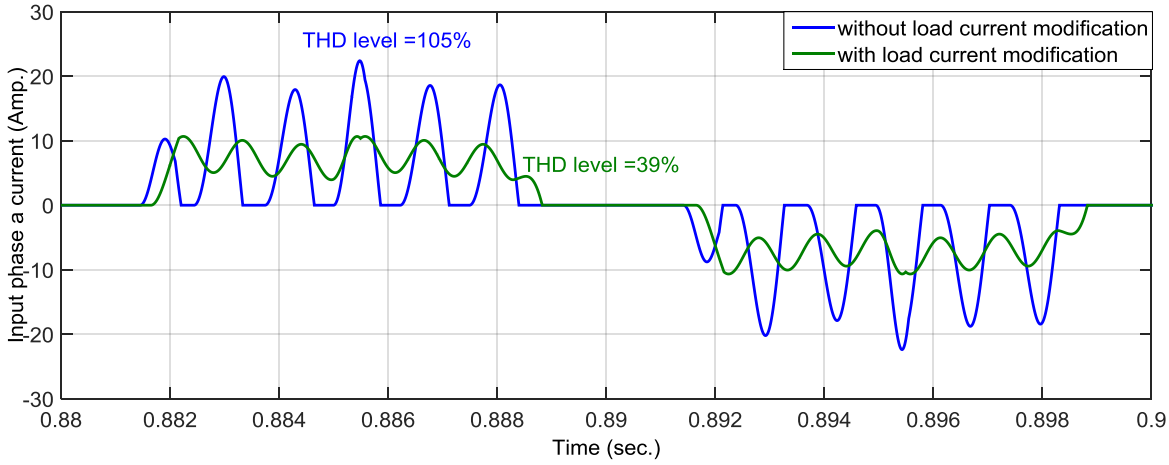

Figure 35. Comparison of input current with load current modification and without its modification at line inductance of 1.5 *mH*.

The peak current reduced significantly and it can also be seen earlier THD level was very high of 105%, after employing active balancing THD level falls to 35%.

This type of active control of load current, output power now contains high frequency ripple. Output power and its harmonics are shown in Figure 36. These harmonics are 6n times of the fundamental frequency. It will increase the losses in the loads associated to these frequencies. If an electrical machine is connected through an inverter, these high frequency will result high loses in the machine windings and poor shaft performance. Winding currents electrical machine will be having harmonics of 6n±1 times of the fundamental frequency. The low performance applications, this active stabilization of intermediate DC bus voltage scheme may be suitable and might work with limited variation in grid condition, but for high performance applications it is not a good idea. By doing this it is changing the location of the harmonic by moving high frequency components from input side to the load, and compromising load side performance.

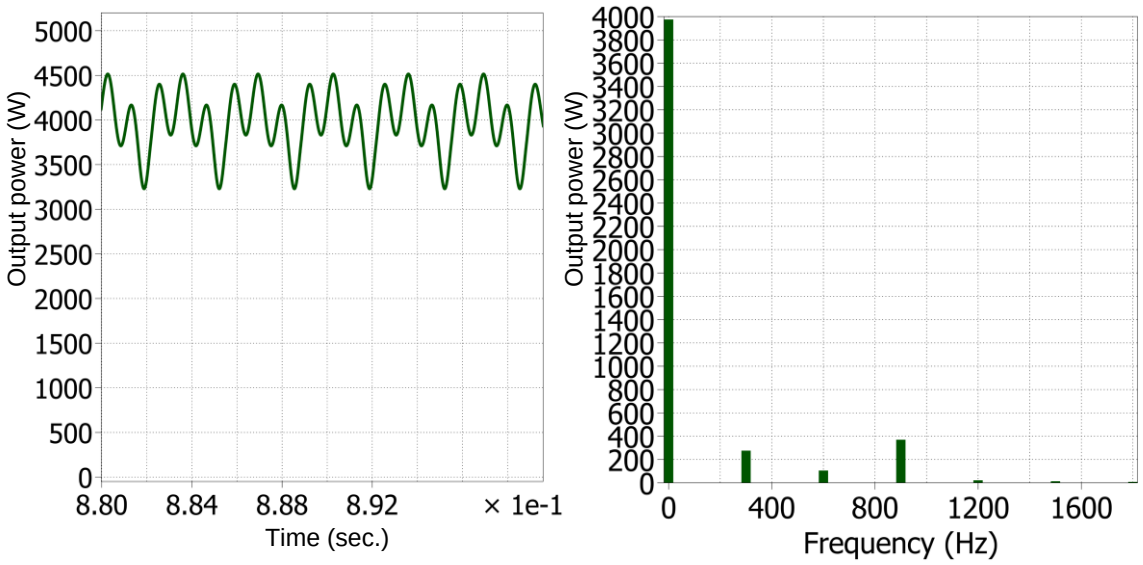

Figure 36. Output power and its harmonic spectrum when load current is modified to reduce the output voltage ripple.

In order to get a better solution without disturbing the load performance, it is necessary to find a solution to reduce the distortions in mains current. If one variable (controlled) ac voltage source can be added in between diode-bridge

and output capacitor in such a way that output capacitor takes only the dc component of the rectified voltage and the added variable ac voltage source provides equal and opposite of the ac ripples in the rectified voltage. By doing so, it is possible to control output voltage to a DC value and to make output current of the diode bridge to constant value equal to dc value of load current. Circuit schematic of the three phase rectifier with such a controlled variable ac voltage source added at the output of the diode bridge rectifier in series with output capacitor and the load is shown in Figure 37.

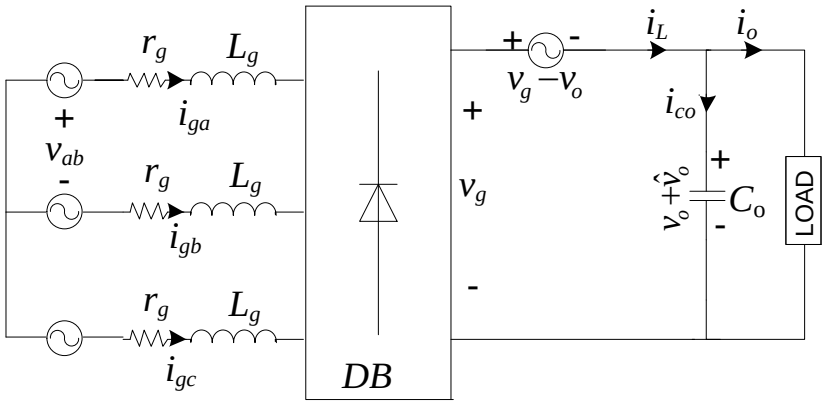

Figure 37. Circuit schematic of a controlled ac voltage source added at the output of the diode bridge rectifier.

Realization of such a controlled variable ac voltage source with a combination of active and passive elements is possible. Details analysis of such type of controlled variable ac voltage source is given in next chapter. This type of voltage compensation for three phase rectifier works very well for all the three different type of loads. Mains current with two different line inductances for all the three different types of load are shown in Figure 38. In this figure two extreme values of line side inductors are used to see the behaviour of this circuit in all three different types of load. In all the situation mains current behaves in a similar way and remain perfectly rectangular. With such a variable voltage source all the disturbances either from input side or from the output side will not affect the performance of the rectifier.

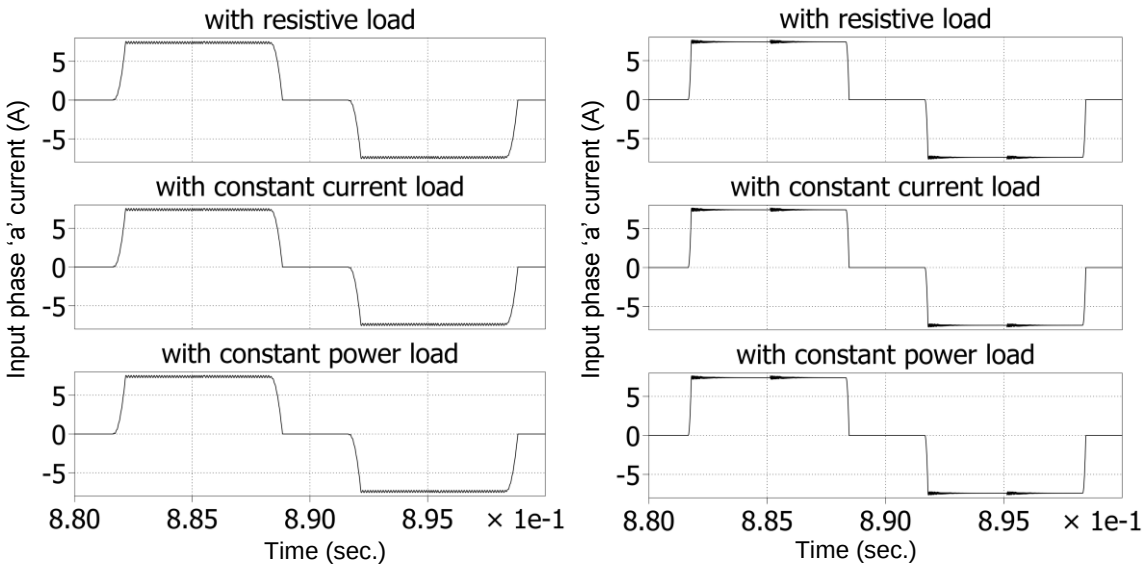

Figure 38. Input phase 'a' current for three different type of load at two different line side inductance.

With this arrangement current coming out from the diode bridge can be controlled to a dc value, it will make circuit to behave as diode bridge connected to a DC current type load. Phase current in such a theoretical case as shown in Figure 39., where the output current of the three phase diode bridge can be estimated as clean DC current, the harmonic current frequencies of a 6-pulse three phase rectifier are 6n±1 times the fundamental frequency.

The line current is then rectangular in shape with 120° blocks. The order numbers h are calculated from the formula below:

$$i_l(t) = I_1 \sin(\omega t) + \sum I_h \sin(h\omega t) \qquad \textbf{3-11}$$

Where $I_h = (-1)^k \frac{I_1}{h}$; and $h = 6k \pm 1$ & $k = 1,2,3,...\infty$

The Total Harmonic Distortion block (in simulation package) calculates the total harmonic distortion (THD) of a periodic distorted signal.

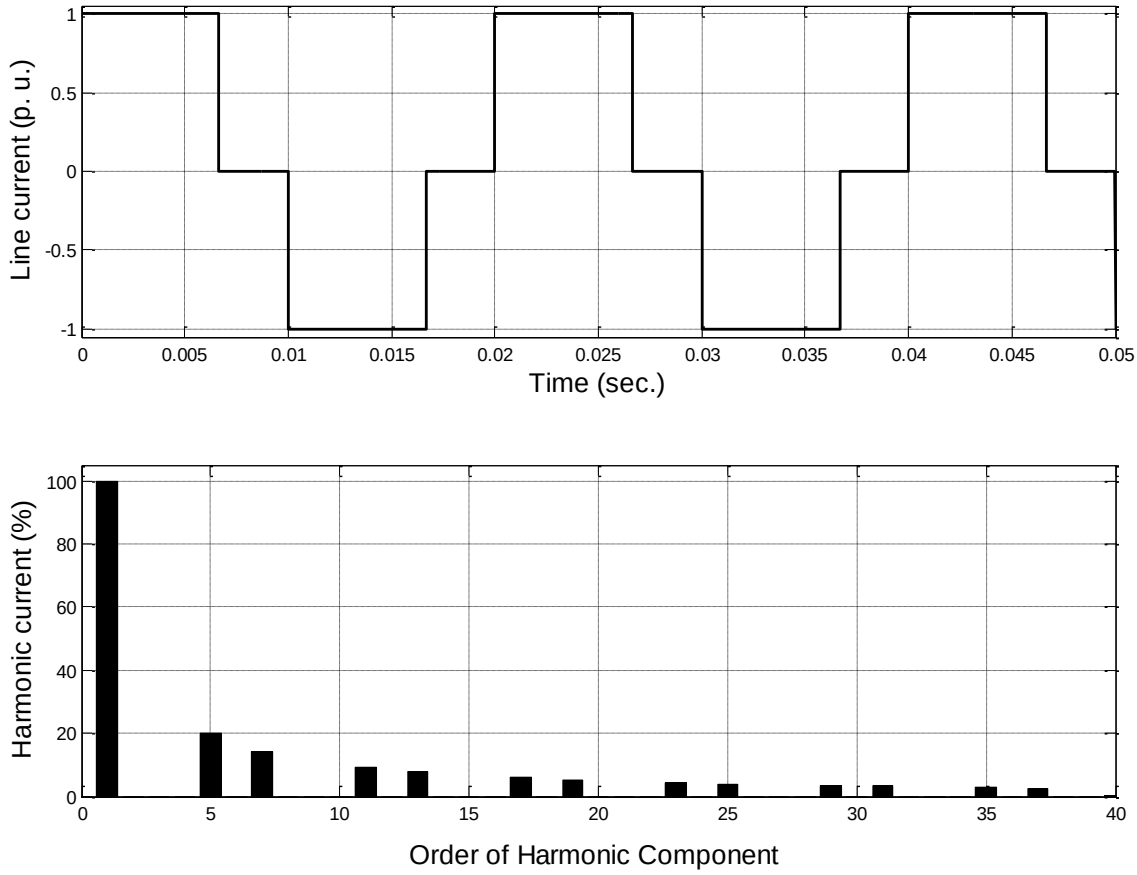

Figure 39. Waveform and harmonic content in a theoretical rectangular current of a 6-pulse standard rectifier.

3.4 Summary and conclusion

The three phase electric drives are used in variable speed drive application. Efficiency and quality of the currents drawn from the grid are two major issues with these variable speed drives. The diode bridge based rectifier fed drives are usually chosen for variable speed drive application as they can offer very high efficiency and comply with standards with the help of filter.

Different types of loads have different impact on the performance of the front end converter connected to the grid. With the help of the standard rectifier it can be very difficult to operate three phase rectifier with high performance for wide range of load and with large variation in the grid side. In order to improve the

performance of these types of drives, some modification in the form of active filter is necessary while maintaining good performance at the load side as well.
It is possible to achieve continuous conduction of the current which is coming out from the rectifier and also to control it to a dc value by adding one controlled ac voltage source in between diode bridge and output capacitor. It will also allow controlling the output voltage to a dc value and reducing or eliminating ripples. This controlled ac voltage source may pave the way to use reduced size of passive components.

Chapter 4. Electronic smoothing inductor based three-phase rectifier

4.1 Background

Filter inductors are commonly used to reduce total harmonic distortions (THDs) level of input current as discussed in detail in the previous chapter. Weight and volume of filter inductor has to come down drastically to make suitable power converter for motor integrated variable speed drive. Introduction of active power electronic switches can ensure very high performance of such inductor with very small size. Such an arrangement is usually referred as "**Electronic Smoothing**" techniques.

In previous chapter addition of a variable voltage source in between the output of the diode bridge and intermediate capacitor as a series arrangement was proposed. This variable voltage source is termed as electronic smoothing inductor (ESI). The ESI can be compared to a passive smoothing inductor which is having infinite inductance to smooth current coming out of the rectifier. If losses of the ESI are neglected, then it behaves like a pure energy storage element. The ESI realizes the energy storage characteristic required for smoothing by the dc-link capacitor of the ESI. Electrolytic capacitors, however, being usually applied for this reason show a very high specific energy storage density as compared to the magnetic energy storage capability of coils of dc inductor.

The basic approach of the ESI based converter is the functional replacement of the passive smoothing inductor by a small power electronic unit whose output voltage in the steady state compensates the voltage ripple of the diode bridge and guarantees a well damped dynamic behaviour by proper control.

4.2 Circuit topology of the electronic smoothing inductor based rectifier

The basic circuit configuration of the ESI connected to the diode bridge output is shown in Figure 40. ESI consists of an inductor (L_{DC}), two MOSFETs (T_1 and T_2) two diodes (D_1 and D_2), and a DC-link capacitor (C). The inductor current i_L is controlled to a constant value by operating T_1 and T_2 with a variable duty cycle. The ESI behaves similar to an inductor that has controlled variable impedance. The ESI voltage is the difference between the rectified input voltage and the output voltage. The ESI realizes the energy storage characteristics required for smoothing by the intermediate dc-link capacitor of the ESI.

Electrolytic capacitors, however, being usually applied for this reason show a very high specific energy storage density as compared to the magnetic energy storage capability of coils of the dc inductor. Losses because of high frequency current ripple flowing in these capacitors produce heat and increase the temperature. Life of electrolytic capacitor reduces when continuously operated at an elevated temperature.

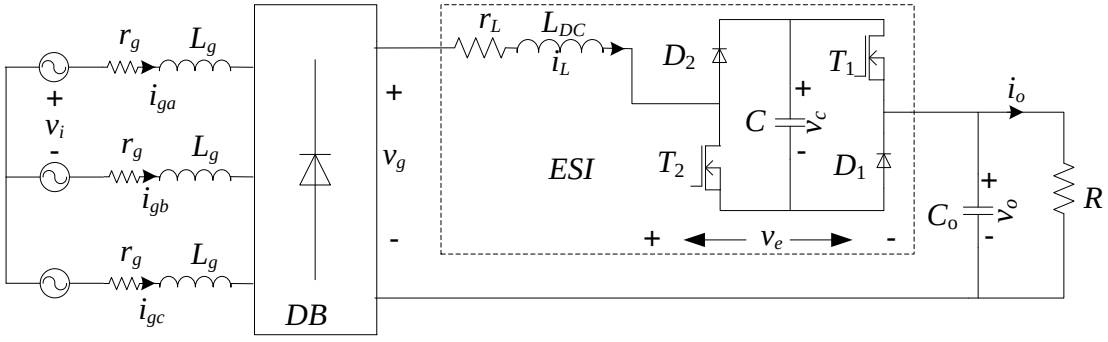

Figure 40. Circuit topology of the ESI based three phase rectifier.

The ESI is able to control a diode bridge output current to a dc value and makes it possible to reduce not only the mains current harmonics but also the output voltage ripple. Ripple reduction in the inductor current and output voltage offer the size reduction of dc-link filter. The ESI helps to reduce size of passive com-

ponents significantly by employing active components and one extra capacitor which is rated for low voltage. Size reduction of the passive components is necessary to achieve high power density while maintaining good quality of the input currents at the mains.

The power circuit of the ESI has to be designed only for the voltage ripple of the diode rectifier and not with respect to the total dc output voltage. Therefore, the power circuit of the ESI for practical realizations typically shows a rated power of only 10% to 15% of the output power of the drive [7]. The higher conduction losses introduced by the bridge are offset by the improved diode rectifier performance, the low voltage devices used in the bridge, and the use of smaller L-C filter components. Although switching frequency of the ESI H-bridge is high (70 kHz), yet the switching losses of the ESI converter remains very low as the switching voltage is relatively low and energy loss associated with each switching is very small.

It is also possible to utilize the same controller for the ESI converter which is already placed for drive control with slight modifications. High power density of the power converter enables integration of the power converter with electrical machines and makes a perfect case for motor integrated variable speed drives (VSDs). These motor integrated VSDs are suitable for several industrial applications like pumps, compressors, ventilators etc.

4.3 Different voltage levels of the ESI based three-phase rectifier

It is important to find a simplified model of the ESI based rectifier to understand different voltage levels and modes of operation. An ideal situation is considered to understand the output voltage of a three phase diode bridge rectifier. These three phase voltages connected to diode bridge rectifier are shown in Figure 41. A constant current source is connected at the output of the rectifier as with ESI it

is possible to control output current to a dc value, which is equal to the average value of the load current.

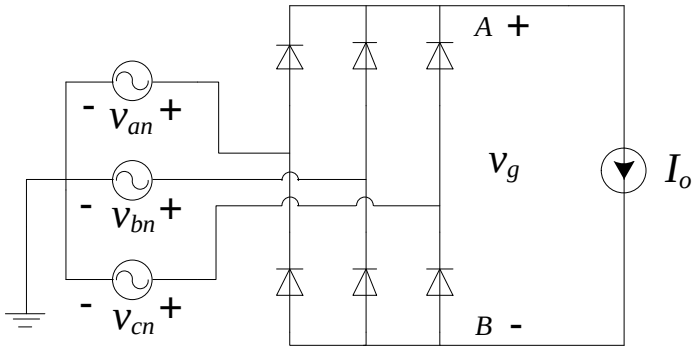

Figure 41. Three phase standard rectifier connected to a constant current output.

If $\hat{v}_i$ is the amplitude of the input phase voltage and ω is angular frequency of the grid voltage, then three input phase voltages of the grid can be written as follows:

$$\begin{aligned} v_{an} &= \hat{v}_i \cos(\omega t) \\ v_{bn} &= \hat{v}_i \cos\left(\omega t - \frac{2\pi}{3}\right) \\ v_{cn} &= \hat{v}_i \cos\left(\omega t - \frac{4\pi}{3}\right) \end{aligned} \qquad \textbf{4-1}$$

In Figure 41., A and B are representing positive and negative rail respectively and V_A and V_B are representing voltage of positive and negative rail with respect to neutral point of the grid respectively. Waveforms of these two voltages are shown in Figure 42. The normal operation of the diodes in the diode bridge in continuous conduction results in a positive output terminal voltage equal to the maximum of the all three phase voltages.

$$\begin{aligned} v_A &= \max(v_{an}, v_{bn}, v_{cn}) \\ v_A(t) &= \frac{3\sqrt{3}}{\pi}\hat{v}_i\left[\frac{1}{2} + \sum_{n=1}^{\infty}\frac{(-1)^{n+1}}{(3n)^2 - 1}\cos(3n\omega t)\right] \end{aligned} \qquad \textbf{4-2}$$

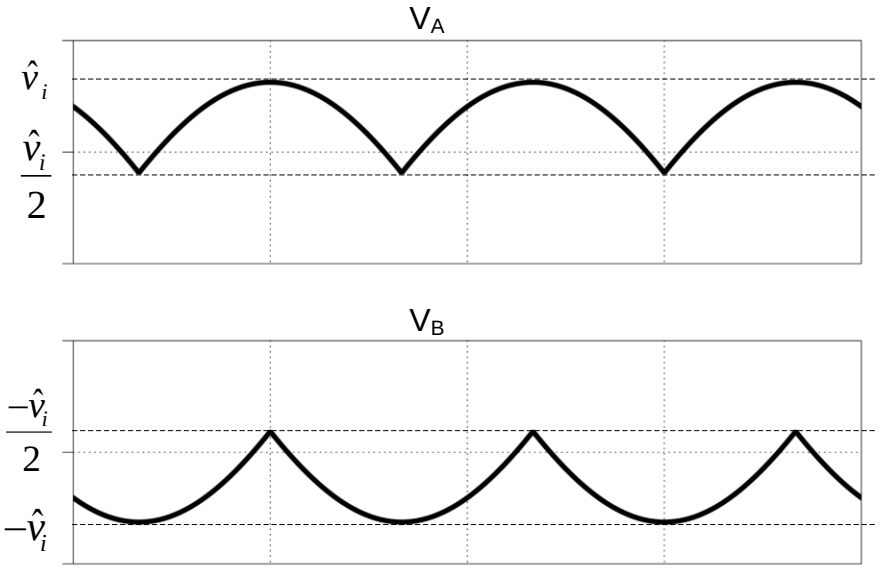

Figure 42. Voltage waveforms of positive and negative rails of an ideal three phase diode bridge rectifier.

Similarly the operation of the diodes in the diode bridge in continuous conduction results in a negative output terminal voltage equal to the minimum of the all three phase voltages.

$$v_B = \min(v_{an}, v_{bn}, v_{cn})$$

$$v_B(t) = \frac{3\sqrt{3}}{\pi}\hat{v}_i\left[-\frac{1}{2} + \sum_{n=1}^{\infty}\frac{1}{(3n)^2 - 1}\cos(3n\omega t)\right] \qquad \textbf{4-3}$$

Both Fourier series expansions contain spectral components at multiples of tripled line frequency, i.e., at triples of the line frequency. The corresponding spectral components of V_A and V_B at odd triples of the line frequency at $3(2k-1)\omega$, where $k \in N$, are the same, having the same amplitudes and the same phases. On the other hand, the corresponding spectral components at even triples of the line frequency, at $6k\omega$, have the same amplitudes, but opposite phases. The rectified output voltage is nothing but the difference of the positive and negative rail voltages and it is shown in Figure 43.

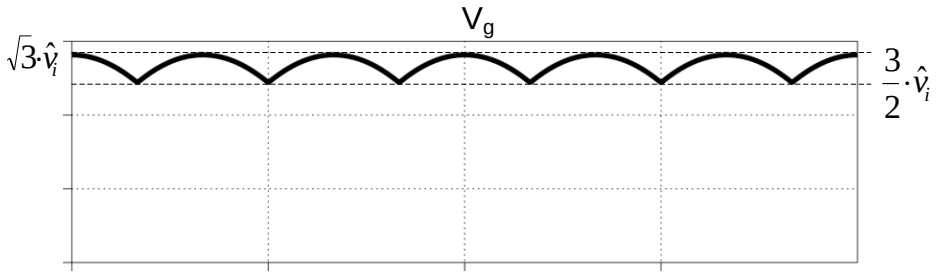

Figure 43. Voltage waveform of output voltage of an ideal three phase diode bridge rectifier.

With the help of eq. (4-2) and eq. (4-3), the diode bridge output voltage v_g can be expressed in Fourier series given by the following expression:

$$v_g = v_A - v_B$$

$$v_g(t) = \frac{3\sqrt{3}}{\pi}\hat{v}_i\left[1 - \sum_{n=1}^{\infty}\frac{2}{(6n)^2 - 1}\cos(6n\omega t)\right] \qquad \textbf{4-4}$$

The rectified output voltage of the three phase diode-bridge rectifier v_g can also be expressed by a simplified expression as:

$$v_g(t) = \sqrt{3}\hat{v}_i\cos(\omega t)$$

$$\omega t \in \left[-\frac{\pi}{6}, \frac{\pi}{6}\right] \qquad \textbf{4-5}$$

This ideal rectified voltage $v_{g,}$ is shown in shown in Figure 44. It is periodic waveform with a frequency six times of the mains frequency. The rectified output voltage of the three phase diode-bridge rectifier v_g, is a combination of a dc and many ac voltages.

The dc value of the output capacitor voltage $\overline{v}_o$ is expressed in (4-6).

$$\overline{v}_o = \frac{3\sqrt{3}}{\pi}\hat{v}_i \qquad \textbf{4-6}$$

Different voltages of the ESI based three phase rectifier are shown in Figure 44. The ESI voltage is the difference between the rectified input voltage and the output capacitor voltage. The ESI voltage v_e, is expressed in (4-7).

$$v_e = v_g(t) - \frac{3\sqrt{3}}{\pi}\hat{v}_i = -\frac{3\sqrt{3}}{\pi}\hat{v}_i\left[\sum_{n=1}^{\infty}\frac{2}{(6n)^2-1}\cos(6n\omega t)\right] \quad \textbf{4-7}$$

The ESI voltage v_e is a periodic function in nature and is given by (4-7) and also shown in Figure 44. The ESI voltage v_e is purely ac in nature and has zero average value over one period of the waveform. The ESI voltage varies in the range given by the following expression in (4-8).

$$\frac{3}{2}\hat{v}_i - \bar{v}_o \le v_e \le \sqrt{3}\hat{v}_i - \bar{v}_o \quad \textbf{4-8}$$

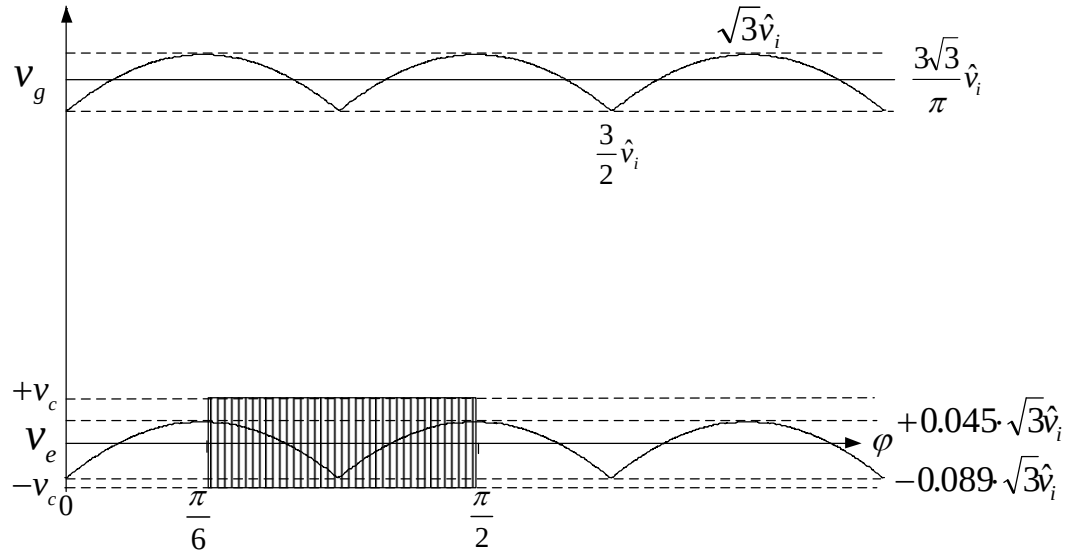

Figure 44. Different voltage levels of the ESI based three phase rectifier.

A low voltage rated (150V) dc-link capacitor *C* is connected to positive and negative rails of the ESI asymmetrical H-bridge and its voltage v_c is utilized to construct the desired ac voltage of the ESI with the control of power semiconductors (MOSFETs) of the ESI asymmetrical H-bridge. The inductor current of the ESI H-bridge, i_L is controlled to a dc value (average load current) by operating T_1 and T_2 with a variable duty cycle with the help of proper control.

4.4 Different modes of operation of the ESI based three phase rectifier

As it is discussed earlier, The ESI consists of two MOSFETs (T_1 and T_2) two diodes (D_1 and D_2), as power semiconductors. It is important to understand flow of current in different switching states of the converter.

During the turn-off period of both T_1 and T_2, the ESI capacitor C is charged and current flows through the diodes D_1 and D_2, and inductor current i_L decreases. On the other hand, C is discharged and i_L increases when both transistors are turned on.

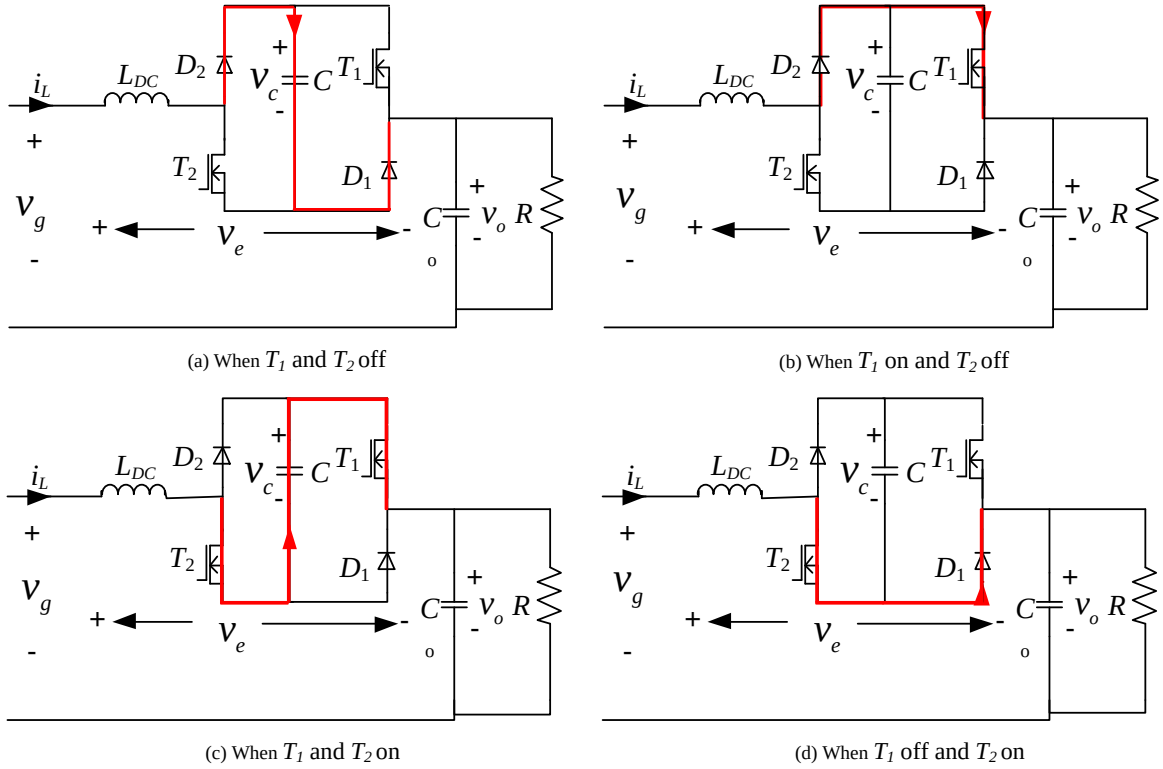

(a) When T_1 and T_2 off

(b) When T_1 on and T_2 off

(c) When T_1 and T_2 on

(d) When T_1 off and T_2 on

Figure 45. Different modes of operations of the ESI based three-phase rectifier.

In the time period when only one of T_1 and T_2 is turned on, i_L does not flow through the ESI capacitor C. In this mode of operation, the inductor current i_L goes through the active switch which is in ON position and diode of other leg of

the ESI H-bridge and the ESI capacitor C is bypassed. The inductor current i_L will increase if the output voltage of the diode bridge v_g is higher than the output capacitor voltage v_o, whereas it decreases if v_g is lower than v_o. The three-level operation can be achieved by shift in gate pulses by half of the time period of the switching frequency. Effective switching frequency through the inductor will be doubled if three level operation of asymmetrical H-bridge is utilized. Conduction path of the current in the ESI for different switching states is shown by red line in Figure 45.

4.5 Summary and conclusion

Diode bridge based rectifier fed drives are natural choice as they can offer very high efficiency and comply with current standards with the help of a hybrid filter such as electronic inductor based filter. To achieve high power density, this modification should involve power electronics and passive component which are rated for low voltage and losses involve in this system should also be low. By taking these things into account, Electronic smoothing inductor based drives appears to be a better choice.

The ESI based converter is easy to integrate in the existing power circuit of a VSD and does not demand too many changes either in power circuit or in control. Volume and weight of these drive with ESI is smaller and it is very much suitable for integration with electrical motor.

Chapter 5. Modelling of the ESI based three-phase rectifier

5.1 Background

Modeling of a power converter is one of the necessary steps to analyze transient and steady state behaviour of an electrical and electronic circuit. Modeling of a circuit is the representation of physical phenomena by mathematical means through simplified equations and transfer functions. In engineering, it is desired to model the important dominant behaviour of a system, while neglecting other insignificant phenomena to build a simplified linear model. Modeling process involves use of approximations to neglect small but complicating phenomena, in an attempt to understand what is most important in the circuit behaviour. Approximate models are an important tool for gaining understanding and physical insight of the circuit topologies.

Switching ripple in capacitor voltage and inductor current is small in a well-designed converter operating in continuous conduction mode (CCM). Hence, one can ignore the switching ripple, and model only the underlying ac variations in the converter waveforms to create a linear model. For example, suppose that some ac variation is introduced into the converter duty cycle *d(t)*, such that

$$d(t) = D + D_m \cos \omega_m t \qquad \textbf{5-1}$$

Where D and D_m are constants and the modulation frequency w_m is much smaller than the converter switching frequency. The objective ac modelling efforts is to predict and analyse this low-frequency component.

A simple method for deriving the small-signal model of CCM converters is explained in this chapter. The switching ripples in the inductor current and

capacitor voltage waveforms are removed by averaging over one switching period. Hence, the low-frequency components of the inductor current and capacitor voltage waveforms are modelled by means of mathematical equations. Average voltage of an inductor and average current flowing into a capacitor can be represented as given in the following equation:

$$L\frac{d<i_L(t)>_{T_s}}{dt}=<v_L(t)>_{T_s}$$
$$C\frac{d<v_c(t)>_{T_s}}{dt}=<i_c(t)>_{T_s} \qquad \textbf{5-2}$$

Where $<x(t)>_{T_s}$ denotes the average of $x(t)$ over an interval of length T_s.

$$<x(t)>_{T_s}=\frac{1}{T_s}\int_{t}^{t+T_s}x(\tau)d\tau \qquad \textbf{5-3}$$

The averaged inductor voltage and capacitor current given in eqs. (5-2) are, in general, nonlinear functions of the signals in the converter, and hence these eqs. (5-2) constitutes a set of nonlinear differential equations. Indeed, the spectrum also contains harmonics of the modulation frequency w_m. In most converters, these harmonics become significant in magnitude as the modulation frequency w_m approaches the switching frequency w_s or as the modulation amplitude D_m approaches the quiescent duty cycle D.

Nonlinear elements are not uncommon in power electronic converters; indeed, all semiconductor devices do have nonlinear behavior. To obtain a linear model that is easier to analyze, it is advisable to construct a small-signal model that has been linearized about a quiescent operating point, in which the harmonics of the modulation or excitation frequency are neglected. So by employing the basic approximation of removing the high-frequency switching ripple by averaging over one switching period will help to create linear model. Yet the average value is allowed to vary from one switching period to the next, such that low-frequency variations are modelled.

One should note that the principles of inductor volt-second balance and capacitor charge balance predict that the right-hand sides of Eqs. (5-2) are zero when the converter operates in steady state. Equations (5-2) describe how the inductor currents and capacitor voltages change when nonzero average inductor voltage and capacitor current are applied over a switching period during the transient operation of the power converter.

5.2 Modeling approach of the ESI based rectifier

The basic circuit configuration of the ESI connected to output of the three phase diode bridge output is shown in Figure 46. In this circuit, three phase diode bridge is represented by a block. It contains three lags where each lag has two diodes connected one after another forming a bridge; joint of the diodes is connected to the phase of a grid. These diodes are naturally line commuted. This circuit also has the ESI circuit plugged into the rectifier. In order to analyze circuit behaviour, it is necessary to find simplified equivalent circuit model of the ESI based rectifier.

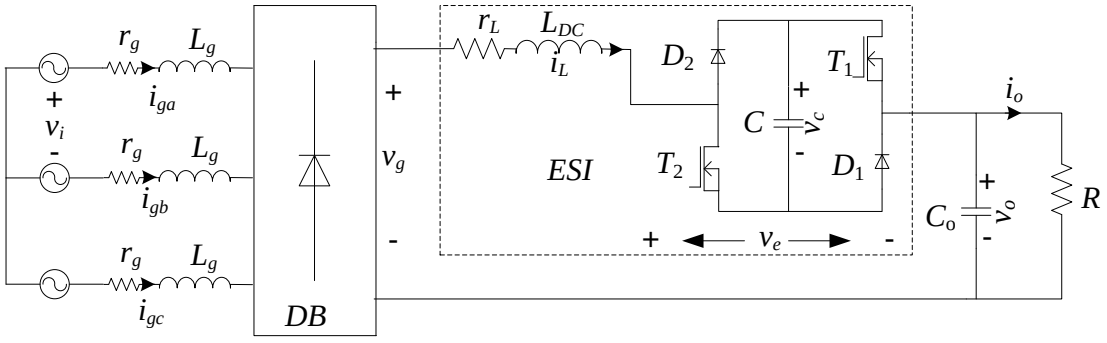

Figure 46. Circuit topology of the ESI based three phase rectifier.

In order to develop equivalent circuit of the ESI based three phase rectifier, it is necessary to separate ESI H-bridge from standard three phase diode bridge rectifier for a while, later it will be plugged into the circuit once simplified linear equivalent circuit for rectifier is developed. For simplicity resistive load connected to the rectifier is considered here.

Circuit simplification of a standard three phase diode bridge rectifier is shown in Figure 47. This circuit has three phase AC voltages with its line impedance on left side of three phase diode bridge and load with DC filter on right side.

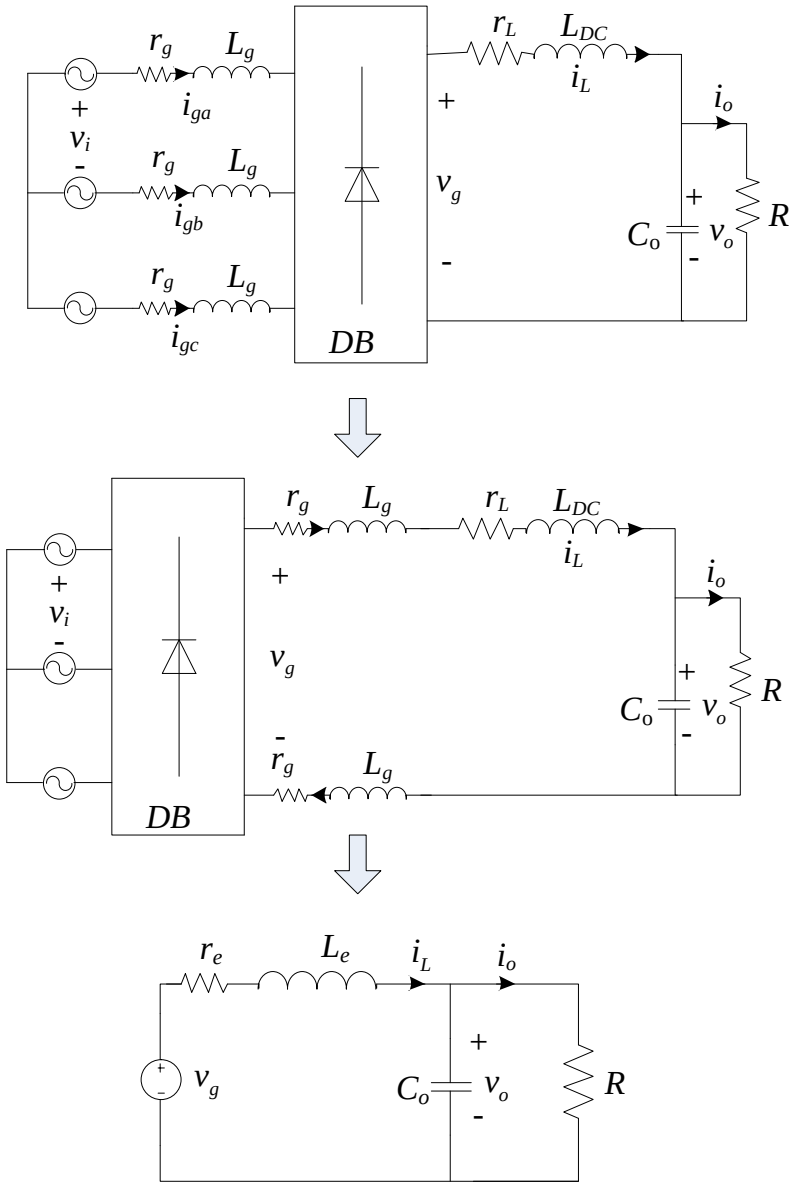

Figure 47. Simplification of circuit of a three phase diode bridge rectifier.

5.2.1 Non-linear circuit model of standard three phase rectifier

For simplifying the non-linear circuit model, impedance of two lines from mains side has been shifted to DC side.

$$r_e = r_L + 2 * r_g$$
$$L_e = L_{DC} + 2 * L_g \qquad \textbf{5-4}$$

The winding resistance of this inductor is r_L. The front end of the three phase rectifier is connected to a three phase grid. The value of line resistance (r_g) and line inductance (L_g) per phase is assumed to be 0.01 Ω and 1 *mH* respectively.

This simplified circuit model holds true in case of continuous conduction and does not take care of commutation of diodes. There is difference in steady state output voltage in this model as compare to practical three phase diode bridge rectifier as it involves commutation of diodes, to accommodate this effect, eq. (5-4) can be modified to the following equation.

$$r_e = r_L + 2r_g + \frac{3\omega_g L_g}{\pi}$$
$$L_e = L_{DC} + 2L_g \qquad \textbf{5-5}$$

The last term in the expression of equivalent resistance r_e, related to non-ohmic voltage drop due to natural commutation in the diodes of the front end rectifier. Effect of any change in input voltage on output voltage of the two circuit schematic is same in steady state as well as in transient state in both the circuit. This circuit can be further simplified to last circuit as shown in Figure 47.

Input to output transfer function of simplified linear circuit can be written as:

$$G_{vg}(s) = \frac{\hat{v}_o(s)}{\hat{v}_g(s)} = \left(\frac{R}{s^2 L_e R C_o + s(L_e + r_e R C_o) + r_e + R} \right) \qquad \textbf{5-6}$$

In order to prepare simplified non-linear model, two legs diode bridge are considered as out of three phases only two phases conducts at a given time if commutation is neglected. Grid inductance is transferred to DC side. Source voltage is constructed from a function which gives maximum of absolute value

of three phase line to line voltages i.e. six-pulse voltage which is given in equation (4-4) in previous chapter. Circuit representation of equation (5-6) is given in Figure 48. This is a linear circuit in which all the linear passive circuit elements are represented with the help of PLECS (circuit simulator). An equivalent voltage source v_g is also applied to this circuit model. In this circuit an equivalent voltage source v_g is used which represents the six-pulse voltage of three-phase ideal diode bridge rectifier.

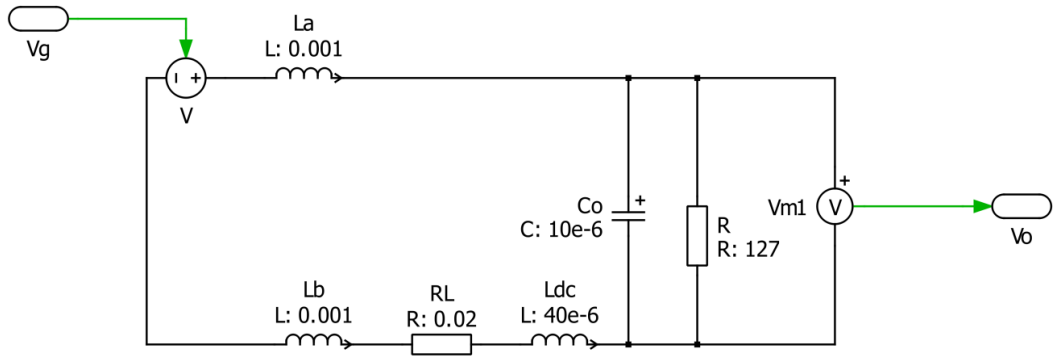

Figure 48. Linear circuit model in PLECS with all linear components from PLECS library.

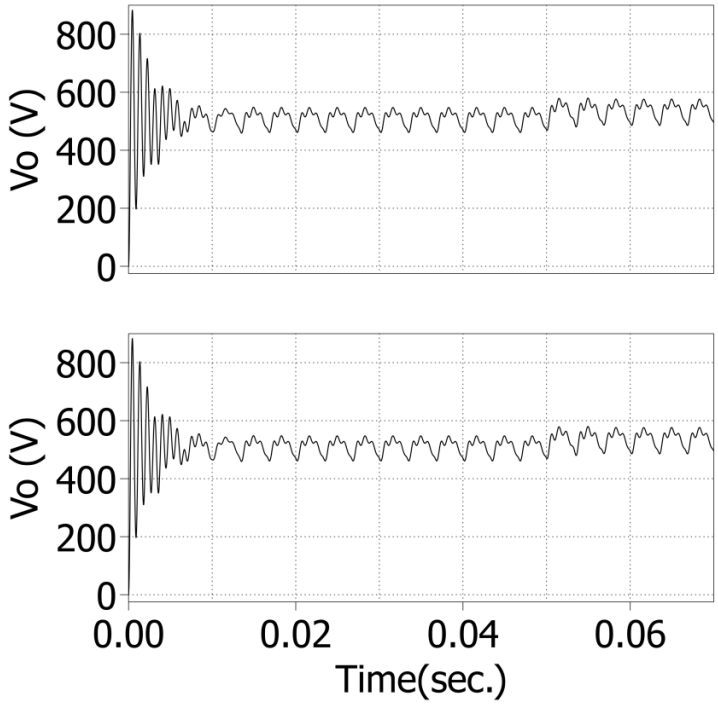

Figure 49. Response of linear circuit in PLECS and transfer function of output to input linear mathematical model.

Response of Output voltage from PLECS linear circuit is compared with the response of transfer function of Mathematical model of equivalent circuit of the standard three phase diode bridge rectifier is shown in Figure 49.

In both situation, response matches exactly at large disturbance of 0.95 times of the full input at time t=0, and small disturbance at t=0.05 from 0.95 time to full input voltage. It is on expected line as circuit model is constructed from all linear elements of the component library of the PLECS package.

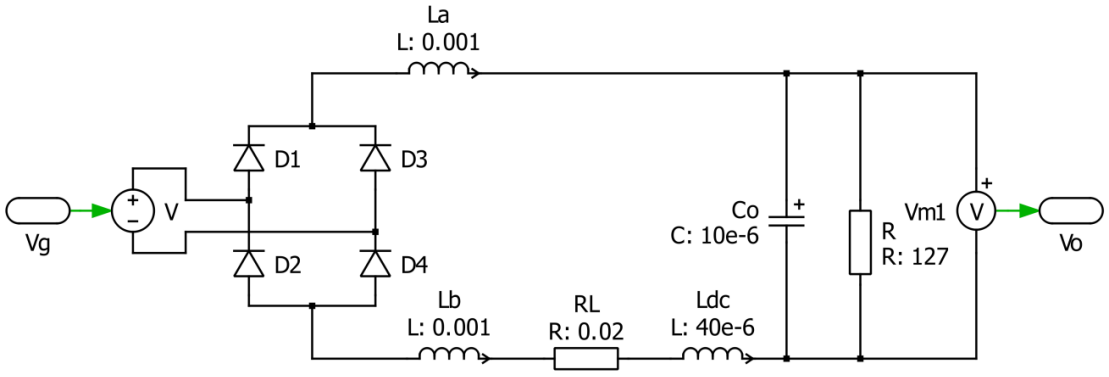

Figure 50. Simplified non-linear model with diodes and impedances of conduction path are connected on DC side.

In order to verify the steady state and transient behaviour of this circuit, an equivalent non-linear circuit is prepared in PLECS and it as shown in Figure 50. This is a linear circuit in which all the passive circuit elements are represented with the help of PLECS (circuit simulator). An equivalent voltage source v_g is also applied to this circuit model. This nonlinear circuit is shown in Figure 50. In this circuit line inductance is moved to DC side from mains. Source voltage vg is equivalent voltage of six-pulse rectified voltage.

It is one step further to include non-linear model of diodes and to observe the behaviour of the linear and the non-linear circuit models in the direction to achieve a better model. Comparison of response of output voltage in PLECS linear model and non-linear model is shown in Figure 51. In the beginning at time t=0, a large step is provided similar to previous case, response of two circuit model is different in transient but same in steady state. Diode current

goes into discontinuous, and because of inherent property of diode current can flow only in one direction, for large step transient response is not matching. But at time t=0.5 sec., a small step of 0.05 times is given (changed from 0.95 time to full input voltage), Both transient and steady state response matches exactly as non-linear characteristic of diodes does not play any role because diode current remain continuous.

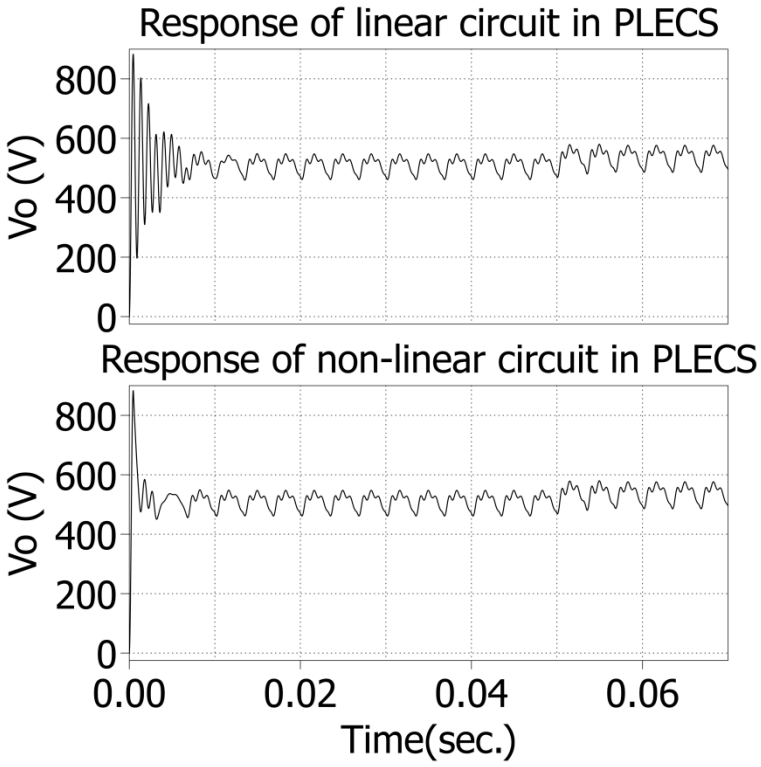

Figure 51. Comparison of response of output voltage from linear model and non-linear circuit model in PLECS.

So far all the inductances of the conduction path are considered on the DC side of the circuit. As only two phases conducts at a given time in standard three phase diode bridge, if commutation time is not considered, therefore line impedances of those two phases are moved to source side and non-linear circuit in PLECS is prepared. This non-linear circuit with commutation effect in PLECS is shown in Figure 52. Forward voltage drop of each diode is considered to be 0.7V, which is a typical value. Response from two different non-linear circuits of Figure 50., and Figure 52., is shown in Figure 53.

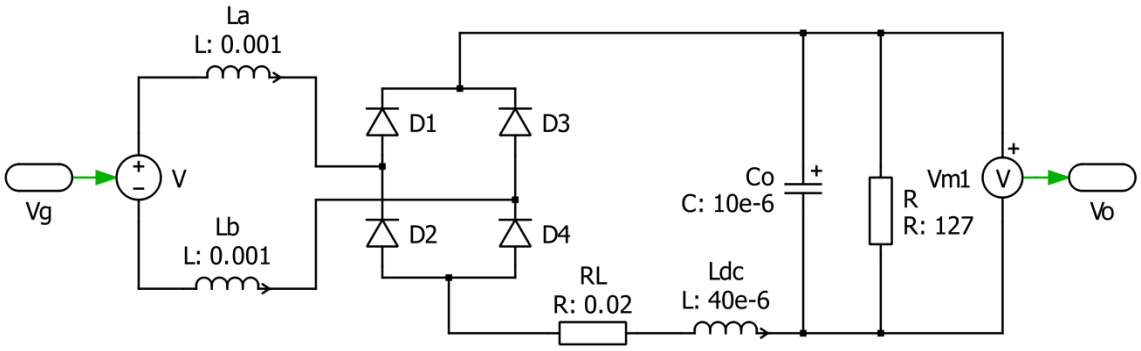

Figure 52. Simplified non-linear model with diodes and line impedances of conduction path are connected on AC side.

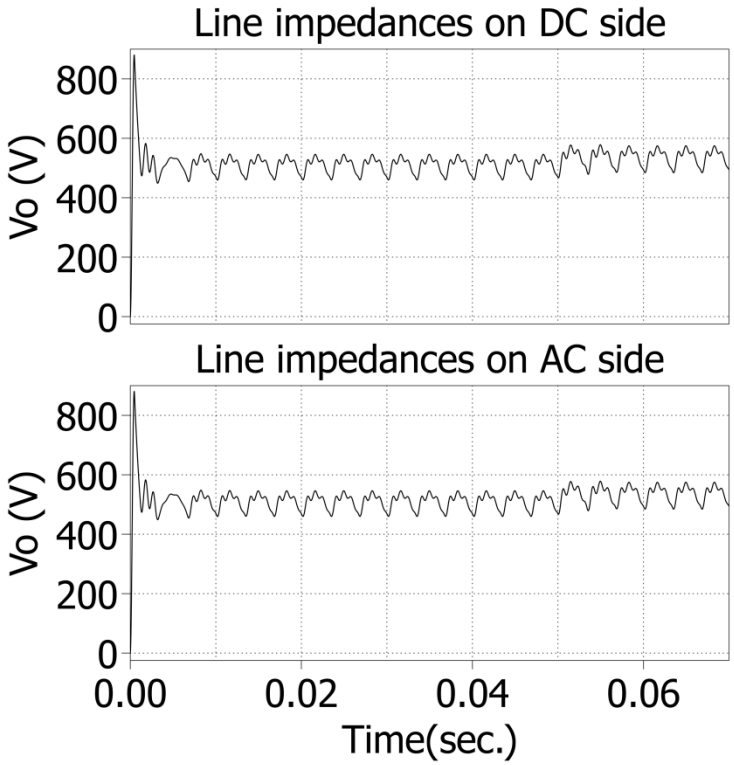

Figure 53. Comparison of response of output voltage from two different non-linear models with different position of line impedances.

Response of output voltage in both the situations matches exactly, because conduction path in these two non-linear circuits remains same all the time. As earlier explained for large step, transient response is different from linear circuit but steady state response is still same, and for small step both transient and steady state response matches exactly to the linear circuit. Moving line imped-

ance from DC side to AC side in this situation does not create any deviation in the response of output voltage.

So Far, only two conducting phases are considered and comparison of linear circuit model with non-linear circuit model has been done. Now line side inductors will be placed in its original positions i.e. in series with the phase voltages and effect of commutation of diodes will also be observed.

In order to compare response of linear model and non-linear circuit behaviour of a three-phase diode bridge rectifier, circuit schematics of the linear and the non-linear circuit are prepared.

Non-linear circuit in PLECS is shown in Figure 54. This circuit contains three balanced voltages sources of a three-phase system, and line impedances connected to standard three-phase diode bridge rectifier.

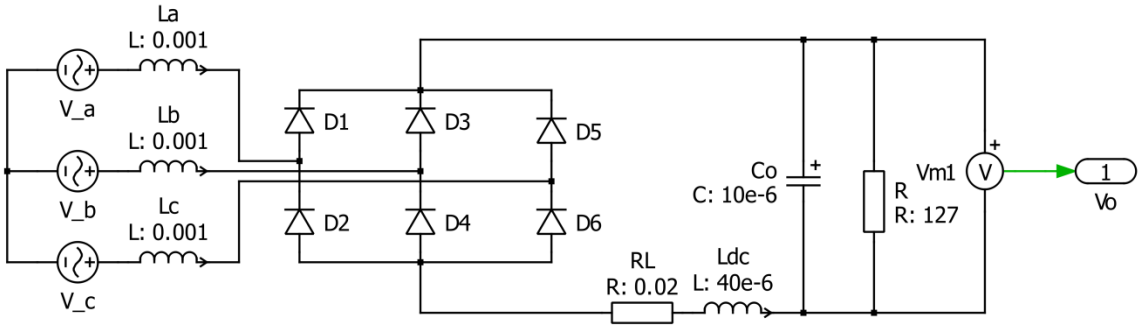

Figure 54. Non-linear circuit model of standard three-phase diode bridge rectifier in PLECS.

Response of the output voltage of the standard three-phase diode bridge rectifier from linear and non-linear circuit model is compared in Figure 55. In this figure step response is presented, in the beginning at time t=0 sec, there is a big step of full input voltage is provided. It is observed that steady state and transient behaviour are slightly different in these two models. Reason for this small difference is diode commutation, in simplified model diode commutation doses not take place as conduction path never changes, but in case of standard three phase diode bridge rectifier, diode commutation takes place and has minor impact on its response which is visible in Figure 55.

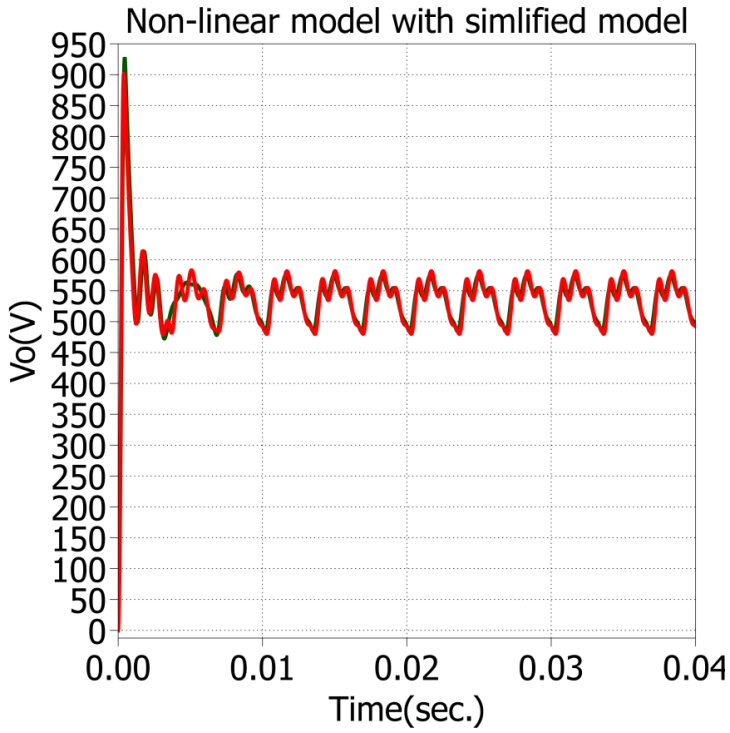

Figure 55. Response comparison of actual non-linear circuit model (red) and simplified non-linear model (Green).

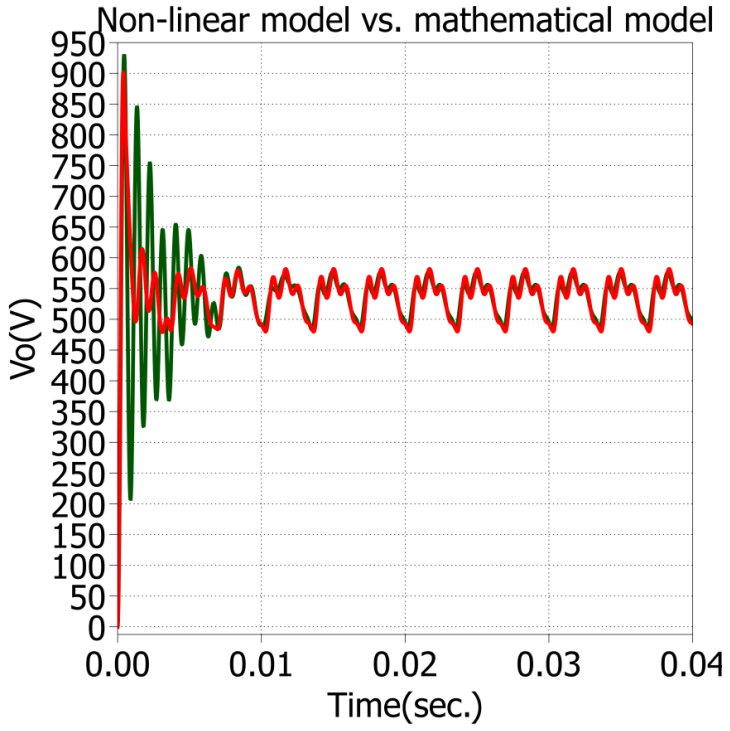

Figure 56. Response comparison of actual non-linear circuit model (red) and mathematical model (green).

Comparison of response of standard three phase diode bridge rectifier with output to input transfer function of the mathematical model based on the equivalent circuit of the three phase diode bridge rectifier is shown in Figure 56.

From Figure 56., It is clear that in steady state mathematical model shows good agreement with actual non-linear circuit model for the standard three phase rectifier.

5.2.2 Non-linear circuit model of the ESI based three phase rectifier

Asymmetrical H-bridge can be modelled as shown in Figure 57. Here DC-link capacitor voltage is assumed constant. Voltage of asymmetrical H-bridge is represented by equivalent voltage source v_e, given by following expression.

$$v_e = v_c(t) * (1 - 2d(t)) \qquad \textbf{5-7}$$

A non-linear circuit of the ESI asymmetrical H-bridge is constructed and this non-linear circuit model of the ESI is plugged into three-phase diode bridge rectifier, the complete non-linear circuit model is derived as shown in Figure 58. This circuit receives gate signals from PWM generator block, which process the modulation signal.

This non-linear circuit of the ESI based three-phase rectifier will be used to construct transfer functions and their verifications in next chapter. In order to find small signal ac model, an averaged circuit is required.

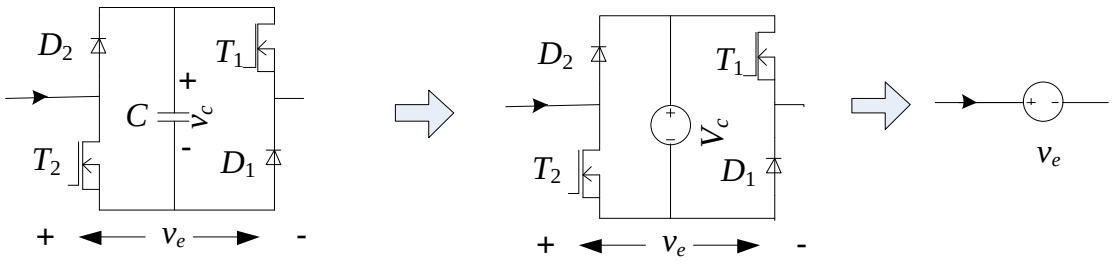

Figure 57. Simplification of asymmetrical H-bridge circuit of the ESI.

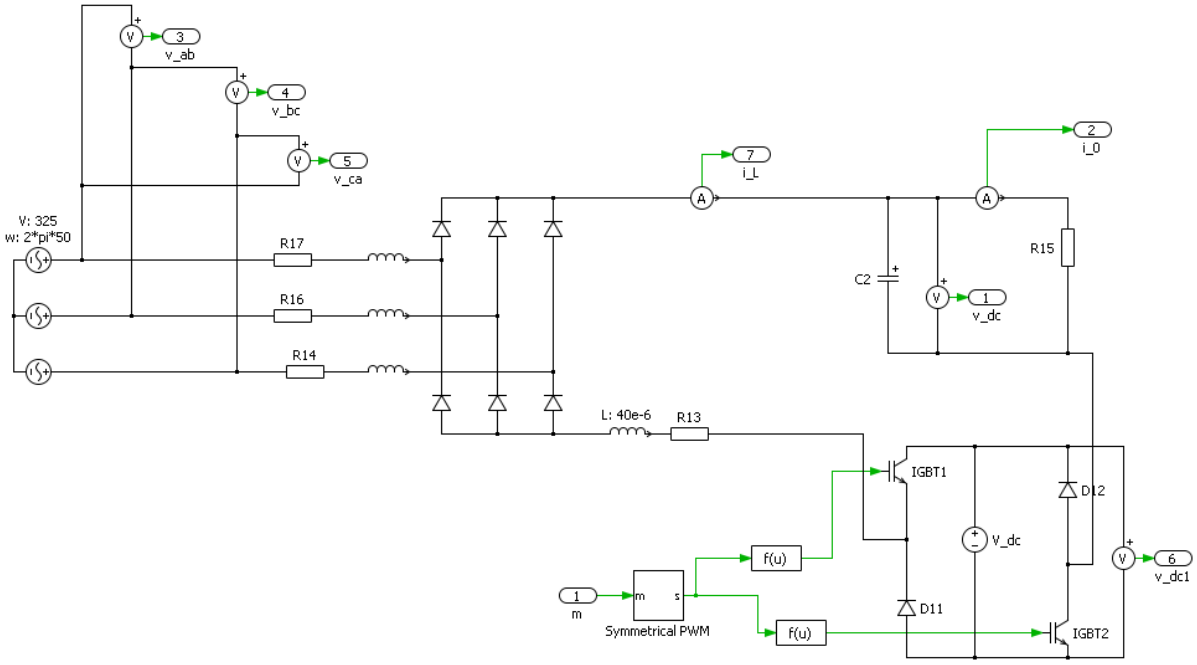

Figure 58. Non-linear circuit of ESI based three phase rectifier.

5.3 The Basic AC Modelling Approach

The analysis begins as usual, by determining the voltage and current waveforms of the inductor and capacitor. It is assumed that the converter is operating in continuous conduction mode; i. e. current in inductor is always flowing.

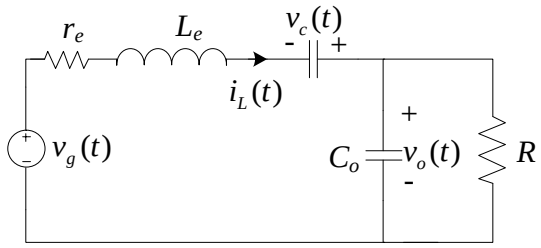

(a)

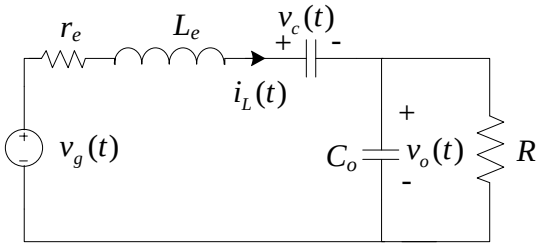

(b)

Figure 59. ESI converter circuit: (a) when both switches are ON, (b) when both switches are OFF.

When T_1 and T_2 are ON (position 1), simplified circuit is shown in Figure 59(a). Inductor voltage and current in ESI capacitor C is given by following equations:

$$v_L(t) = L_e \frac{di_L(t)}{dt} = v_g(t) - r_e i_l(t) + v_c(t) - v_o(t) \quad \textbf{5-8}$$

$$i_c(t) = C \frac{dv_c(t)}{dt} = -i_L(t) \quad \textbf{5-9}$$

We now make the small-ripple approximation. By replacing $v_g(t)$, $i_L(t)$, $v_c(t)$ $v_c(t)$ and $v_o(t)$ with their low-frequency averaged values $< v_g(t) >_{T_s}$, $< i_L(t) >_{T_s}$, $< v_c(t) >_{T_s}$ and $< v_o(t) >_{T_s}$. Equations (4.8) and (4.9) then become

$$v_L(t) = L_e \frac{di_L(t)}{dt} = < v_g(t) >_{T_s} - r_e < i_L(t) >_{T_s} + < v_c(t) >_{T_s} - < v_o(t) >_{T_s} \quad \textbf{5-10}$$

$$i_c(t) = C \frac{dv_c(t)}{dt} = - < i_L(t) >_{T_s} \quad \textbf{5-11}$$

Hence, during the first subinterval, the inductor current $i_L(t)$ and the capacitor voltage $v_c(t)$ change with the essentially constant slopes given by Eqs. (5-10) and (5-11). When T_1 and T_2 are OFF (position 2), simplified circuit is shown in Figure 59(b). Inductor voltage and current in ESI capacitor C is given by following equations:

$$v_L(t) = L_e \frac{di_L(t)}{dt} = v_g(t) - r_e i_l(t) - v_c(t) - v_o(t) \quad \textbf{5-12}$$

$$i_c(t) = C \frac{dv_c(t)}{dt} = i_L(t) \quad \textbf{5-13}$$

Use of the small-ripple approximation, By replacing $v_g(t)$, $i_L(t)$, $v_c(t)$ $v_c(t)$ and $v_o(t)$ with their low-frequency averaged values $< v_g(t) >_{T_s}$, $< i_L(t) >_{T_s}$, $< v_c(t) >_{T_s}$ and $< v_o(t) >_{T_s}$. Equations (5-12) and (5-13) then become

$$v_L(t) = L_e \frac{di_L(t)}{dt} = < v_g(t) >_{T_s} - r_e < i_L(t) >_{T_s} - < v_c(t) >_{T_s} - < v_o(t) >_{T_s} \quad \textbf{5-14}$$

$$i_c(t) = C \frac{dv_c(t)}{dt} = < i_L(t) >_{T_s} \quad \textbf{5-15}$$

During the second subinterval, the inductor current and capacitor voltage change with the essentially constant slopes given by Eqs. (5-10) and (5-11).

Circuit remain in position 1 for $t_1 \le t \le t_1 + dT_s$

And circuit remain in position 2 for $t_1 + dT_s \le t \le T_s$

The low-frequency average of the inductor voltage is found by evaluation the inductor voltage during the first and second subintervals, are averaged:

$$< v_L(t) >_{T_s} = \frac{1}{T_s} \int_t^{t+T_s} v_L(\tau) d\tau$$

$$L_e \frac{d < i_L(t) >_{T_s}}{dt} = d(t)(< v_g(t) >_{T_s} - r_e < i_L(t) >_{T_s} + < v_c(t) >_{T_s} - < v_o(t) >_{T_s}) + \quad \textbf{5-16}$$

$$(1-d(t))(< v_g(t) >_{T_s} - r_e < i_L(t) >_{T_s} + < v_c(t) >_{T_s} - < v_o(t) >_{T_s})$$

$$L_e \frac{d < i_L(t) >_{T_s}}{dt} = < v_g(t) >_{T_s} - r_e < i_L(t) >_{T_s} - < v_c(t) >_{T_s} (1-2d(t)) - < v_o(t) >_{T_s}$$

This equation describes how the low-frequency components of the inductor current vary with time.

In a similar way, averaging the capacitor current for the ESI capacitor *C*.

$$< i_c(t) >_{T_s} = \frac{1}{T_s} \int_t^{t+T_s} i_c(\tau) d\tau$$

$$C \frac{d < v_c(t) >_{T_s}}{dt} = d(t)(- < i_L(t) >_{T_s}) + (1-d(t))(< i_L(t) >_{T_s}) = < i_L(t) >_{T_s} (1-2d(t)) \quad \textbf{5-17}$$

If we can define a modulation function $m(t)$ in such a way that:

$$m(t) = 1 - 2d(t) \quad \textbf{5-18}$$

Average model for circuit can be constructed from these equations. Averaging the inductor voltage yields the following:

$$L_e \frac{d < i_L(t) >_{T_s}}{dt} = < v_g(t) >_{T_s} - r_e < i_L(t) >_{T_s} - < v_c(t) >_{T_s} m(t) - < v_o(t) >_{T_s} \quad \textbf{5-19}$$

$$C \frac{d < v_c(t) >_{T_s}}{dt} = < i_L(t) >_{T_s} m(t) \quad \textbf{5-20}$$

This is the basic averaged equation which describes dc and low-frequency ac variations in the capacitor voltage. Equivalent circuit representing by eq. (5-19)

and eq. (5-20) is analysed. A dc equivalent circuit is constructed by combining all the average circuit equations and it is shown in Figure 60.

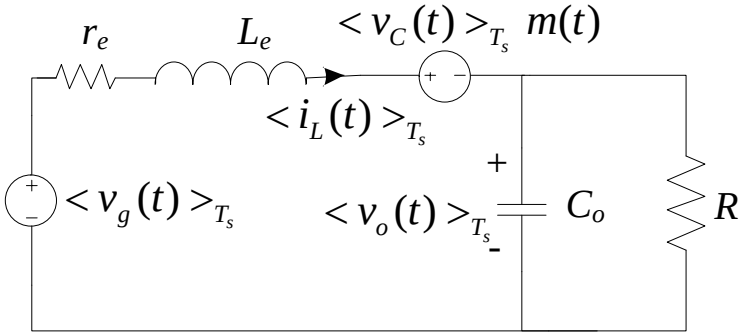

Figure 60. Circuit equivalent to inductor loop equation.

An equivalent circuit with the concept of ideal dc transformer for understanding the circuit operation for large signal is prepared and it is shown in Figure 61.

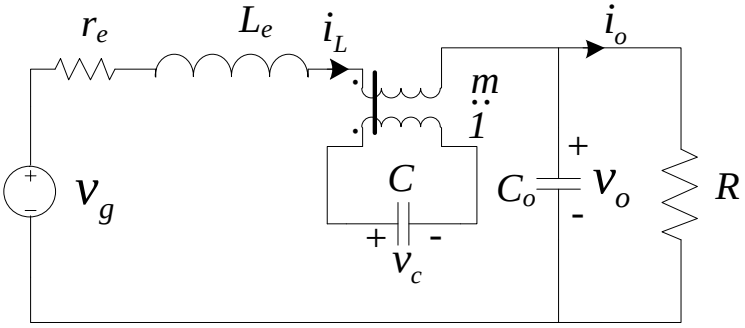

Figure 61. Equivalent circuit with ideal dc transformer.

5.3.1 Perturbation and Linearization

In the perturbation and linearization step, it is assumed that an averaged voltage or current consists of a constant (dc) component and a small-signal ac variation around the dc component is added. In general, the linearization step amounts to taking the Taylor expansion of a nonlinear relation and retaining only the constant and linear terms.

So far a nonlinear set of differential equations related to the ESI based rectifier is developed, and hence the next step is to perturb and linearize these differential

equations, to construct the converter small-signal ac equations which can be used to derive transfer function of the converter.

It is assumed that average value of the converter input voltage $v_g(t)$ and the modulation function $m(t)$ can be expressed as quiescent values plus small ac variations, as follows:

$$\begin{aligned} &< v_g(t) >_{T_s} = V_g + \hat{v}_g(t) \\ &m(t) = M + \hat{m}(t) \end{aligned} \qquad \textbf{5-21}$$

In response to these inputs, and after all transients have decayed, the average converter waveforms can also be expressed as quiescent values plus small ac variations:

$$\begin{aligned} &< i_L(t) >_{T_s} = I_L + \hat{i}_L(t) \\ &< v_c(t) >_{T_s} = V_c + \hat{v}_c(t) \\ &< v_o(t) >_{T_s} = V_o + \hat{v}_0(t) \end{aligned} \qquad \textbf{5-22}$$

With these substitutions, the large-signal averaged inductor equation becomes

$$L_e \frac{d\hat{i}_L(t)}{dt} = V_g + \hat{v}_g(t) - r_e I_L - r_e \hat{i}_L(t) - V_c M - V_c \hat{m}(t) - \hat{v}_c(t) M - \hat{v}_g(t)\hat{m}(t) - V_o - \hat{v}_o(t) \qquad \textbf{5-23}$$

$$C \frac{d\hat{v}_c(t)}{dt} = \hat{i}_L(t) M + I_L \hat{m}(t) + I_L M + \hat{i}_L(t)\hat{m}(t) \qquad \textbf{5-24}$$

As usual, this equation contains three types of terms. The dc terms contain no time-varying quantities. The first-order ac terms are linear functions of the ac variations in the circuit, while the second-order ac terms are functions of the products of the ac variations. Comparing DC terms, we get

$$V_c = \frac{V_g - r_e I_L - V_o}{M} \qquad \textbf{5-25}$$

Collecting first order linear terms, circuit equations become

$$L_e \frac{d\hat{i}_L(t)}{dt} = \hat{v}_g(t) - r_e \hat{i}_L(t) - V_c \hat{m}(t) - \hat{v}_c M - \hat{v}_o(t) \qquad \textbf{5-26}$$

$$C \frac{d\hat{v}_c(t)}{dt} = \hat{i}_L(t) M + I_L \hat{m}(t) \qquad \textbf{5-27}$$

From eq. (5-26) and eq. (5-27) an equivalent circuit in time domain is constructed and it is shown in Figure 62.

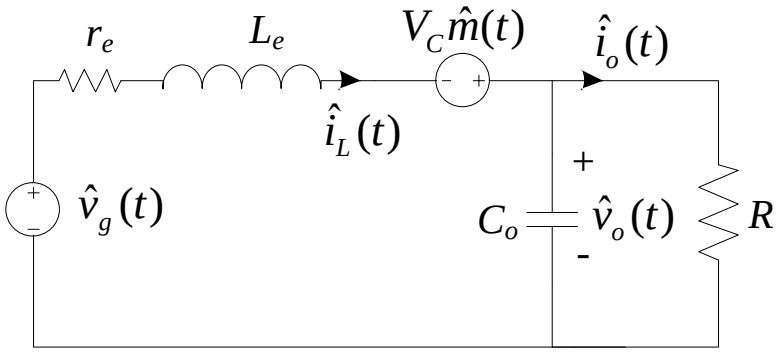

Figure 62. Equivalent circuit of ESI based rectifier in time domain.

From time domain equivalent circuit, by converting quantities from time (t) domain to frequency (s=jw) domain, one will get equivalent circuit in frequency domain and it is shown in Figure 63. In the frequency based equivalent circuit model the ESI based three-phase rectifier contains two independent ac input: the control input $\hat{m}(s)$ and, the line input $\hat{v}_g(s)$, and the output capacitor voltage disturbance is $\hat{v}_o(s)$.

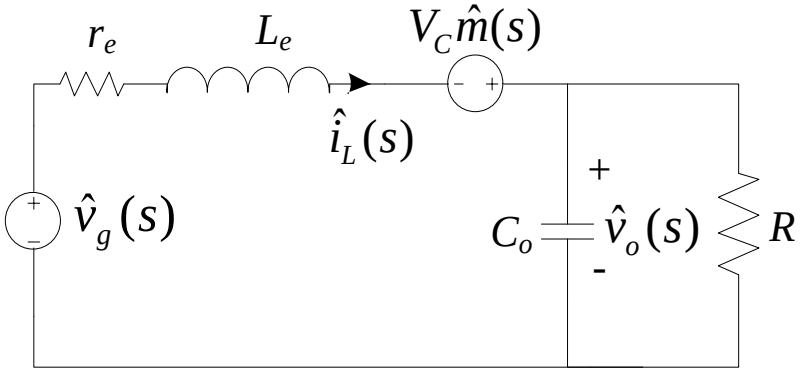

Figure 63. Equivalent circuit of ESI based rectifier in frequency domain.

5.4 Model parameters of the equivalent circuit

5.4.1 Selection of input line impedance

Input line impedance depends on various things such as distribution transformer connected in line or other equipment connected at point of common coupling (PCC). For verification of circuit behaviour it has been selected to 1 *mH* for each phase in this thesis for evaluation. Grid inductance varies from few hundreds of

μH to some mH, depending on no. of transformers connected in transmission and distribution system and their leakage inductances.

5.4.2 Selection of output capacitor

Output capacitor of 10 uF is constructed by putting two film capacitor of 5uF in parallel, these capacitors are rated to operate at 800V at 70 deg C and 700V at 80 deg C. High frequency ripple current will flow in the output capacitor of the ESI based rectifier. RMS current rating of each capacitor is 5A at 10 kHz and ESR value is 7mΩ, So the effective rms current rating of output capacitor is 10A and ESR value is 3.5 mΩ.

5.4.3 Selection of Inductor of ESI asymmetrical H-bridge

The average value of duty cycle is 0.5 and therefore the current stress on the active switches and diodes is equal to half of the rated current and this is explained in detail in [7]. For an output power of 4kW, the dc inductor is chosen to be 40 μH, it is calculated on the basis of maximum allowed ripple current of 20%. Effective ripple frequency will be twice of the switching frequency in case of phase shifted gate signals are applied to the active power semiconductors of the ESI asymmetrical H-bridge. By using phase-shifted gate signal a three level operation of the converter will be realized. Required inductance value of the ESI based converter is found by the following expression:

$$L_{DC} = \frac{\left(\frac{3}{2}\right)\hat{v}_i - (v_o - v_c)}{0.4 I_L \times 2 f_s} D_{\max} \qquad \textbf{5-28}$$

5.4.4 Selection of the ESI capacitor of asymmetrical H-bridge

The ESI capacitor C stores the energy corresponding to the ac portion of the diode bridge output voltage and its voltage has a ripple corresponding to six time the frequency of the mains to perform good regulation on output voltage of the ESI based rectifier.

For two level operations when both the active switches are turned ON together and turned OFF together at the same time, rms value of the current through ESI capacitor is equal to the ESI inductor current, but this current is ac in nature as against the inductor current. For low voltage rated capacitor ESR value is relatively higher and there will be significant losses in the ESI capacitor for two level operation of the ESI converter. The rms value of current through the ESI capacitor is given by the following expression [54]:

$$I_{C,rms} = I_L \cdot \sqrt{\frac{\hat{v}_g}{\bar{v}_c}} \cdot \sqrt{\frac{36}{\pi^2}\left[\sqrt{\frac{\pi^2}{9}-1} - \arctan\sqrt{\frac{\pi^2}{9}-1}\right]} \qquad \textbf{5-29}$$

For three level operation, rms value of the ESI capacitor current depends on the ratio of peak value of the diode rectified voltage and the ESI capacitor voltage. This expression of the rms value of the current flowing in the ESI capacitor can be simplified into the following:

$$I_{C,rms} = (0.186) I_L \cdot \sqrt{\frac{\hat{v}_g}{\bar{v}_c}} \qquad \textbf{5-30}$$

The reference voltage for the ESI capacitor *C* is selected to 70V, which is higher than the lower limit of the ESI voltage v_e. For 4 kW output power, rms value of the ESI capacitor is 3.91A. Current ripples depend on the PWM scheme used in control and it is discussed in detail in chapter 7.

The output capacitor is selected to be 10 μF, and ESI capacitor is 200 μF. There is one film capacitor of 0.22 uF is connected in parallel to electrolytic capacitor for the high frequency ripple components of the current. Dissipation factor of a film capacitor is very small and in order of 10^{-3}.

In the selection of ESI capacitor *C*, one should note that it stores the energy which is because of ripple on output voltage of three phase diode-bridge. ESI capacitor C is rated to be 150V because it will hold low voltage of 70V. Peak to peak voltage ripple depends on the full load current as it will work as buffer to store the energy which has frequency six times of the mains frequency. This

peak to peak voltage should not be more than 20 V, otherwise in lower voltage of the ESI capacitor, it will not able to construct the required voltage difference for ESI bridge.

5.5 Verification of the non-linear model of the ESI based three phase rectifier

In order to analyze front end performance of this drive, three phase rectifier is operated to resistive load, schematic of this circuit is presented in Figure 64. Input side is fed through a three phase grid connected to rectifier by a three phase auto transformer. Line impedance of such arrangement is represented by series connected resistance of r_g and inductance of L_g. Grid voltage is standard 400V line to line at frequency of 50 Hz. One auto transformer is used to make variable grid voltage. Different circuit parameters used in the ESI based three phase rectifier are given in Table 3.

Table 3. Circuit Parameters of the ESI based three phase rectifier.

Equivalent resistance, r_e	0.34 Ω
Equivalent inductance, L_e	2.04 mH
ESI Inductor, L_{dc}	40 μH
ESI Capacitor, C	200 μF
Output Capacitor, C_o	10 μF
Load Resistance, R_{Load}	71.5 Ω
Switching frequency, F_{sw}	70 kHz
ESI semiconductors ratings	200V/20A

This lab setup was operated by different input voltage conditions (400V, 300V and 200V line to line rms voltages) with resistive load of 127Ω after bypassing the ESI bridge. Bypass arrangement was created with the help of an electronic

relay. Circuit schematic of the test arrangement of standard three phase diode bridge is shown in Figure 64.

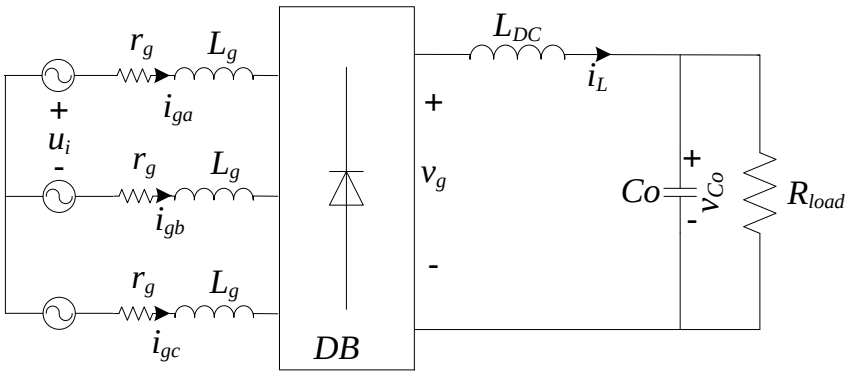

Figure 64. Three phase rectifier operating with resistive load.

Response of the output DC-link voltage is shown in Figure 65. The output DC-link voltage v_{Co} has 300 Hz ripple in its waveform. Peak to peak ripple in output voltage is close to 15%. Similar circuit was simulated in MATLAB with the help of PLECS circuit simulator. Value of resistance of r_g and inductance of L_g were selected as 0.1Ω and $1mH$, obtained results of output voltage is presented in Figure 66.

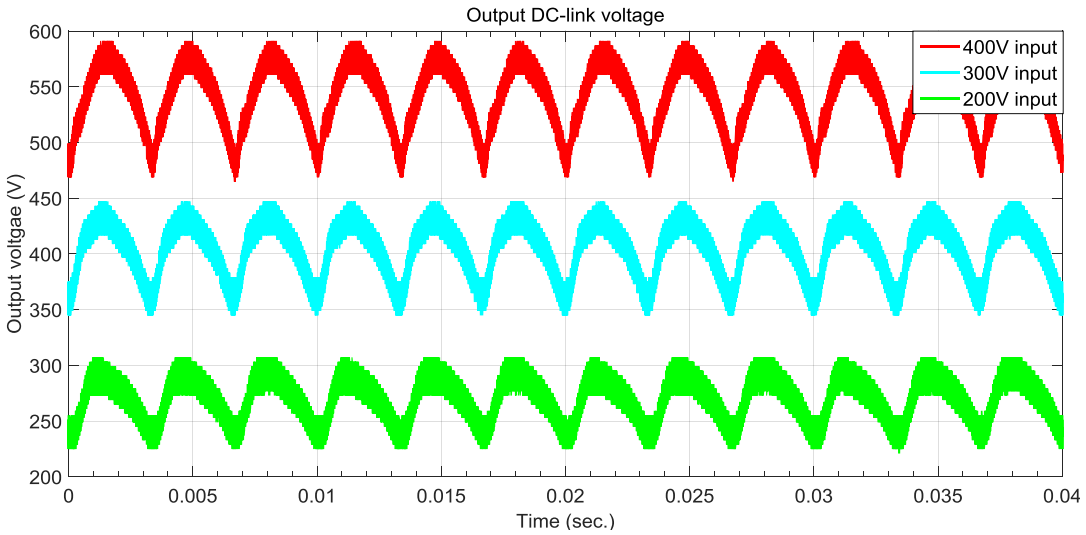

Figure 65. DC link voltage at different input voltage conditions from lab setup.

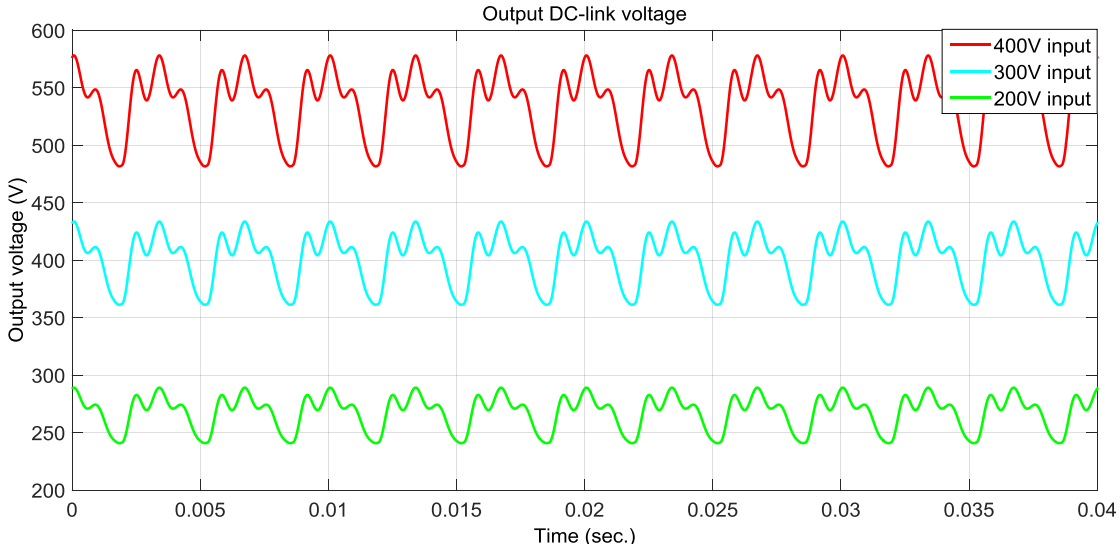

Figure 66. DC link voltage at different input conditions from non-linear PLECS simulation model.

In simulation results along with 300Hz ripple there are high frequency ripples, which are corresponding to resonating frequency of output capacitor and input inductor. It should be noted that peak to peak ripple matches very closely in experimental result and simulated result.

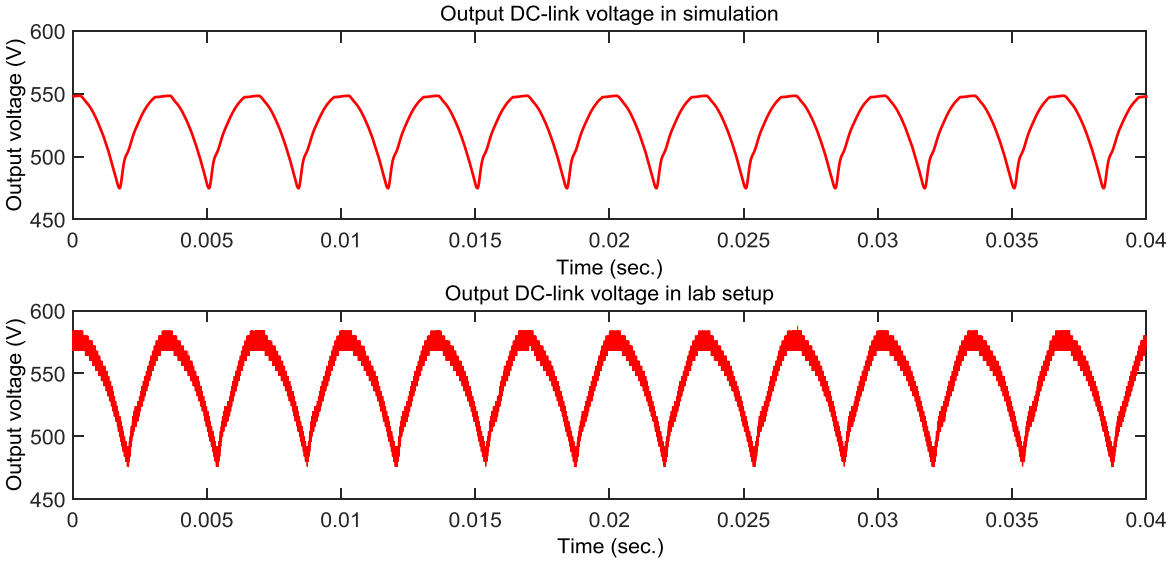

Figure 67. Verification of DC link voltage with higher damping.

In order to get rid of high frequency ripple in output voltage, grid inductance is increased from $1mH$ to $8mH$ and grid resistance also increased from 0.1Ω to 0.8Ω

to achieve better damping. In experimental setup one auto transformer was connected in between the grid and diode-bridge based rectifier.

In this situation which is shown in Figure 67., although high frequency ripples are disappeared but peak to peak voltage ripple increased from 15% to 25%. Similar measurements and simulations have been performed on inductor current in three different input conditions.

Although Output voltage of lab setup contains only 300Hz ripple, but inductor current has very small and much damped high frequency ripples, it can be seen very clearly in Figure 68.

When simulation results obtained from increased value of grid impedance peak to peak ripple in inductor current increased significantly and high frequency ripples were eliminated totally. Verification of the circuit model for the inductor current is shown in Figure 68.

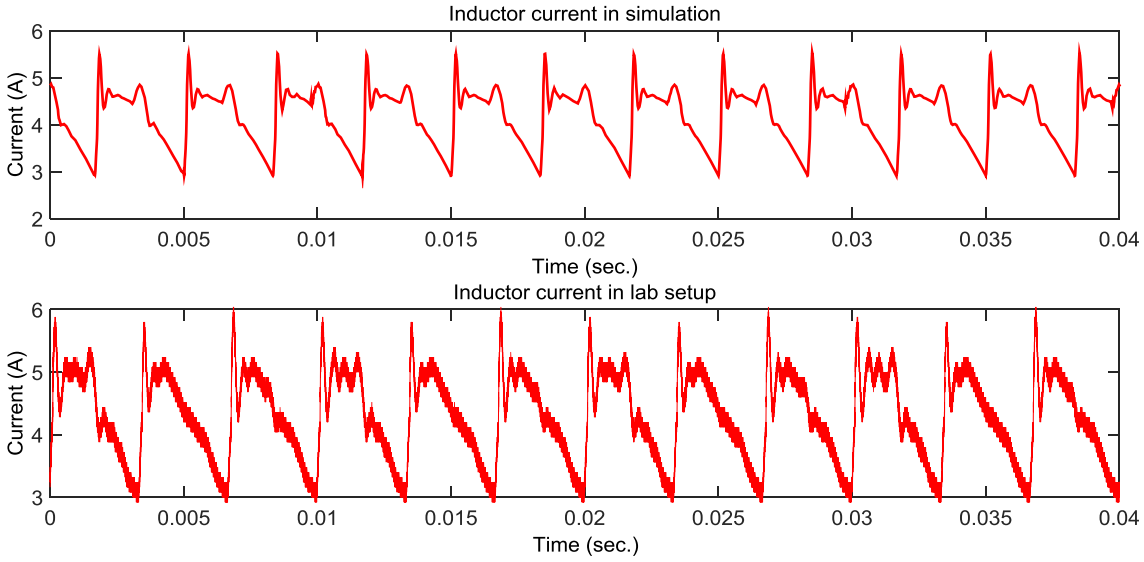

Figure 68. Verification of inductor current with higher damping in grid side.

Response of the inductor current is very similar in non-linear simulation model and lab prototype. The non-linear simulation circuit model was operated at different input voltages and response of the output voltage is shown in Figure 69. As compared to earlier response of Figure 67., now high frequency terms

from the output voltage are disappeared. Peak to peak voltage ripple is now increased 15% to 30%. Now simulation results matches to experimental results as obtained in Figure 65.

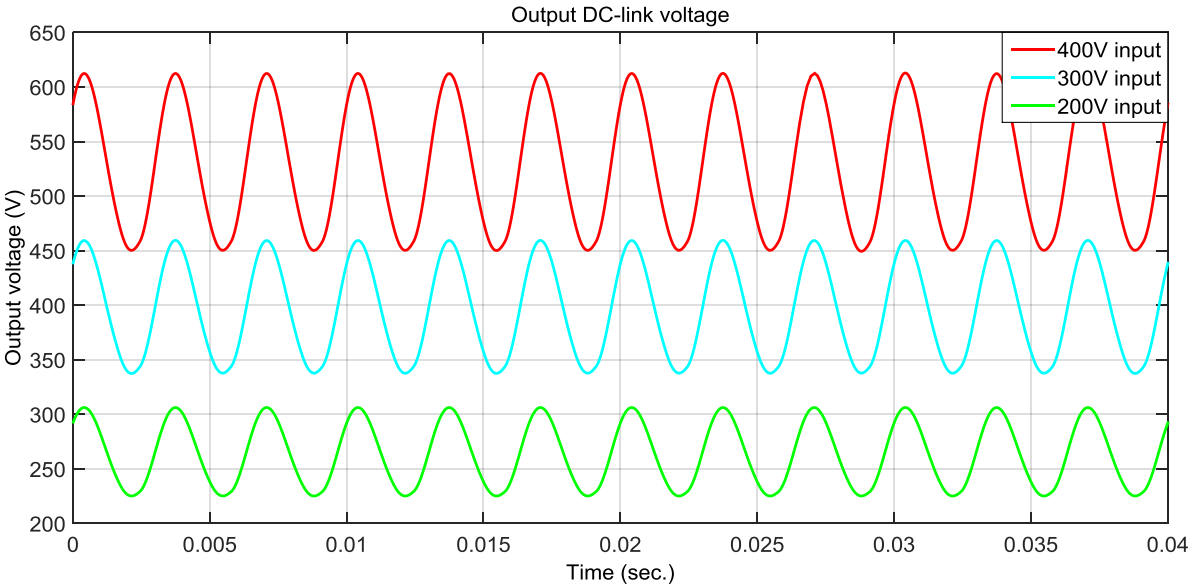

Figure 69. DC-link voltage at different input conditions from PLECS simulation model with high damping.

Response of the inductor current in this situation of different input voltages is shown in Figure 70.

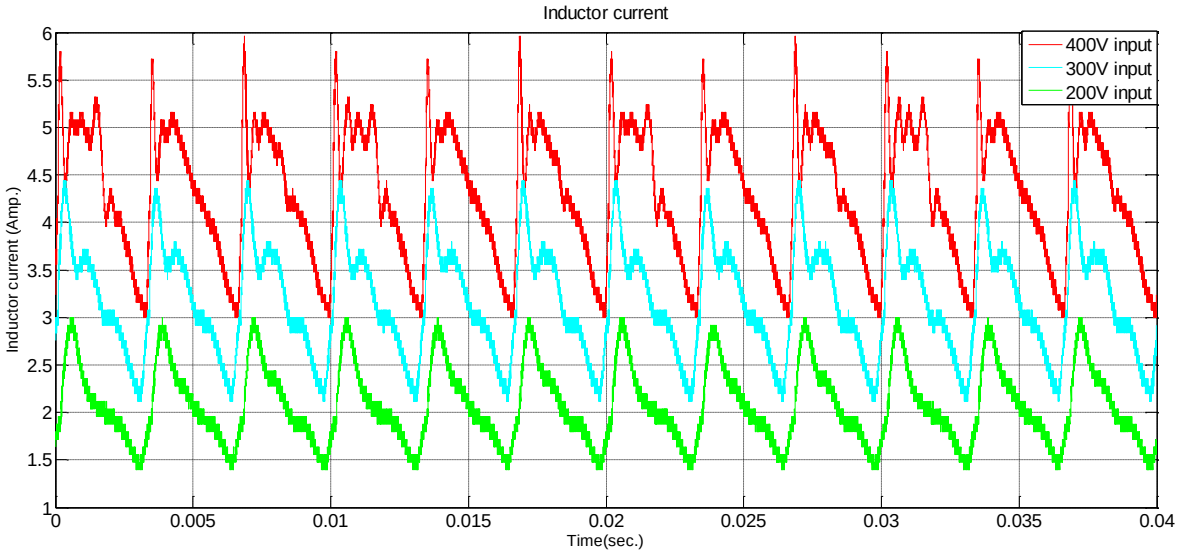

Figure 70. Inductor current at different input conditions from lab setup.

At lower voltage high frequency components in inductor current are not dominating, but at high input voltage condition, they can be clearly seen. Response of the inductor current in non-linear simulation model without additional inductor is presented in Figure 71.

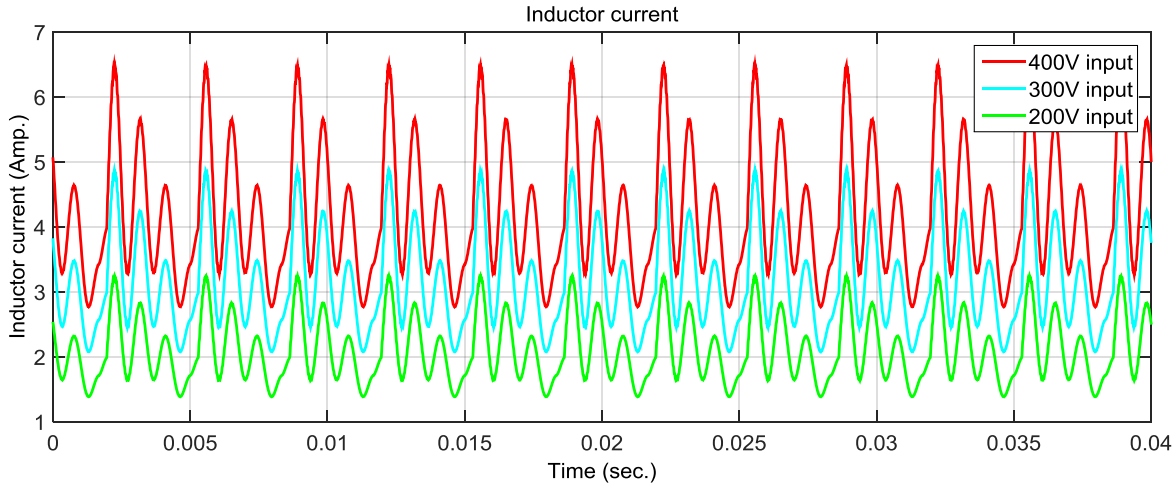

Figure 71. Inductor current at different input conditions from PLECS simulation model without additional line side inductor.

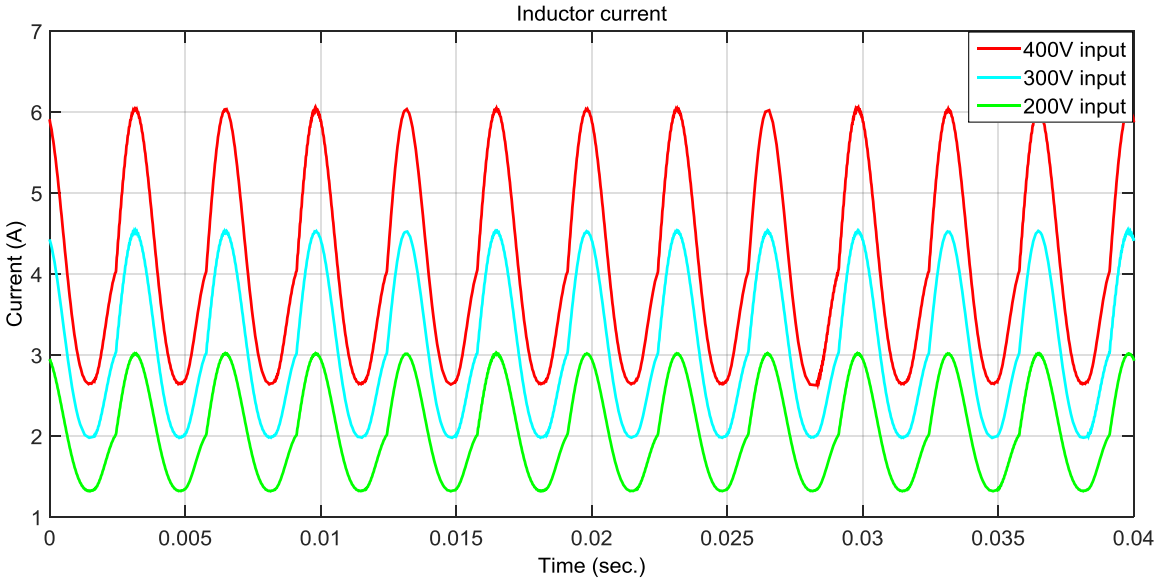

Figure 72. Inductor current at different input conditions from PLECS simulation model with additional line side inductors.

This response is at lower damping and contains high frequency terms and to get rid of these terms one should increase damping. After improving damping by

introducing more resistance in grid impedance, improved response of the inductor current in non-linear PLECS circuit model is shown in Figure 72.

In order to analyze behaviour of this circuit topology of the ESI based power converter, a lab prototype has been build and plugged in a commercially available standard drive. When modulating signals, which used to generate gate pulses for MOSFETs of ESI are generated from a fixed frequency and magnitude level, similar response is observed from the power converter.

In Figure 73, modulation signal was 25Hz sine wave with amplitude of 0.1. It can be seen clearly that ESI capacitor follows the similar behaviour in voltage.

Similar signal is passed to simulation circuit and it was observed that although frequency of ESI capacitor voltage is same but its magnitude is not same, it can be seen in Figure 74. It is also seen that in Lab setup ESI capacitor voltage was with an offset. Ripple in ESI capacitor voltage seems to be same magnitude. In lab setup there is dead-band in gate pulses of two MOSFETs of the same leg of the ESI bridge, it may be a reason why voltage is with an offset. In lab setup four MOSFETs were placed in the circuit, although only the diodes of two MOSFETs were used in the operation of the circuit.

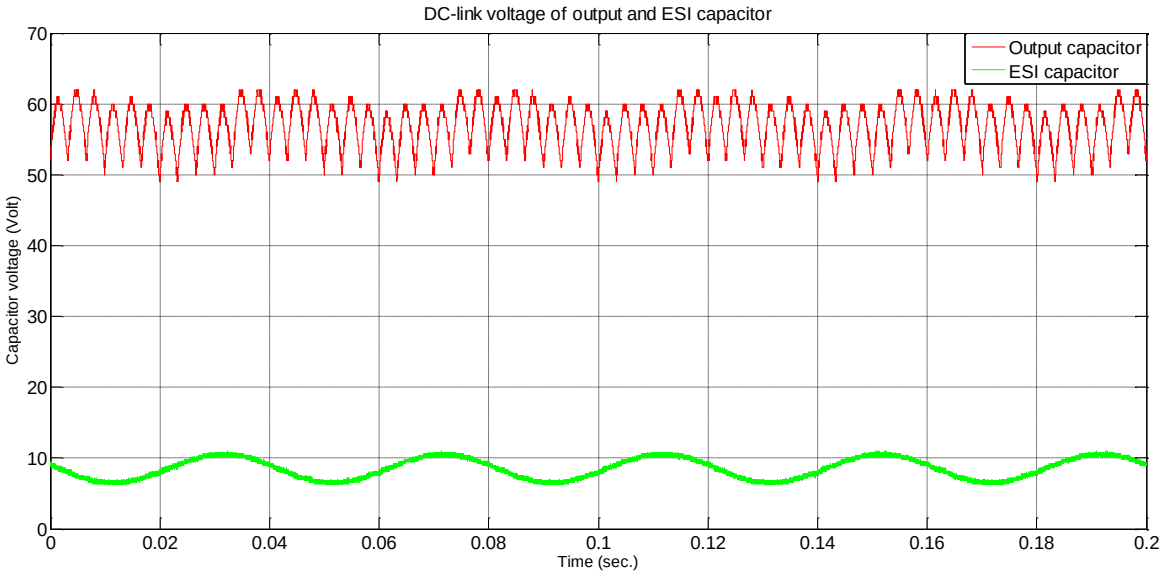

Figure 73. DC-link voltage of output and ESI capacitor.

When frequency of modulating signal is increased from 25Hz to 50Hz peak to peak ripple in ESI capacitor voltage reduced. This effect can be seen in both experimental and simulated results which are presented in Figure 75., and Figure 76., for 50 Hz sinusoidal modulating signal used in experimental and simulation respectively. Response of the ESI capacitor voltage is mot matching each other.

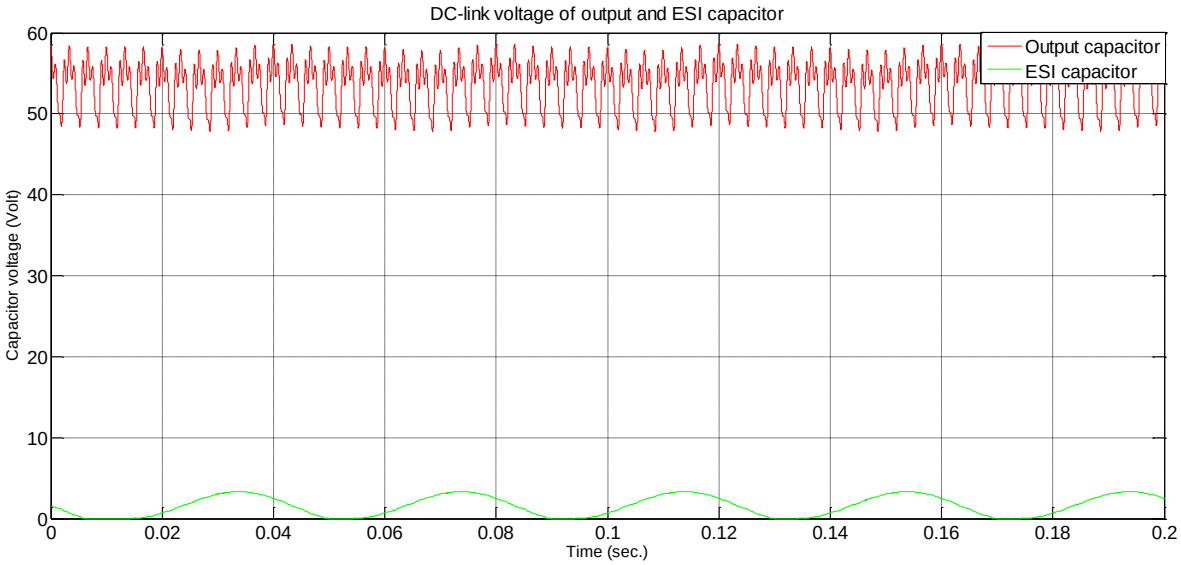

Figure 74. DC-link voltage of output and ESI capacitor in PLECS simulation.

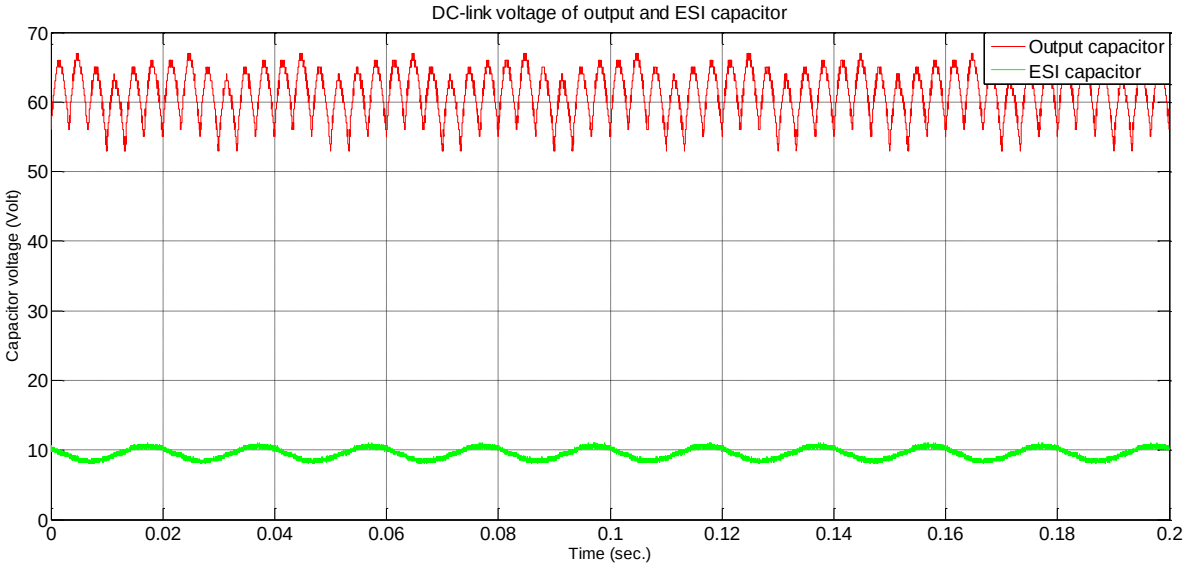

Figure 75. DC-link voltage of output and ESI capacitor.

If Dead-band compensation of the active switches is included in modulating signal than the inductor current waveform looks very similar to simulating result and it is shown in Figure 77.

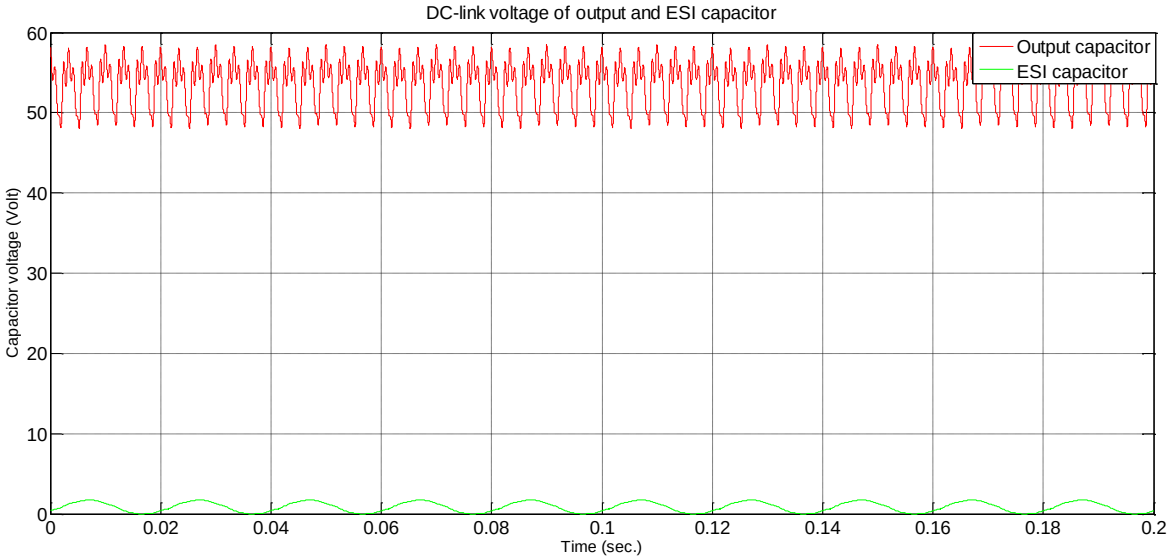

Figure 76. DC-link voltage of output and ESI capacitor in PLECS simulation.

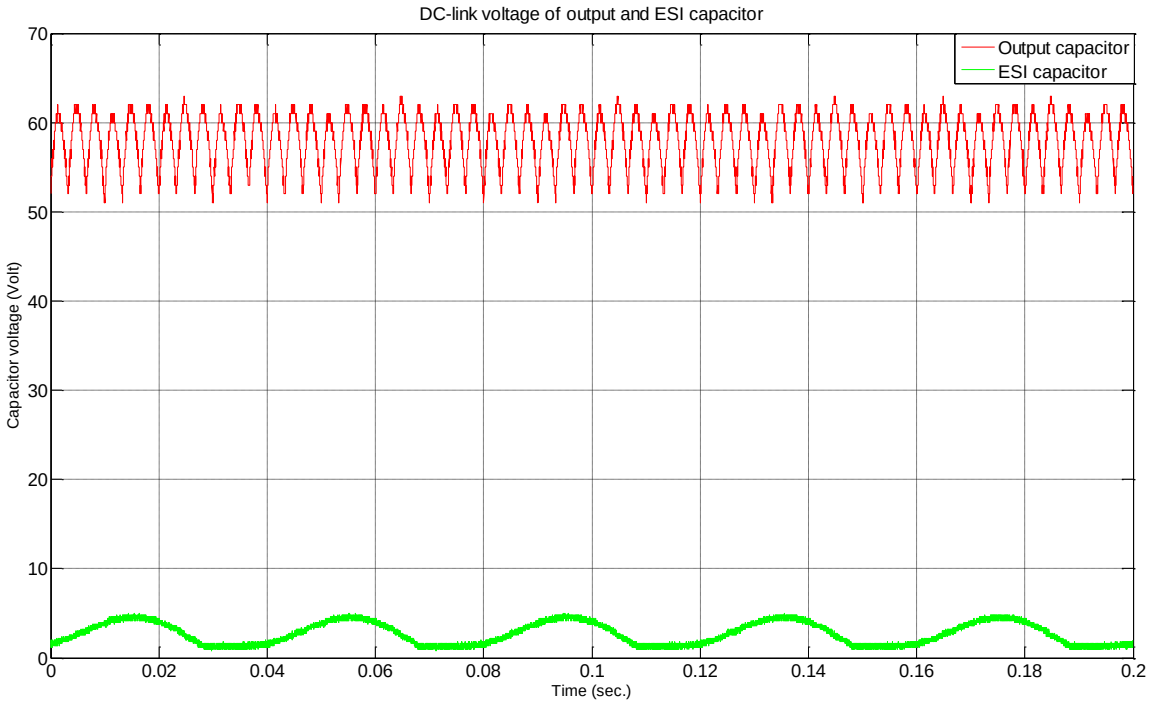

Figure 77. DC-link voltage of output capacitor and the ESI capacitor with dead-time compensation.

Modulating signal in lab setup was tested with an offset of 0.13. One should note here, now experimental results match with simulation very closely. It verifies the non-linear circuit model of the ESI converter in PLECS is closely representing the actual circuit.

When extra inductance of 3mH is inserted at input side of rectifier then peak value of inductor current is increased and resonating frequency is decreased. The inductor current with and without an external inductance of 3mH in the individual phases of the mains is shown in Figure 78. With introduction of an additional inductances in the mains high frequency components of the inductor current are very well damped.

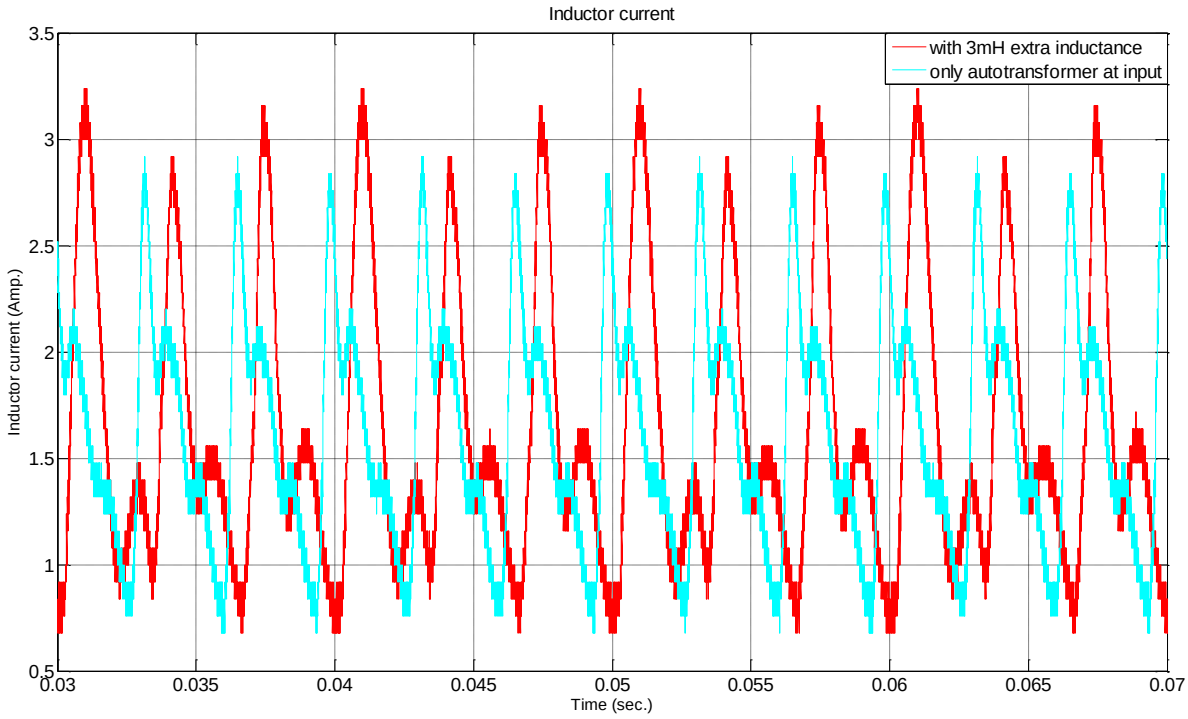

Figure 78. Inductor current with and without external inductance of 3*mH* in mains.

A three phase 400V line to line voltage source was used in non-linear simulation model and experimental test set-up. An external three phase inductor of 3mH per phase has been inserted between the grid and the front end of the system. These additional inductors are inserted to minimize the effect of grid imped-

ance, as this impedance value is higher than the grid impedance. Experimental test results are stored in data format and reproduced with the help of MATLAB.

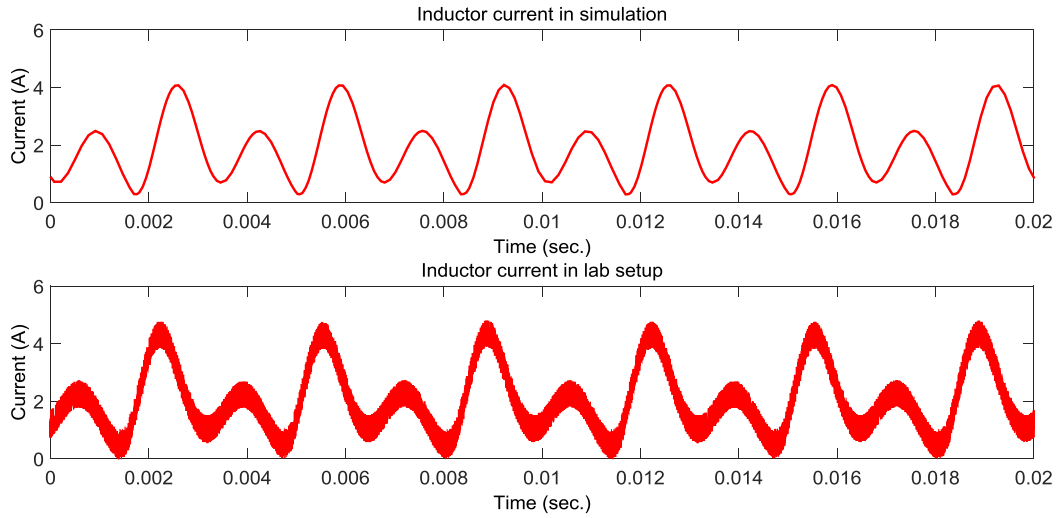

Figure 79. Inductor current in simulation and lab setup with external inductance of 3*mH* in mains.

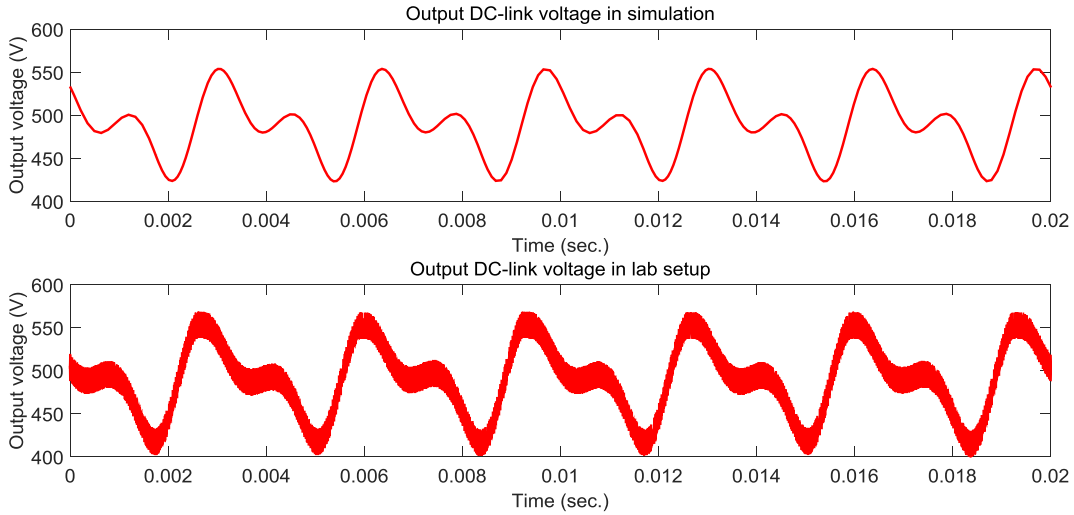

Figure 80. Output voltage in simulation and lab setup with external inductance of 3*mH* in mains.

In Figure 79. and Figure 80., both the inductor current and the output voltage are same in shape and magnitude in the simulation model and the experimental lab setup. Damping in experimental setup is slightly higher than the simulation results of both the output voltage and the inductor current.

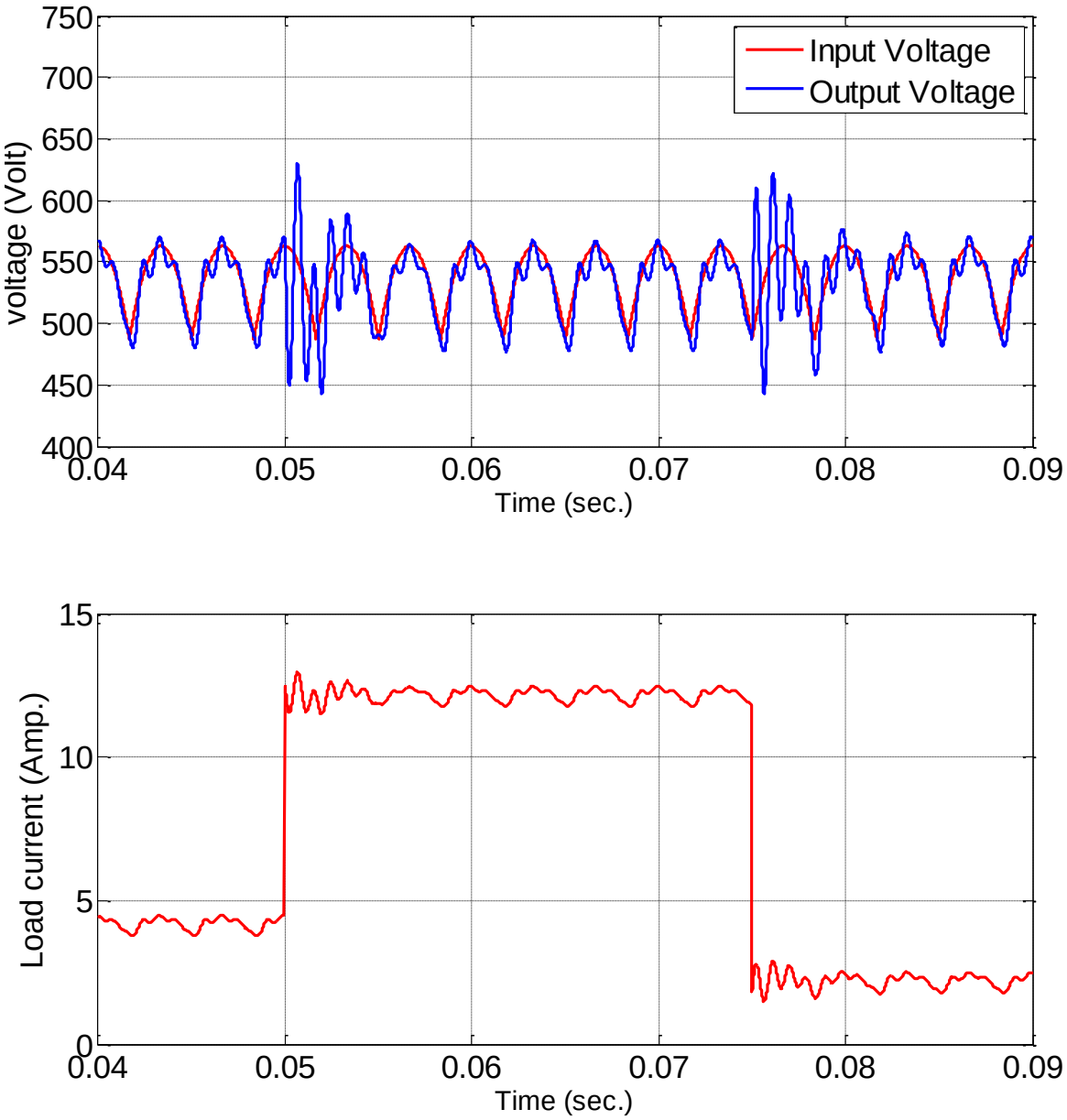

Figure 81. Step load on uncontrolled three phase rectifier without ESI.

A load step response of a three phase standard rectifier is shown in Figure 81. Step in load is performed from 4A to 12A at time instant t=0.05sec, and from 12A to 2A at time instant t=0.075 sec in the simulation. The output voltage shows natural response of a second order system and it takes long time to come back in steady state.

5.6 Summary and conclusion

Since most of the power electronics based switching converters are nonlinear systems, it is desirable to construct small-signal linearized models to have a better understanding of its behaviour. This task is accomplished by perturbing and linearizing the averaged model about a quiescent operating point. When the switches are the only time-varying elements in the power converter, then circuit averaging affects only the switch network of the converter.

Based on different switching states of the ESI based rectifier, a small signal and a large signal equivalent circuit is prepared. This equivalent linear circuit model paves a way forward to find out different transfer functions of the ESI based three-phase rectifier stage of the drive and allows the design of control scheme.

In next two chapters transfer functions and control will be presented, and then response of controlled circuit will be presented.

Chapter 6. Transfer functions of the ESI based rectifier

6.1 Background

An objective of this chapter is the construction of Bode plots of the important transfer functions of the ESI based three phase rectifier. A Bode plot is a plot of the magnitude and phase of a transfer function or other complex-valued quantity, vs. frequency. Magnitude in decibels, and phase in degrees, are plotted vs. frequency, using semilogarithmic axes.

The magnitude plot is effectively a log-log plot, since the magnitude is expressed in decibels and the frequency axis is logarithmic. The Bode diagram of a transfer function containing several pole, zero, and gain terms, can be constructed by simple addition. At any given frequency, the magnitude (in decibels) of the composite transfer function is equal to the sum of the decibel magnitudes of the individual terms. Likewise, at a given frequency the phase of the composite transfer function is equal to the sum of the phases of the individual terms.

6.2 Reduced circuit model of the ESI based rectifier

The small-signal equivalent circuit model of the converter from previous chapter is shown in Figure 62. Two equivalent circuits of ESI topology one with ideal dc transformer and another small signal ac average circuit model are shown in Figure 82. In the equivalent circuit m is modulation signal which is used to generate gate pulses for T_1 and T_2. If D is duty cycle of T_1 and T_2 then value of m will be $1\text{-}2D$. This modulation index is similar to the full bridge inverter. Value of ESI capacitor C is much higher than the output capacitor C_o, and in one

switching period ESI capacitor C is subjected to charging and discharging both, therefore its voltage v_c is considered as constant and $\overline{v}_c$, while deriving the transfer functions for the output voltage v_o and the inductor current i_L. Control objective is to reduce the ripple of output capacitor voltage and to make the inductor current to a constant value which is equal to the load current. In Figure 82(b), a linearized small signal equivalent circuit is presented. From the linearized equivalent circuit transfer functions for the output voltage and the inductor current have been derived.

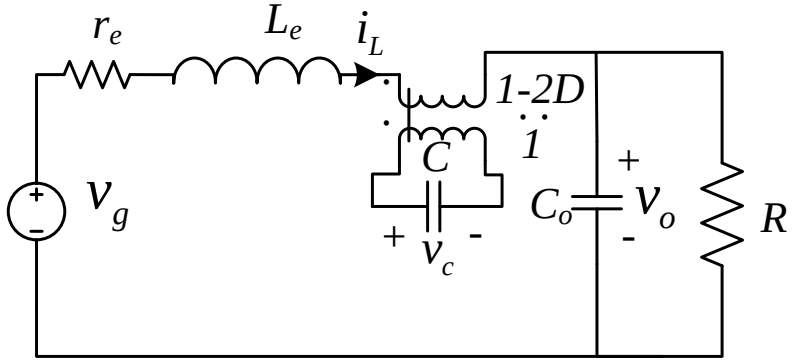

(a) Circuit with ideal dc transformer

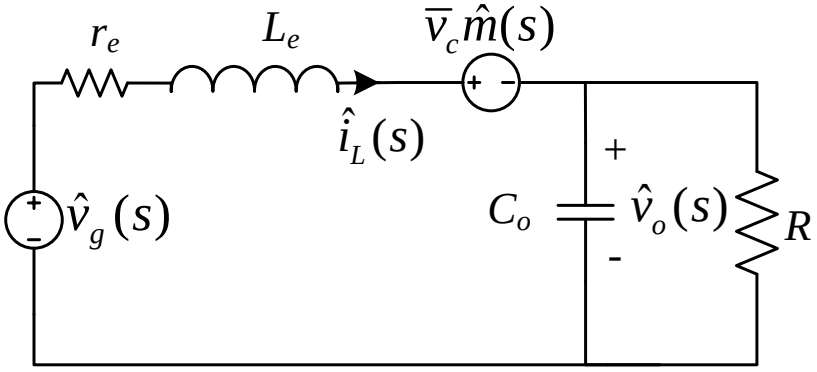

(b) Small signal ac equivalent circuit

Figure 82. Equivalent circuits of ESI based rectifier.

Where M is input as modulation signal which is function of duty cycle for active switches T_1 and T_2. v_g is equivalent voltage, r_e and L_e are equivalent resistance and inductance. Small signal ac model of the ESI based three-phase rectifier is

shown in Figure 83. This is simplified linear circuit and will be used to find out different transfer functions.

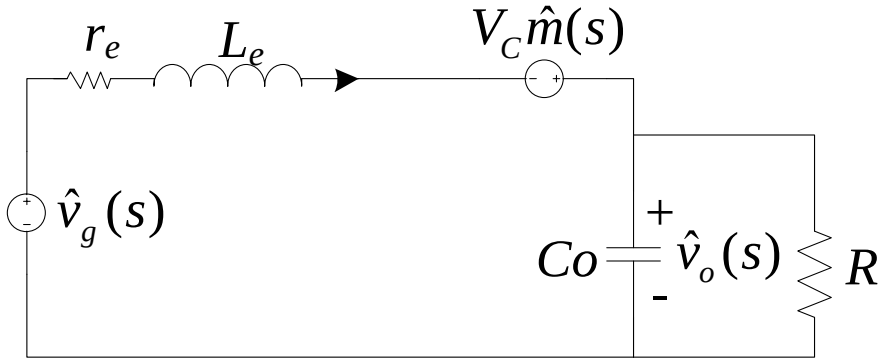

Figure 83. Small signal circuit representation of ESI.

6.3 Derivation of converter open loop transfer functions

Small signal ac model of the ESI based three-phase rectifier contains two independent ac input variations: control input $\hat{m}(s)$, and line input $\hat{v}_g(s)$.

The ac output voltage variations of the output capacitor voltage $\hat{v}_o(s)$ can be expressed as the superposition of terms arising from these two independent inputs:

$$\hat{v}_o(s) = G_{vg}(s)\hat{v}_g(s) + G_{vm}(s)\hat{m}(s) \qquad \textbf{6-1}$$

Hence, the transfer functions $G_{vg}(s)$ and $G_{vm}(s)$ can be defined as:

$$G_{vg}(s) = \left.\frac{\hat{v}_o(s)}{\hat{v}_g(s)}\right|_{\hat{m}(s)=0} \qquad \textbf{6-2}$$

$$G_{vm}(s) = \left.\frac{\hat{v}_o(s)}{\hat{m}(s)}\right|_{\hat{v}_g(s)=0} \qquad \textbf{6-3}$$

In above equation, $G_{vg}(s)$ is called input (line) to output voltage transfer function whereas $G_{vm}(s)$ is called control to output voltage transfer function.

6.3.1 Input to output voltage transfer function

The input to output transfer function $G_{vg}(s)$ is found by setting control input control input $\hat{m}(s)$ variations to zero, and then solving the circuit for the transfer function from reduced circuit as shown in Figure 84. Transfer function $G_{vg}(s)$ is calculated by solving this simple circuit using standard circuit equations.

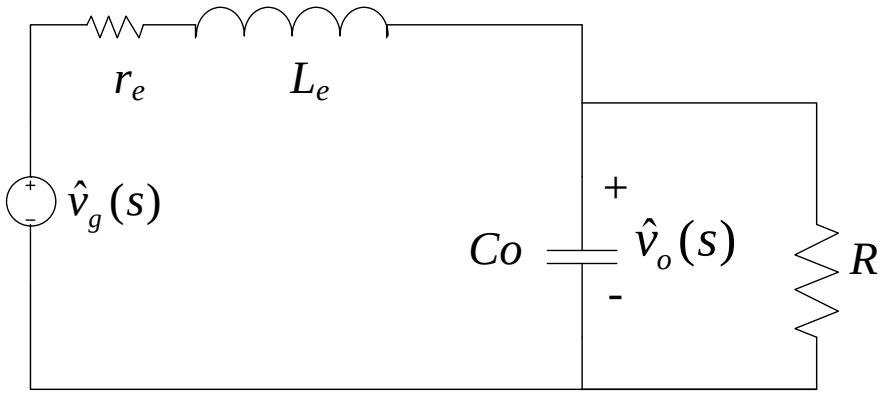

Figure 84. Manipulation of circuit to find input to output voltage transfer function.

$$G_{vg}(s) = \left.\frac{\hat{v}_o(s)}{\hat{v}_g(s)}\right|_{\hat{m}(s)=0} = \left(\frac{R}{s^2 L_e RC_o + s(L_e + r_e RC_o) + r_e + R}\right) \qquad \textbf{6-4}$$

This transfer function describes how variations or disturbances in the applied input voltage $\hat{v}_g(s)$ lead to disturbances in the output voltage $\hat{v}_o(s)$.

It is important in design of an output voltage regulator to control the output capacitor voltage in the specified limits.

Step response of $G_{vg}(s)$ is shown in Figure 85. In the beginning a large step of 95% of the rectified dc voltage (540V) was given, then at t=0.05 sec, additional small step of 5% of the rectified dc voltage was provided to transfer function. Transfer function $G_{vg}(s)$ is second order function with double pole and its step response also confirms the same.

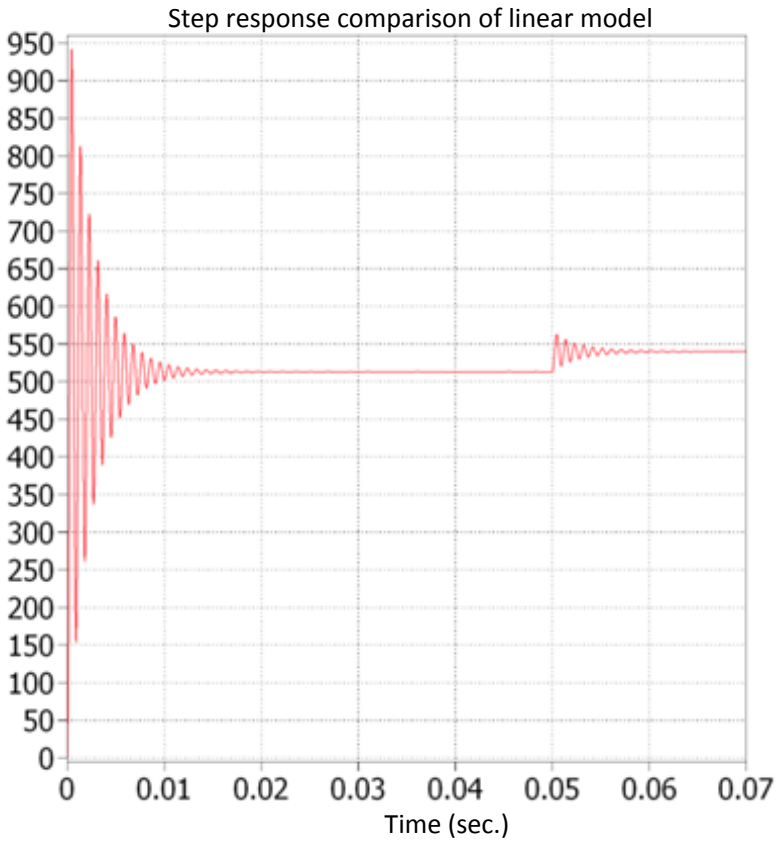

Figure 85 Step response of input to output voltage transfer function (G_{vg}) with large and small step at two different time instance.

6.3.2 Control to output voltage transfer function

The control to output voltage transfer function $G_{vm}(s)$ is found by setting line input variations $\hat{v}_g(s)$ to zero, and then solving for the transfer function from reduced circuit as shown in Figure 86.

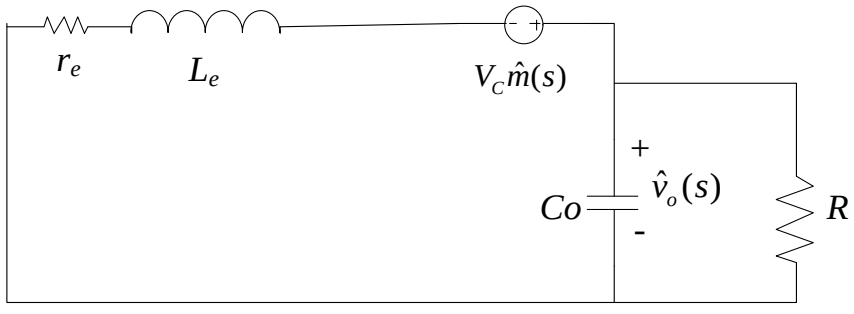

Figure 86. Manipulation of circuit to find control to output voltage transfer function.

$$G_{vm}(s)=\left.\frac{\hat{v}_o(s)}{\hat{m}(s)}\right|_{\hat{v}_g(s)=0}=(-\bar{v}_c)\left(\frac{R}{s^2L_eRC_o+s(L_e+r_eRC_o)+r_e+R}\right) \quad \textbf{6-5}$$

This transfer function describes how control input $\hat{m}(s)$ variations influence the output voltage. In an output voltage regulator system, $G_{vm}(s)$ is a key component of the loop gain and has a significant effect on regulator performance.

Control to output voltage transfer function $G_{vm}(s)$ is similar to line to output transfer function $G_{vg}(s)$ in nature, although its gain is different. Response of control to output transfer function $G_{vm}(s)$ will be similar to line to output voltage transfer function in nature but in this case step will be very small as value of control parameter can vary from -1 to +1 only.

Inductor current i_L is another state variable, which need to be controlled in order to achieve rectangular current from mains. Now, transfer function of inductor current will be investigated. To find these transfer functions, variations of the inductor current, $\hat{i}_L(s)$ can be expressed as the superposition of terms arising from these two inputs:

$$\hat{i}_L(s)=G_{ig}(s)\hat{v}_g(s)+G_{im}(s)\hat{m}(s) \quad \textbf{6-6}$$

Hence, the transfer functions $G_{ig}(s)$ and $G_{im}(s)$ can be defined as:

$$G_{ig}(s)=\left.\frac{\hat{i}_L(s)}{\hat{v}_g(s)}\right|_{\hat{m}(s)=0} \quad \textbf{6-7}$$

$$G_{im}(s)=\left.\frac{\hat{i}_L(s)}{\hat{m}(s)}\right|_{\hat{v}_g(s)=0} \quad \textbf{6-8}$$

In above equation, $G_{ig}(s)$ is called input to inductor current transfer function whereas $G_{im}(s)$ is called control to inductor current transfer function.

6.3.3 Input to inductor current transfer function

The input-to-inductor current transfer function $G_{ig}(s)$ is found by setting line input variations $\hat{m}(s)$ to zero, and then solving for the transfer function from the manipulated circuit as shown in Figure 87.

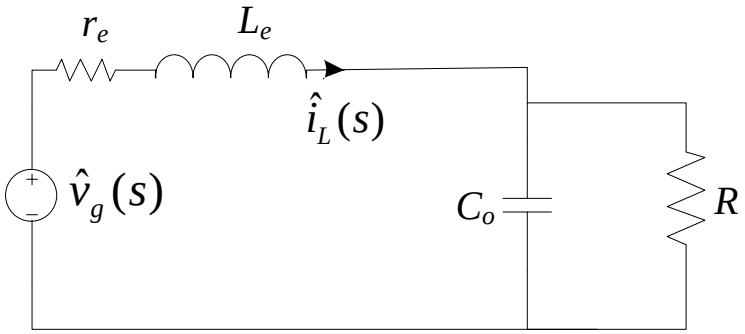

Figure 87. Manipulation of circuit to find input to inductor current transfer function.

$$G_{ig}(s) = \left.\frac{\hat{i}_L(s)}{\hat{v}_g(s)}\right|_{\hat{m}(s)=0} = \left(\frac{sRC_o + 1}{s^2 L_e RC_o + s(L_e + r_e RC_o) + r_e + R}\right) \qquad \textbf{6-9}$$

6.3.4 Control to inductor current transfer function

The control-to-inductor current transfer function $G_{im}(s)$ is found by setting line input variations $\hat{v}_g(s)$ to zero, and then solving for the transfer function from reduced circuit as shown in Figure 88.

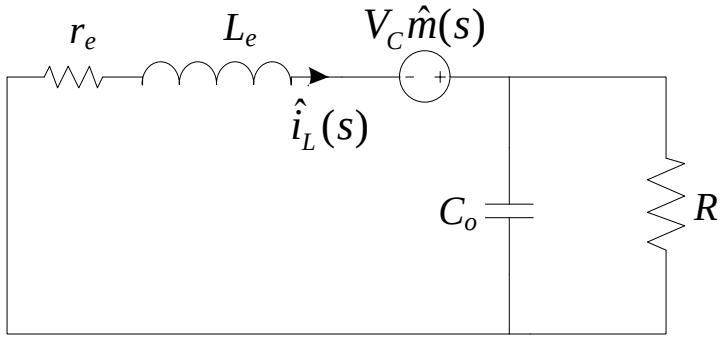

Figure 88. Manipulation of the equivalent circuit for control to inductor current transfer function.

$$G_{im}(s) = \frac{\hat{i}_L(s)}{\hat{m}(s)}\bigg|_{\hat{v}_g(s)=0} = (-\bar{v}_c)\left(\frac{sRC_o + 1}{s^2 L_e RC_o + s(L_e + r_e RC_o) + r_e + R}\right) \qquad \textbf{6-10}$$

The Linear mathematical model of the ESI based converter is constructed from different transfer functions and shown in Figure 89.

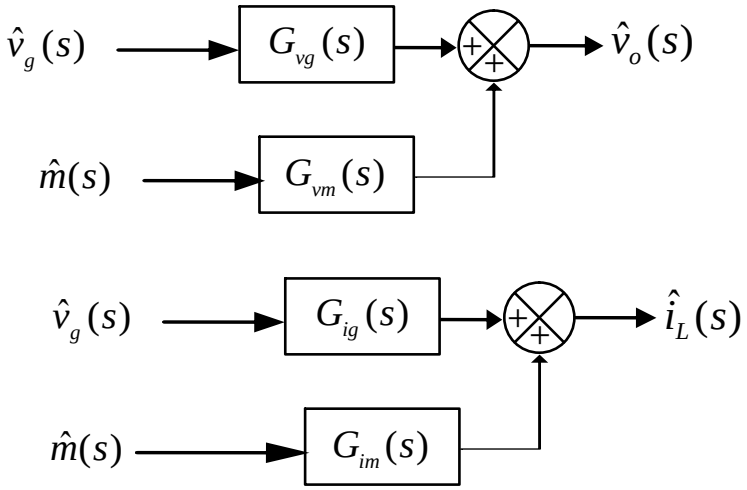

Figure 89. Block representation of open loop transfer functions.

This model has two inputs, one from input(mains) and another from control(modulation index). This model contains different transfer functions derived earlier in this chapter. The load current i_o, is derived by from the linear relationship of the output voltage and the load current. The current through the ESI capacitor C can be calculated by the equivalent circuit as it is multiplication of inductor current and the modulation function of the ESI. To get a linear function, the average value of the inductor current is assumed to be equal to the average load current I_o. It is a fair assumption as there is no loss of energy in the output capacitor in ideal case. To calculate the voltage across the ESI capacitor, linear relationship of its voltage and current has been used.

For simplicity, the load side disturbances and its effects have not been considered for designing the control, if it is needed to include them, those disturbances can be accommodated by adding these to the transfer functions. Load connected to output capacitor affects the steady state and transient behavior of circuit.

If disturbance of load side need to take care, then block diagram of circuit in open loop, will be modified as shown in Figure 90. This model has three inputs, one from mains, one from the control and other form the load side disturbances. In this model G_{vo} and G_{io} are the transfer functions for the load disturbances to the output voltage and the inductor current respectively.

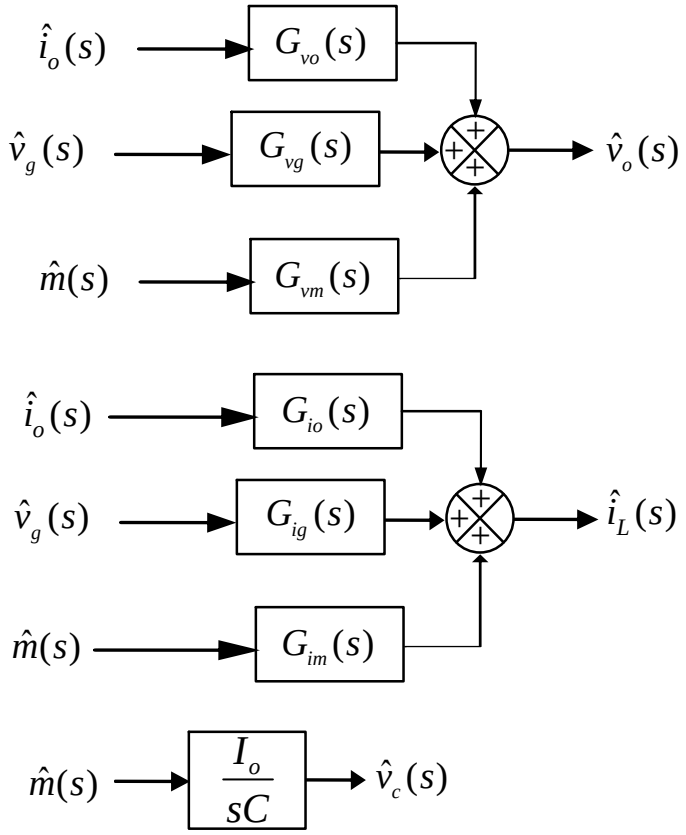

Figure 90. Block representation of transfer functions after including the load side disturbances.

6.4 Summary and conclusion

In this chapter transfer functions of the ESI based three-phase rectifier are derived from the small signal ac circuit model. This small signal ac circuit model was constructed with the help of state space averaging technique. Based on these transfer function a linear mathematical model is constructed. This model will be useful to develop a control scheme in order to achieve control objective.

In next chapter control scheme of the ESI based three-phase rectifier will be discussed.

Chapter 7. Control of electronic smoothing inductor

7.1 Background

For the ESI based rectifier, voltage control has to be performed such that the output voltage v_o is equal to the dc component of the diode bridge output voltage v_g, i.e., that the global average value of v_e (with reference to the fundamental component) is controlled to zero. A two-stage control is applied where the duty-cycle of the switch is determined by an inner current control loop and the constant dc output voltage by a superimposed voltage control.

In all switching converters, the output voltage is a function of the input line voltage the duty cycle, and the load current as well as the converter circuit element values. Stability is another important issue in feedback systems. Adding a feedback loop can cause an otherwise well-behaved circuit to exhibit oscillations, ringing and overshoot, and other undesirable behaviour. An in-depth treatment of stability is not considered in this thesis; however, the simple phase margin criterion for assessing stability is used here. When the phase margin of the loop gain is positive, then the feedback system is stable. Moreover, increasing the phase margin causes the system transient response to be better behaved, with less overshoot and ringing. It is well known that adding a feedback loop can cause an otherwise stable system to become unstable [63-65]. Even though the transfer functions of the original converter, as well as of the loop gain *T(s)*, contain no right half-plane poles, it is possible for the closed-loop transfer functions to contain right half-plane poles. The feedback loop then fails to regulate the system at the desired quiescent operating point, and oscillations are

usually observed. It is important to avoid this situation. And even when the feedback system is stable, it is possible for the transient response to exhibit undesirable ringing and overshoot.

7.2 Control scheme

Let's now consider how to design a regulator system, to meet specifications or design goals regarding rejection of disturbances, transient response, and stability. Two different control schemes have been discussed in this section.

7.2.1 Two level Hysteresis control

A calculation of the losses based on the relationships given in the previous section results for the switch-mode stage on total in less than 1% of the rectifier output power. Without any counter-measures these losses would have to be covered by an auxiliary power supply feeding the DC link voltage v_c. However, by application of a proper control it is possible to cover the losses out of the power flow through the electronic smoothing stage. The hysteresis control is shown in Figure 91. The loss compensation value P, which is the gain for the current control, is adjustable in order to control the current shape of I_L. A high P-value produces a low six times mains frequency current ripple on the DC-link.

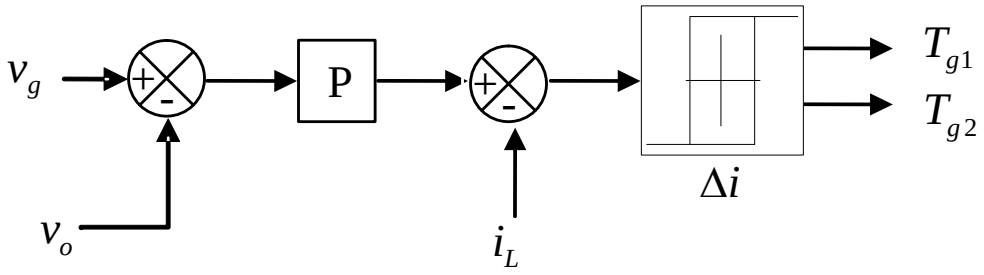

Figure 91. Two level hysteresis control.

In this simulation, the current flowing to the ESI is limited to within ±5% by the hysteresis control. Therefore, the drawbacks of the hysteresis control are variable switching frequency, which brings difficulties in design and/or attenuate switching ripple. With this simple control no free-wheeling states are used

which results in a comparatively high switching frequency for a given width of the control error. In the case of the PWM control, frequency of current ripple is double the switching frequency.

A drawback of the hysteresis control is variable switching frequency, which brings difficulties in design to attenuate switching ripple. With this simple control no free-wheeling states are used which results in a comparatively high switching frequency for a given width of the control error. In the case of the phase shifted PWM control scheme, the frequency of current ripple is twice of the switching frequency. However, the hysteresis control causes two-level operation because the power transistors $T1$ and $T2$ are driven by the same signal. Therefore, a higher switching frequency ripple and/or a higher switching frequency are present if compared to the PWM control. The essential drawback of the hysteresis current control as described before is the two-level switching characteristic. Therefore, the PWM control (3-level behavior) is advantageous and focused on in this thesis.

7.2.2 Three level PWM control

The basic control scheme including the DC-link voltage control and the active damping for reducing resonances is described in this section. The control block diagram is shown in Figure 92.

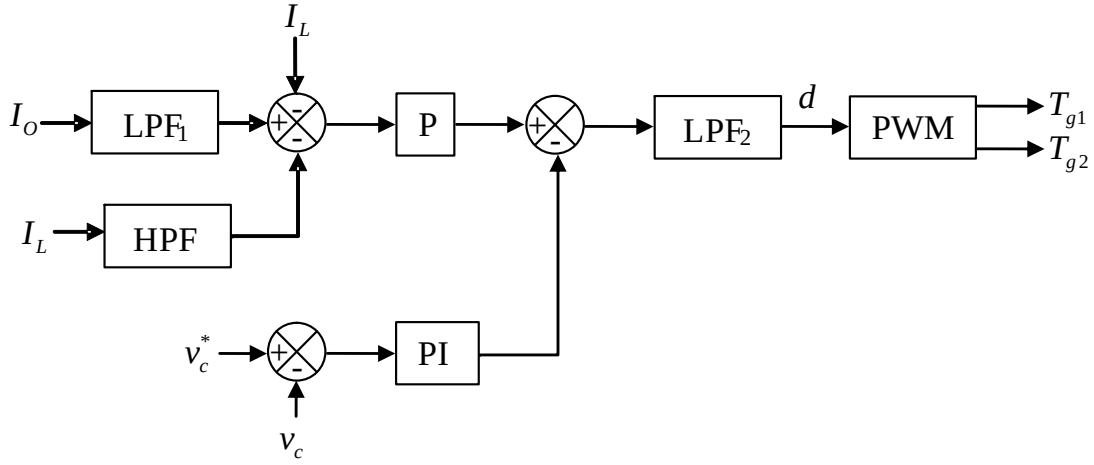

Figure 92. Three level control of the ESI based rectifier.

The ESI can be placed in the negative DC rail to allow measuring all the currents required for the control implementation by shunt resistors which are cheaper and of smaller volume compared to current transducers. The ESI input current I_L is controlled to reach the output current I_O by using a feed forward control. There, a low-pass filter LPF_1 has to be employed for attenuating high frequency components present in the case of pulsating load current such as when the rectifier is supplying a PWM inverter or a DC-DC converter. To detect the average output current, several low pass filters are connected in series in LPF_1 in order to achieve a sufficient attenuation of pulsating load currents as well as minimizing the detection delay time when the load is dynamically changed. In this case, two low- pass filters, each with a cut-off frequency of 5.3kHz, are employed, which has enough attenuation for a pulsing signal higher than 10kHz. It is noted that the number of series connections of the low pass filter can be increased if a higher attenuation is required instead of impairing load dynamic response.

The loss compensation value P, which is the gain for the current control, is adjustable in order to control the current shape of I_L. A high P-value produces a low six times mains frequency current ripple on the DC-line. However the detected signal of I_L has a ripple and the ripple is multiplied by the P-value. For the 5kW ESI, the control circuit P-value is set to 30 in order to keep the low ripple in the control signal line and to achieve sufficient current controllability. For attenuating the equivalent switching frequency ripple, a low pass filter LPF_2 should be employed in the main control loop. The cut-off frequency is selected around 400Hz, which should be higher than the sixfold the mains frequency (300Hz or 360Hz) and enough to reduce the equivalent switching frequency (100kHz) ripple to a sufficient level.

For controlling the DC-link voltage v_c, a PI-type controller is used and connected in parallel to the main control loop. This allows adjusting offset of control signal v_m. If no loss is generated in the DC-link capacitor C, the offset should be zero.

However, an offset is needed to increase the charge current into *C* because the loss in *C* is not zero in practice.

Resonant currents that normally occur at times of diode bridge commutations are detected by using a high-pass filter and are actively damped by feeding back into the main control loop. The high pass filter, *HPF*, is used to sense the resonant currents and to block the low frequency components of the rectifier current such as the six fold mains frequency. The cut-off frequency is adjusted to 723Hz. Finally, the gate signals T_{g1} and T_{g2} are determined by intersecting the control signals and a triangle waveform.

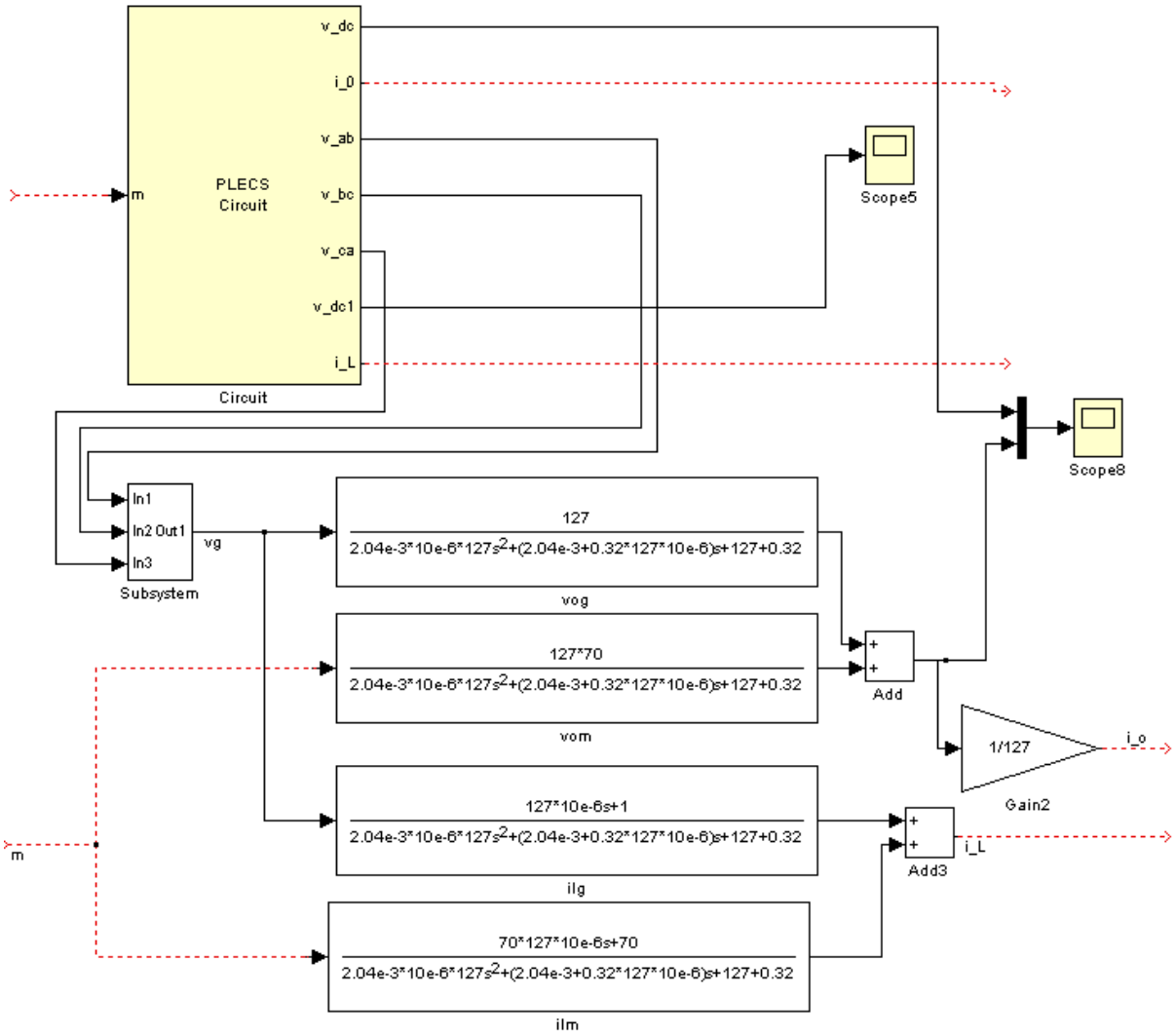

Figure 93. Comparison of a complete linear model of a non-linear circuit of the ESI based three phase rectifier.

Due to the tighter voltage approximation and the doubling of the effective switching frequency the maximum current ripple is reduced to 1/4 as compared to two-level control.

For two level control operation:

$$\Delta I_{\max} = \frac{V_c}{2L_{DC} f_s} \qquad \textbf{7-1}$$

For three level control operation:

$$\Delta I_{\max} = \frac{V_c}{8L_{DC} f_s} \qquad \textbf{7-2}$$

In Figure 93., approximated linear model of non-linear circuit is presented with the help of open loop transfer functions.

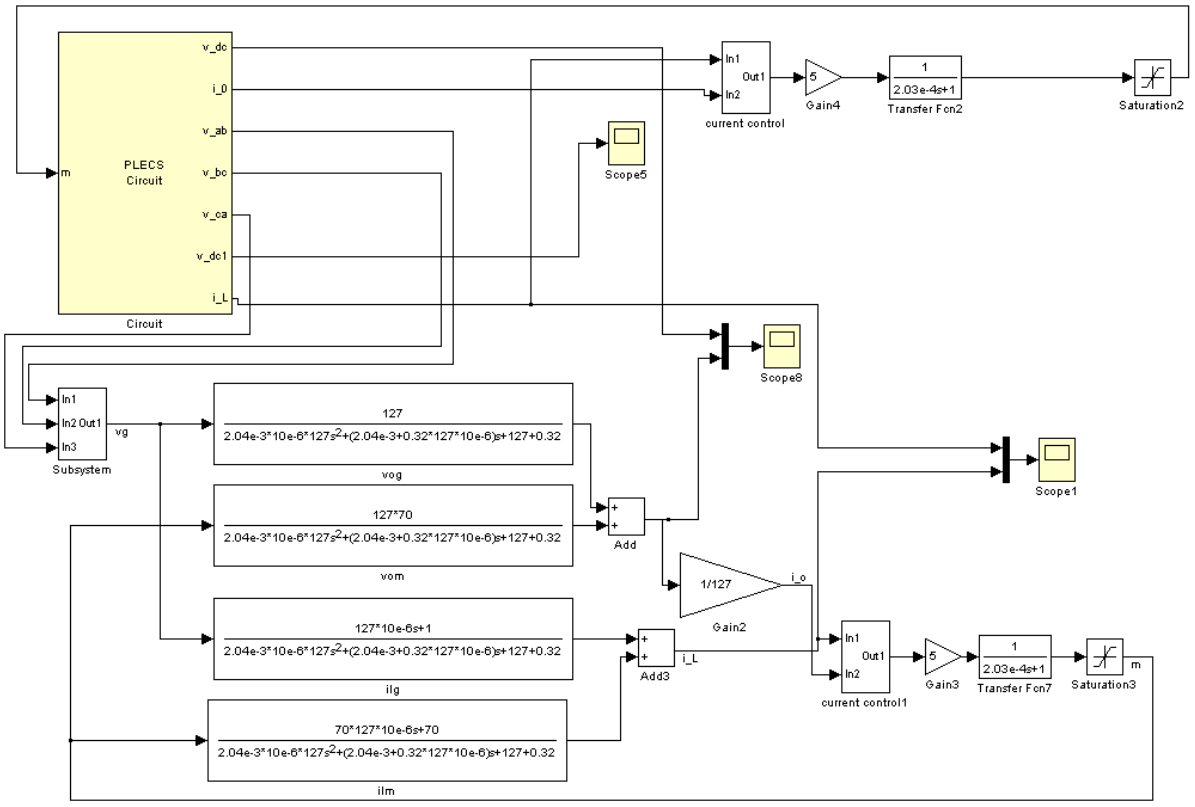

Figure 94. Block representation with simple proportional control for the ESI based three phase rectifier.

This model is compared against a non-linear circuit simulation model constructed in PLESC circuit simulator. Linear and non-linear models of three-phase rectifier are placed in the same simulation. It is easier to compare the response of both the models. Both the models show similarity in its behaviour.

Open loop behaviour of linear and non-linear model has been verified in previous chapter. Integrity of linear model has been already stabilised by verifying its steady state and transient responses.

In order to test controller performance for simple proportional control, the linear and non-linear models have been used are shown in Figure 94. Block representation of complete system is shown in Figure 94. This system is derived from standard three phase voltage source and control variable is produced through closed loop control.

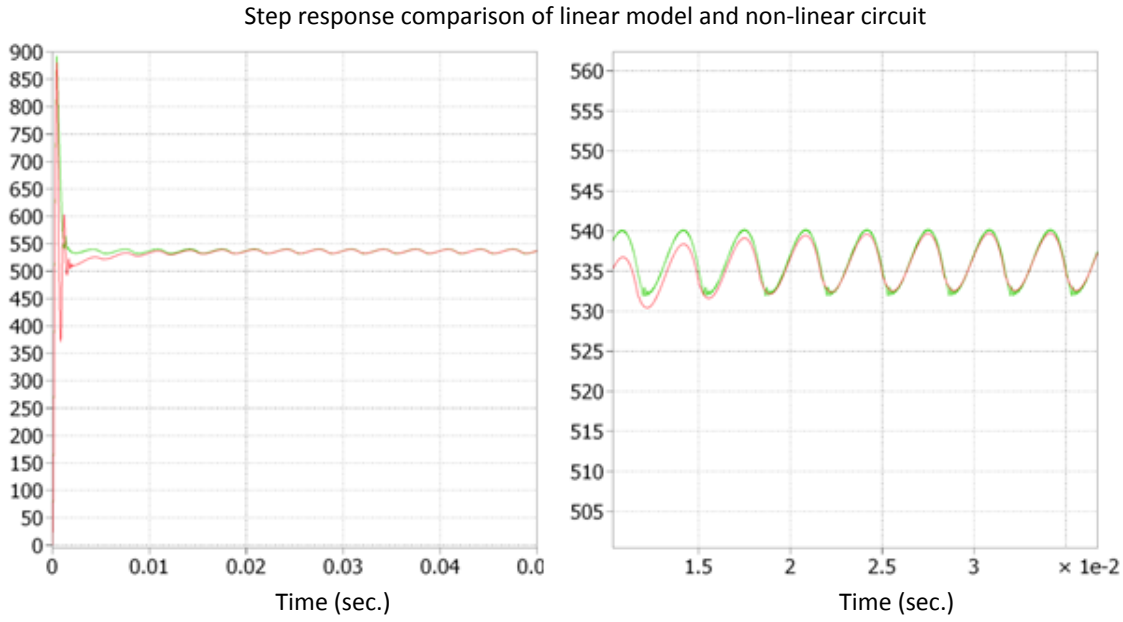

Figure 95. Step response of output voltage from linear and non-linear model of the ESI based three phase rectifier.

Response of output voltage from non-linear circuit simulation and linear model is shown in Figure 95. In the initial transient both model are different but for

steady state both have the same behavior. Response of inductor current is presented in Figure 96.

In non-linear circuit simulation high frequency noise are clearly visible, but one cannot see them in linear model. Linear model is average representation and therefore only average value is matching.

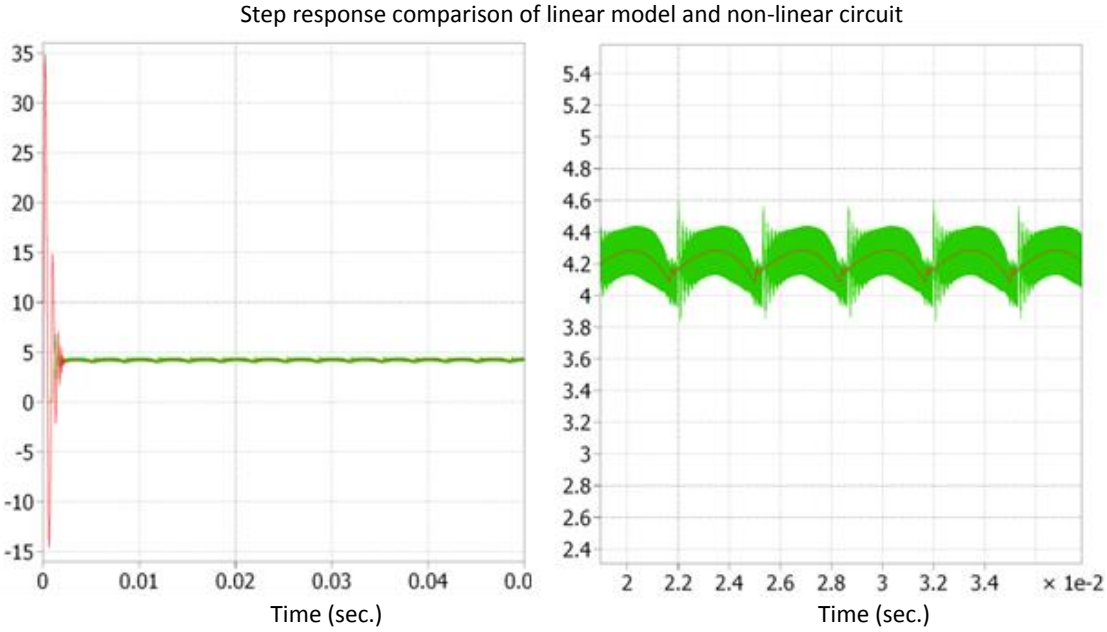

Figure 96. Response of inductor current from linear and non-linear model of the ESI based three phase rectifier.

Response of output voltage is Figure 95. Steady state response is very similar, but transient response is different. This difference is because of non-linear behaviour of diodes for large step.

Similarly response of inductor current is shown in Figure 96. Inductor current from non-linear circuit is having high-frequency switching ripples. The linear circuit is an averaged representation and it is valid for low frequency.

Frequency response in open loop of input to output voltage transfer function (G_{vg}) is shown in Figure 97. Typical value of the grid resistance and the inductance are 0.01 Ω and 1 mH respectively have been used, and load resistance has been chosen according to 4kW output power.

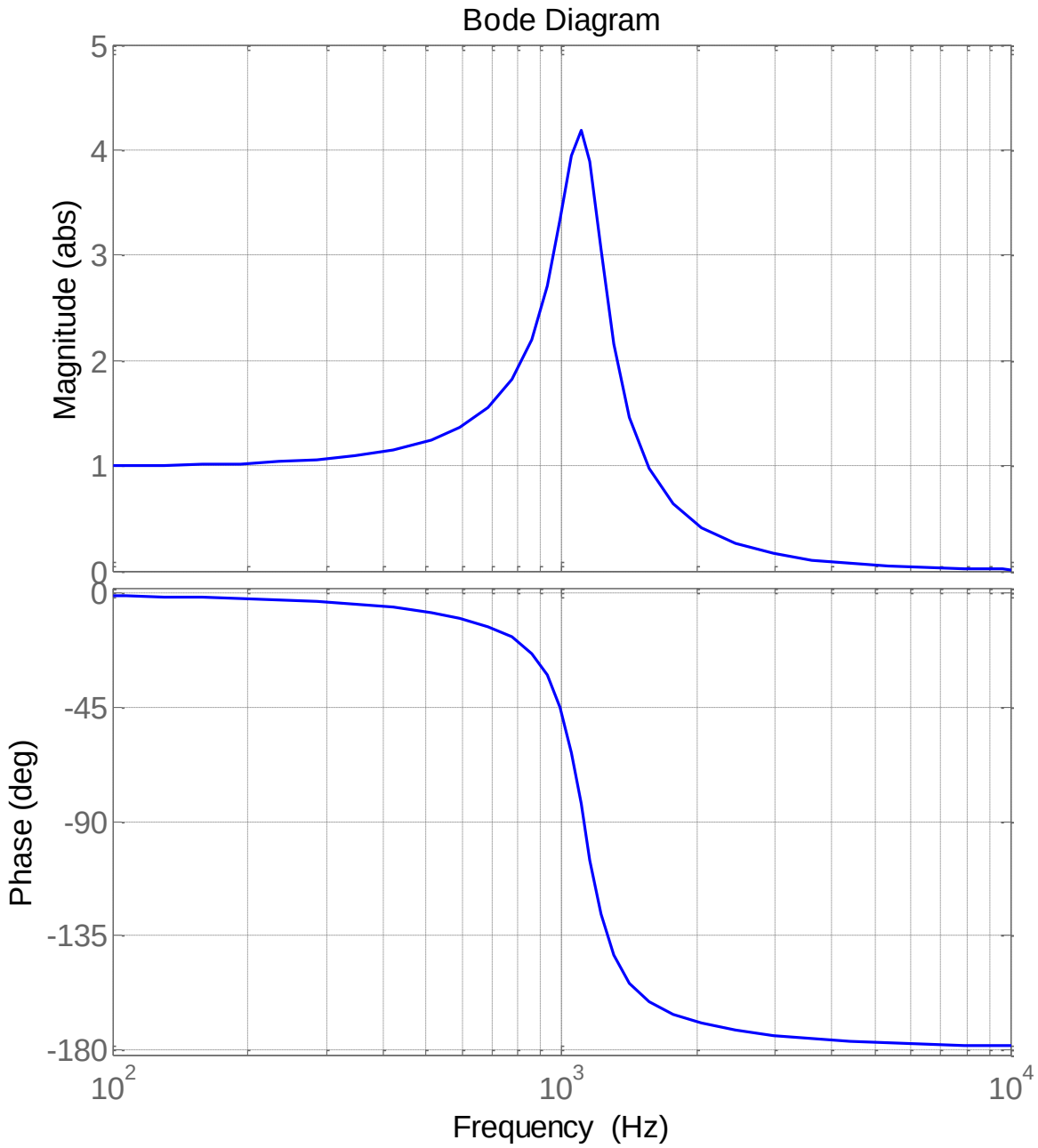

Figure 97. Open loop response of input to output transfer function (G_{vg}).

There is a resonating peak corresponding to the characteristic impedance of input line. At very low frequency close to zero Hz, the magnitude is zero dB, i.e. amplification is unity. This means all the dc value will pass through, and other than dc, signals will either be amplified or damped according to their frequencies. At 300 Hz, absolute magnitude is 1.06 (0.56 dB), which means ripple at this

frequency will be amplified and will be higher than the ac part of the theoretical value of rectified output voltage of three phase diode bridge. For the standard 50 Hz, 400V line to line mains power, output ripple corresponding to 300 Hz will be approximately 89V.

7.3 Control design for the ESI based rectifier

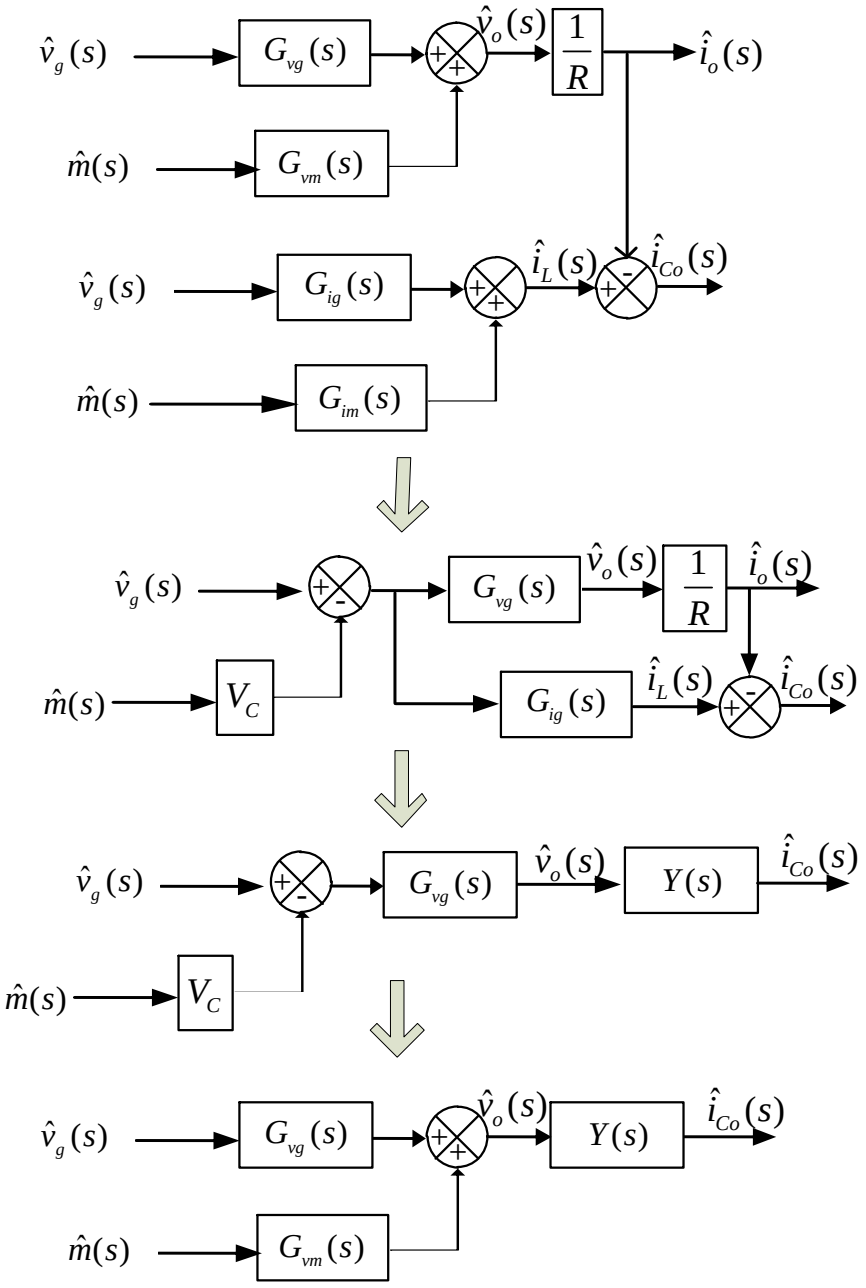

Figure 98. Block diagram of plant prepared by its transfer functions.

To make output voltage of the ESI based rectifier is constant, i.e. free from ripples of input voltage, to reduce ripple less than 3% of DC value. In the event of sudden change in load current, dip or overshoot in voltage should not be more than 10% and it must be settle to steady state value in less than 1 msec.

Neglecting Load disturbance, i.e. $\hat{i}_o(s) = 0$, we can have linear mathematical model of the plant as shown in Figure 98.

This model can be reduced to different levels and simplified. A feedback control $G_C(s)$ can be added and then the closed loop system will look like as shown in Figure 99. Here $Y(s)$ is admittance of output capacitor. In this control strategy idea is to estimate the ripple in output capacitor current and minimize this ripple by feedback control. It is assumed that ESI capacitor voltage V_C is constant.

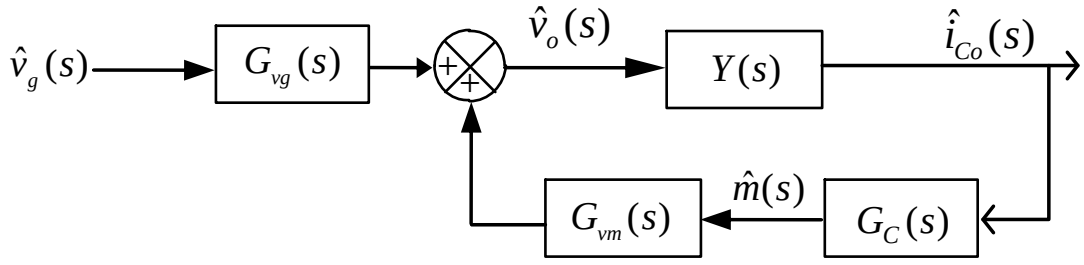

Figure 99. System with feedback control.

$$G_C(s) = P * LPF$$
$$P = 5 \qquad \textbf{7-3}$$
$$LPF = \frac{1}{5.03e-4s+1}$$

$$Y(s) = \frac{sC_o}{sr_cC_o+1} = \frac{s10e-6}{s2e-7+1} \qquad \textbf{7-4}$$

When ESI capacitor voltage required a separate voltage controller $G_V(s)$, Total system with separate ESI voltage controller is shown Figure 100.

Current controller $G_C(s)$ contains proportional (P) gain and a low pass filter. Voltage controller $G_V(s)$ contains proportional and integral type control and a

low pass filter. When the performance of controlled system requires checking against the disturbances at input side small signal linear model can be described as follows.

The output voltage ripple can be further reduced by increasing the value of the gain P. A high P-value produces a low six times mains frequency ripple on the output voltage, but it introduce high frequency ripple in the inductor current. A high pass filter (*HPF)*, is used to sense the high frequency components of inductor current i_L, and to block the low frequency components of i_L.

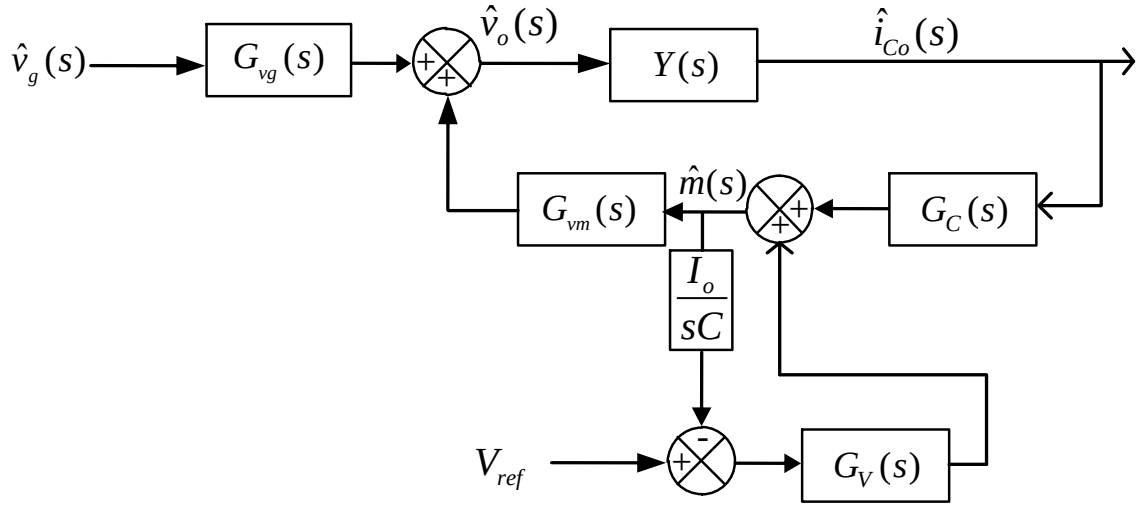

Figure 100. System with feedback control and separate ESI voltage controller.

To control the ESI capacitor voltage v_c, a PI-type controller is employed and connected in parallel with the main control loop. The voltage controller is relatively slow and generates the required current reference for current controller. The voltage controller works on energy balance.

$$G_V(s) = PI * LPF$$

$$PI = \frac{2s+1}{70s} \qquad \textbf{7-5}$$

$$LPF = \frac{1}{5.03e-4s+1}$$

In this reduced model, effect of different disturbance occurring at input and output side of the converter can be easily analyzed. From the linear mathemati-

cal model, of the ESI based three phase rectifier, closed loop system is derived as shown Figure 101. The loop gain of the voltage controller $G_V(s)$ is termed $T(s)$ and is multiplication of different blocks of the forward path of the voltage controller.

$$T(s) = G_V(s)\frac{I_o}{sC} \qquad \textbf{7-6}$$

A reduction of the block diagram representation has also been done in Figure 101. $G_C(s)$ is the current controller and it tries to smooth the inductor current i_L to a dc value. Simplified closed loop control system has been derived.

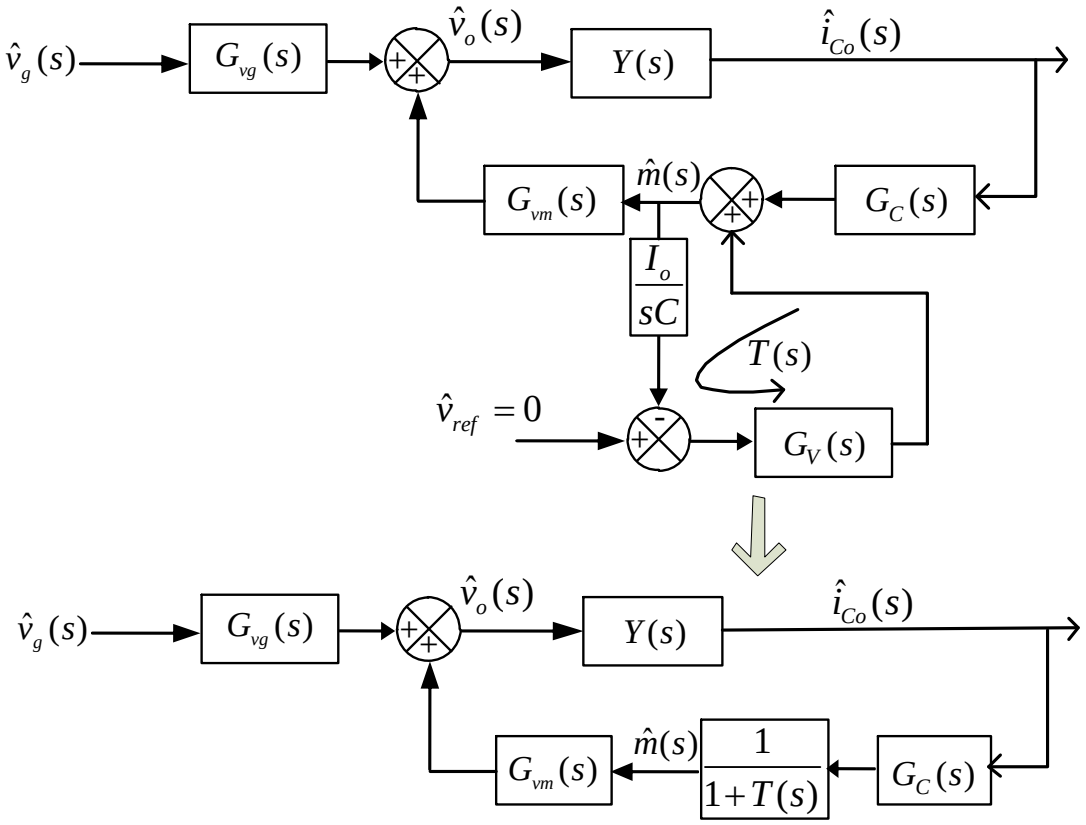

Figure 101. Reduced Model of System with feedback control and separate ESI voltage controller.

Effect of a separate voltage controller for the ESI capacitor voltage is shown in Figure 102. When no separate voltage controller is used, response of closed loop is damped throughout all the frequency range, But by adding a separate voltage controller there is amplification at low frequency range. By changing the gain of this separate voltage controller, the magnitude of the closed loop response can

be controlled. At two different gain of this voltage controller closed loop response is shown in Figure 103.

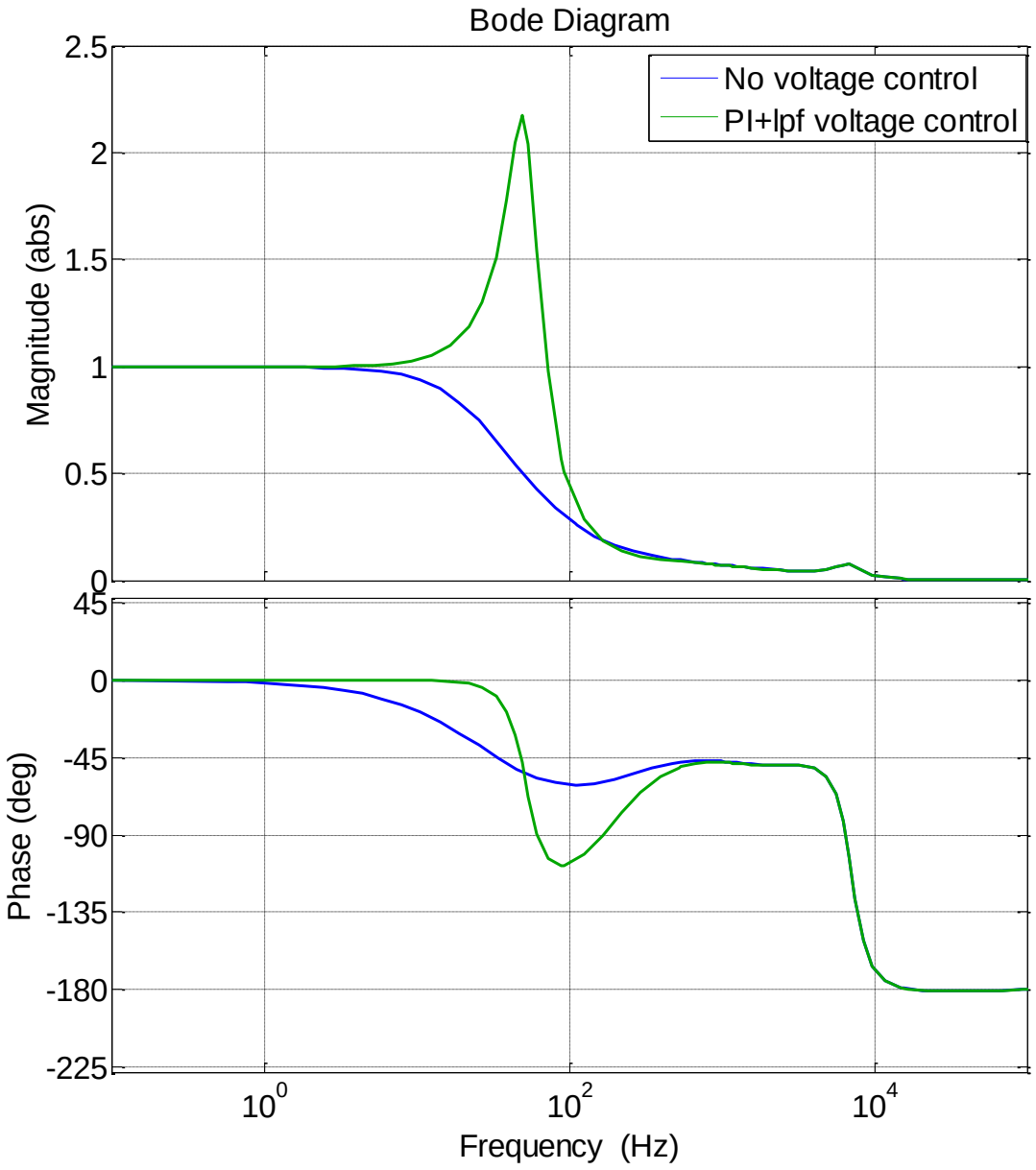

Figure 102. Effect of adding separate voltage controller.

The gain P for the current control is adjustable in order to control the current shape of i_L. For attenuating switching frequency ripple, a low pass filter LPF_2 should be employed in the main control loop [67]. Output voltage ripple can be further reduced by increasing the value of the gain element P. A High P-value

produces a low six times mains frequency current ripple on the DC-line. One high pass filter, *HPF*, is used to sense the resonant current and to block the low frequency components of i_L.

Response of a P+lpf type control on absolute scale is shown in Figure 104. When it is compared against the open loop transfer function, it can be seen that there is significant reduction in amplitude at 300 Hz.

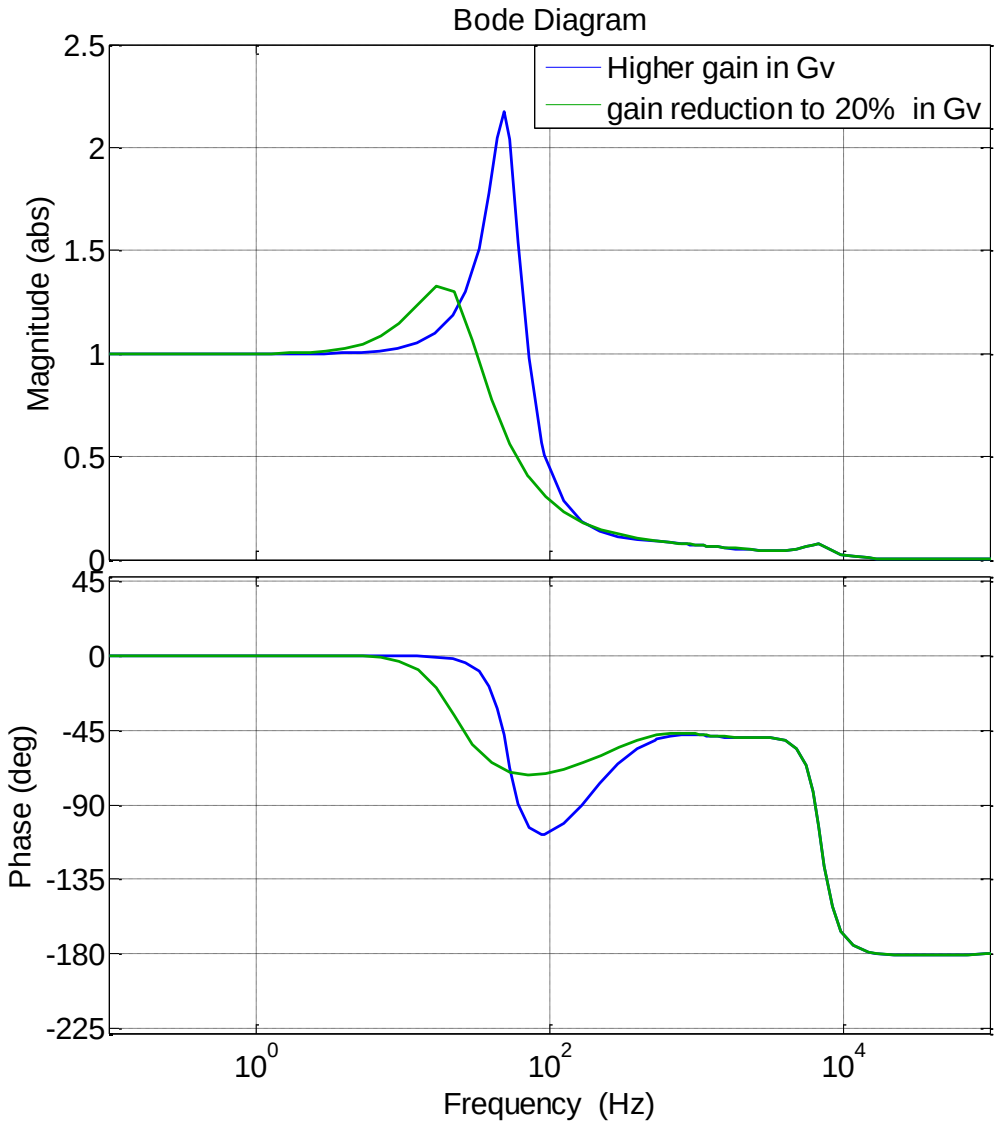

Figure 103. Response comparison of a controller at two different control gain of voltage controller.

At higher frequency P type controller can become unstable or oscillatory at frequencies around 3 kHz. To improve response at this frequency range instead of P type controller, a new PD type controller is proposed and its response is compared in Figure 105.

This PD type controller is given by:

$$G_c(s) = PD * LPF_2$$

$$PD = \frac{30s + 190500}{s + 25400} \qquad \text{7-7}$$

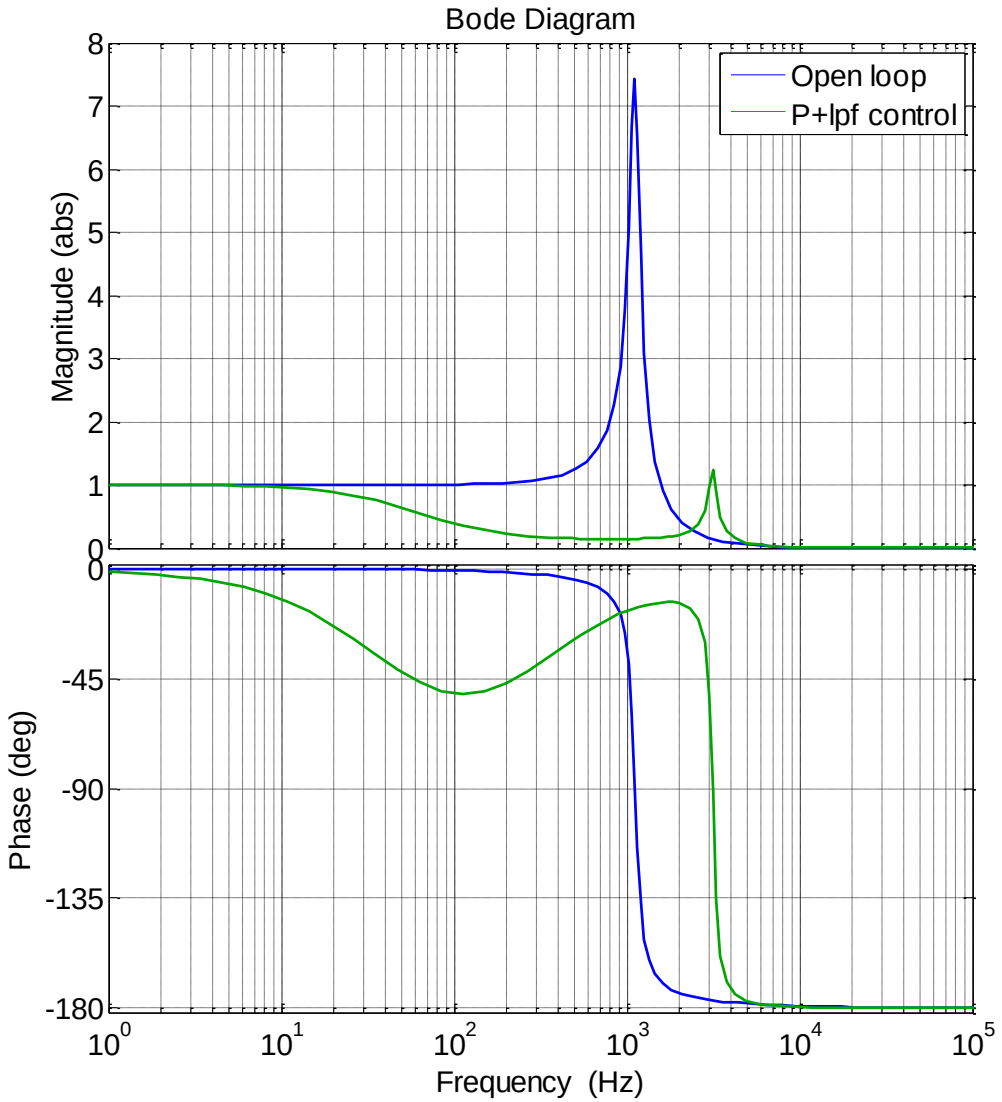

Figure 104. Comparison of closed loop controlled response with open loop on absolute scale.

With PD type controller, it can be clearly seen that response of closed loop at 3 kHz is sufficiently damped. PD type controller contains one pole close to 4 kHz and one zero close to 1 kHz, which are placed in such a way to that controller behavior remains good at lower frequency than switching frequency.

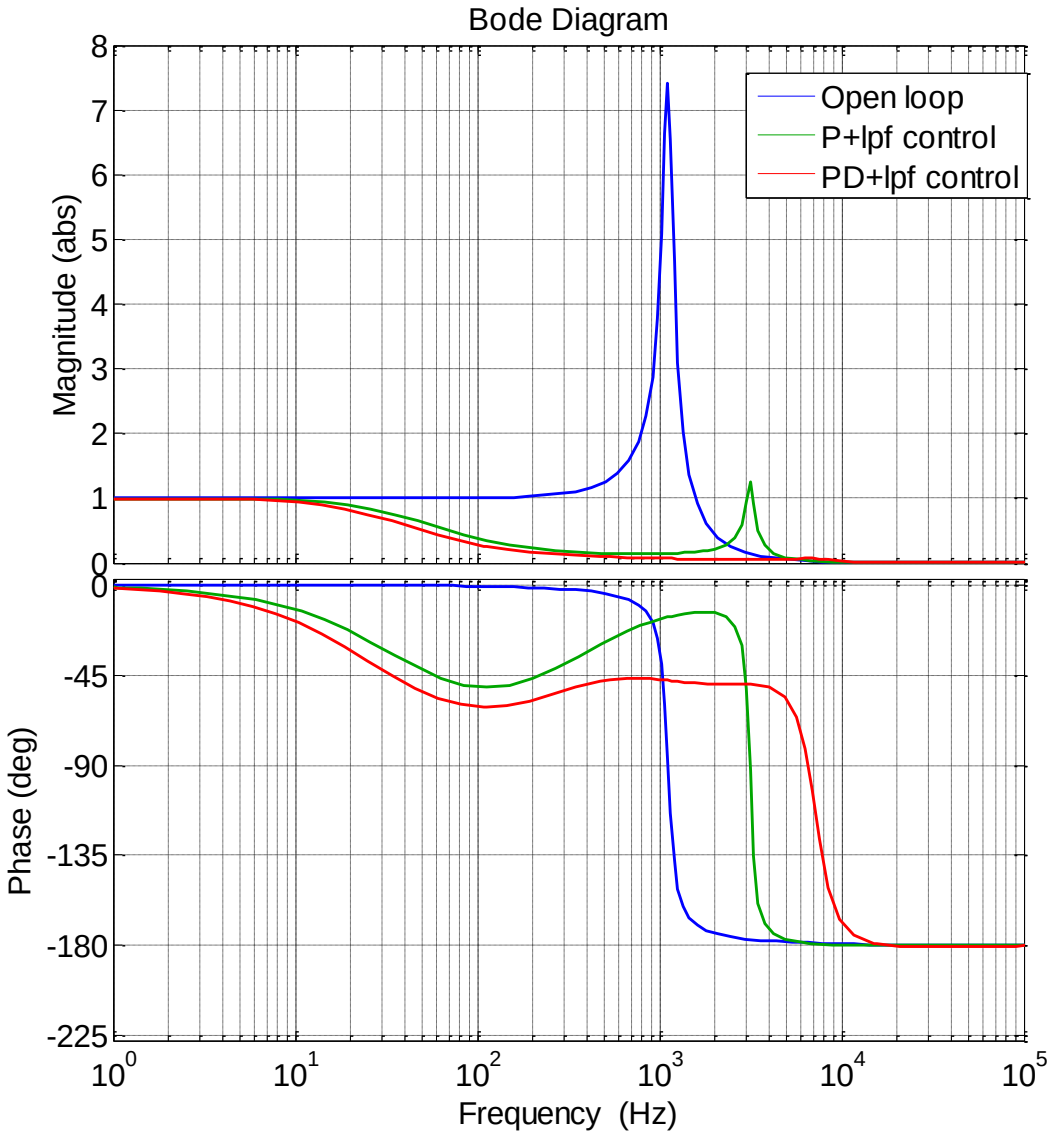

Figure 105. Comparison of on two different controllers with open loop response on absolute scale.

Forward gain of PD type controller is 30. The PD type controller behaves very similar to lag-lead type controller. It offers higher damping in the vicinity of 3 kHz frequency. Grid inductance can change also. At 300uH grid impedance bode plot is shown above. Here open loop transfer function output to input

(G_{vg}) contains a resonating peak at 3kHz. The frequency response in open loop on db scale of the input to the output voltage transfer function (G_{vg}) is shown in Figure 106. There is a resonating peak corresponding to the characteristic impedance of input line. At very low frequency close to zero Hz, the magnitude is zero dB, i.e. amplification is unity.

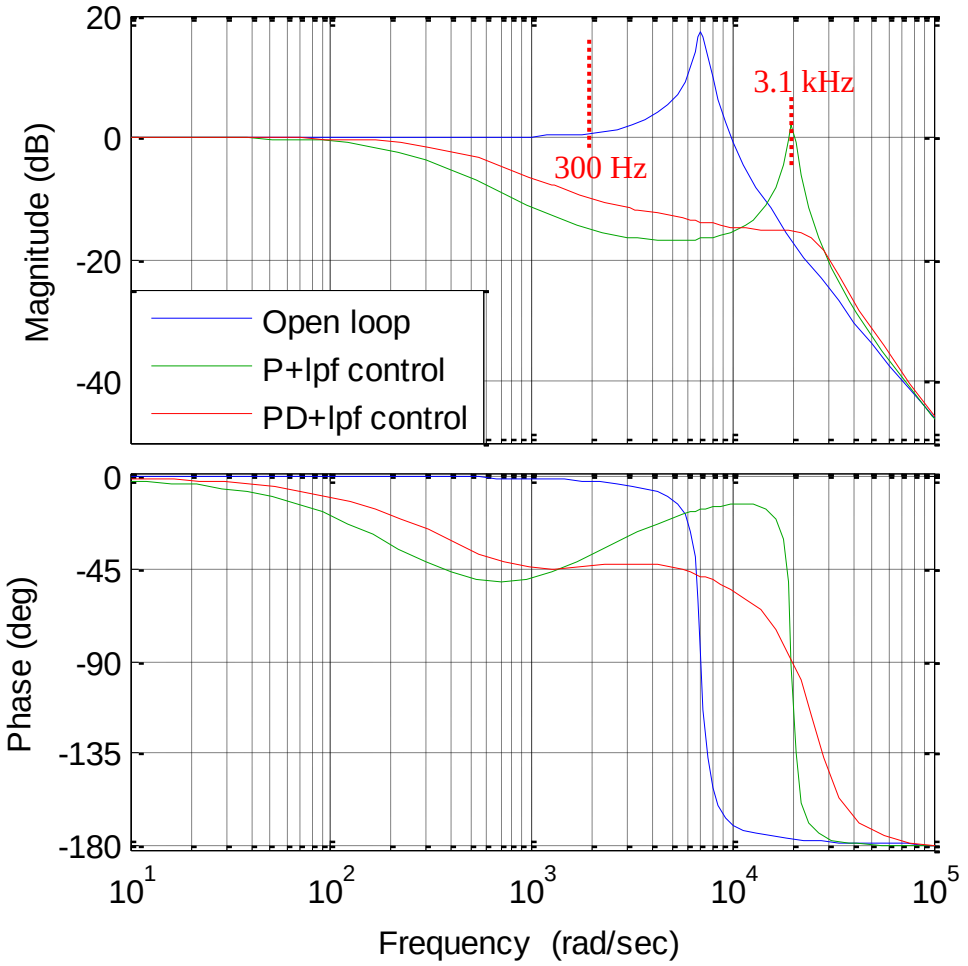

Figure 106. Comparison of two different controllers with open loop response on dB scale.

This means all the dc value will pass through, and other than dc, signals will either be amplified or damped according to their frequencies. At 300 Hz, absolute magnitude is 1.06 (0.56 dB), which means ripple at this frequency will be amplified and will be higher than the ac part of the theoretical value of rectified output voltage of three phase diode bridge. At 300Hz the magnitude is reduced from 0.56 dB to -15 dB. In terms of absolute value, magnitude is reduced from

1.06 to 0.17. This means the ripple at 300 Hz will be reduced by factor of 6.24. With PD type controller, it can be clearly seen that response of closed loop at 3 kHz is sufficiently damped. PD type controller contains one pole close to 4 kHz and one zero close to 1 kHz, which are placed in such a way to that controller behavior remains good at lower frequency than switching frequency. Forward gain of PD type controller is 30. The PD type controller behaves very similar to lag-lead type controller. It offers higher damping in the vicinity of 3 kHz frequency. The inductor current i_L is controlled to a constant value (DC current with superimposed switching frequency current ripple) by operating T_1 and T_2 with a variable duty cycle.

In the turn-on period of both T_1 and T_2, the DC-link capacitor C is discharged and i_L increases. On the other hand, C is charged and i_L decreases when both transistors are turned off. In the period when either of T_1 or T_2 is turned on, i_L does not flow in C. Therefore, a 3-level operation (C is discharged, bypassed, and charged) can be realized. A two-stage control is applied where the duty-cycle of the switch is determined by an inner current control loop and the constant dc output voltage by a superimposed voltage control.

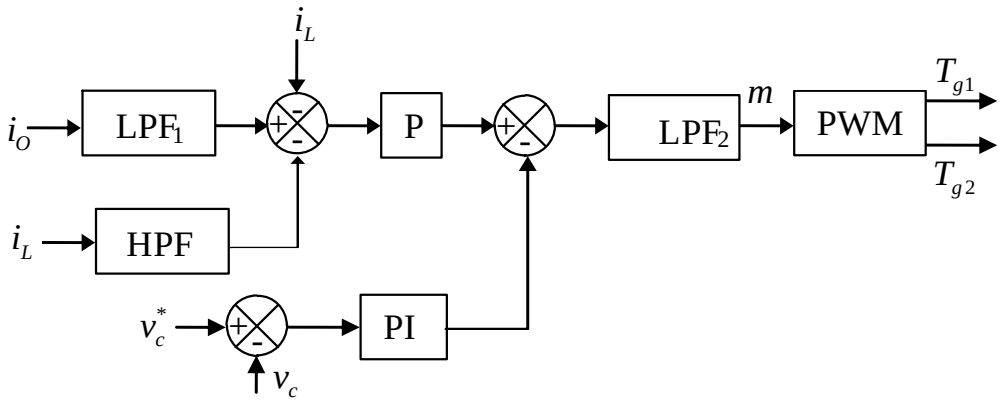

Figure 107. Control scheme of rectifier with ESI.

Control scheme is presented in Figure 107. There, a low-pass filter LPF_1 has to be employed for attenuating high frequency components being present in case of pulsating load current. The gain P for the current control is adjustable in order

to control the current shape of i_L. A High P-value produces a low six times mains frequency current ripple on the DC-line. One high pass filter, *HPF*, is used to sense the resonant current and to block the low frequency components of i_L. For attenuating switching frequency ripple, a low pass filter LPF_2 should be employed in the main control loop.

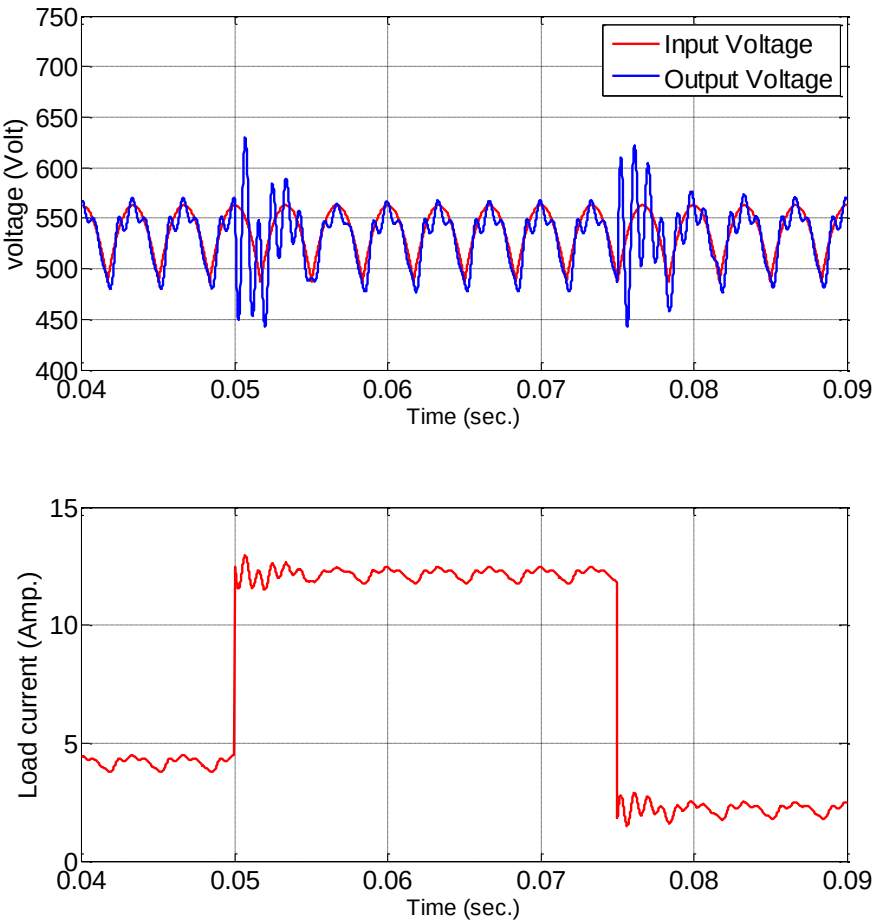

Figure 108. Step load on uncontrolled three phase rectifier without ESI.

The cut-off frequency is designed around 500Hz, which should be a higher frequency of the six times of the mains frequency and it should be able to reduce switching ripple to sufficient level. To control voltage v_c of the ESI capacitor, a PI-type controller is employed and connected in parallel with the main control loop. Gate signals T_{g1} and T_{g2} are determined by comparing the control signal m and a triangle waveform. In Figure 108., the output voltage and inductor current

at the passive mode are shown. The comparison to the active mode as shown in Figure 109., makes us clearly understand that the output voltage ripple can be significantly reduced. The output voltage ripple is then reduced from 81.1V_{pp} to 14.1V_{pp}. This allows use of a much lower volume of output capacitor. In active mode, the power transistors must be driven. Therefore switching losses are generated and the core loss in the inductor is increased because of a high frequency current ripple. Accordingly, the efficiency in the case of the active mode is reduced compared to the passive mode. However, the reduction of the efficiency at the nominal output power is not much. It is also verified that the critical increased loss components such as the switching losses and the loss in the inductors are relatively low. Therefore, the efficiency is not reduced so much when ESI actively operates.

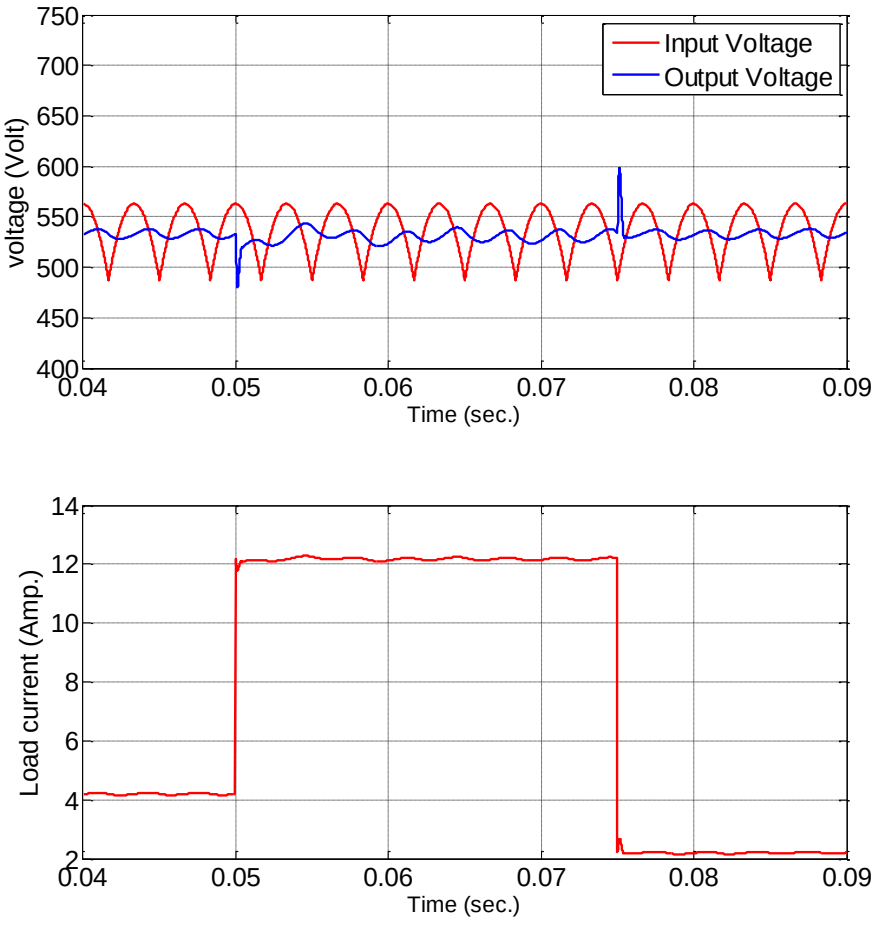

Figure 109. Step load response of the ESI based three phase rectifier.

A load step responses of the output voltage and the inductor current of a three phase rectifier system with the ESI are presented in Figure 109. Without the ESI oscilation at 300 Hz are higher compared to system with the ESI and response of the output voltage towards load change is improved and it settels down quickly. It is possible that without the ESI, the output voltage will become unstable and put higher voltage stress on the power semiconductor. During unstability, when DC link voltage falls, It will be difficult for the drive to provide required stator volatges to the motor connected to it. It can also be seen in ESI based three phase rectifier, the output voltage is more or less controlled to a dc value and peak to peak voltage ripples corresponding to 300 Hz have been reduced significantly. Simillar improvement has been seen in the inductor current response.

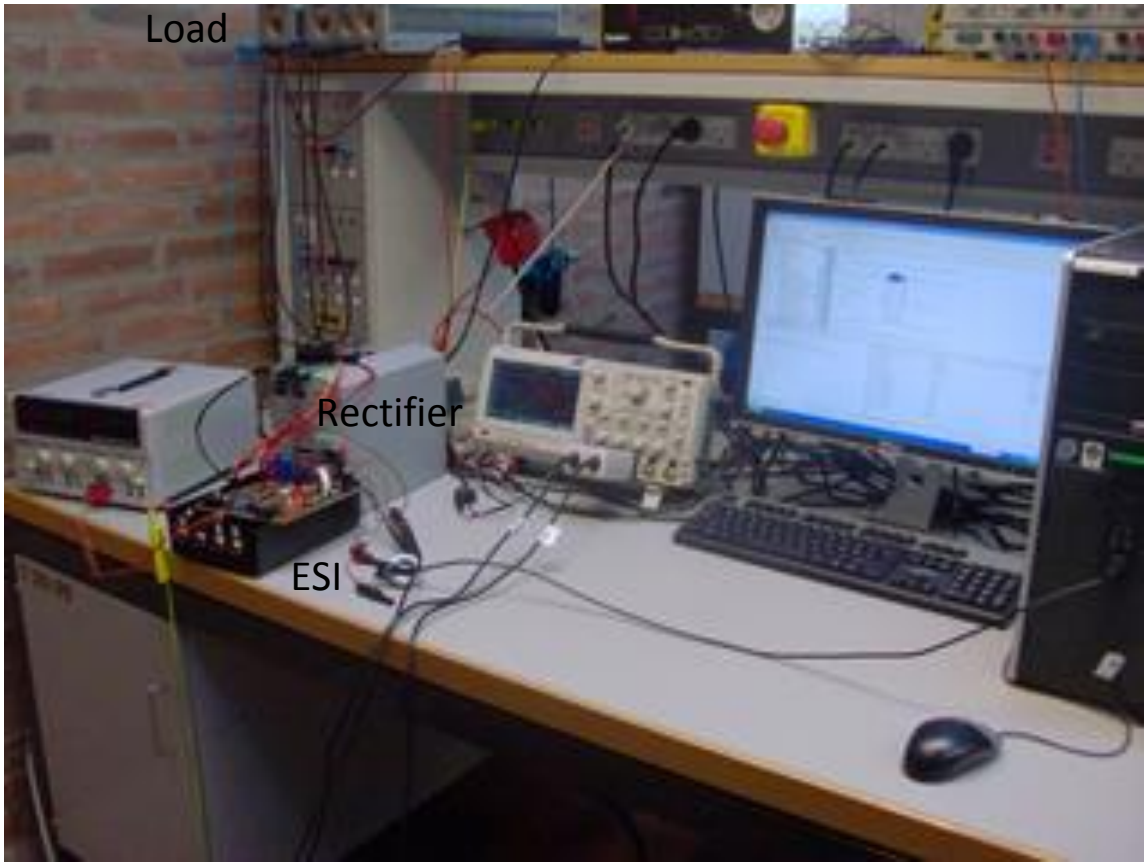

Figure 110. ESI is plugged into a traditional drive.

The experimental setup of laboratory is shown in Figure 110. A traditional drive from *Danfoss* drive, is modified and the ESI based converter is plugged into this drive. A resistive load is connected to output dc-link capacitor of the modified drive. Auxiliary DC power supply was used to power-up the control and sensing electronics.

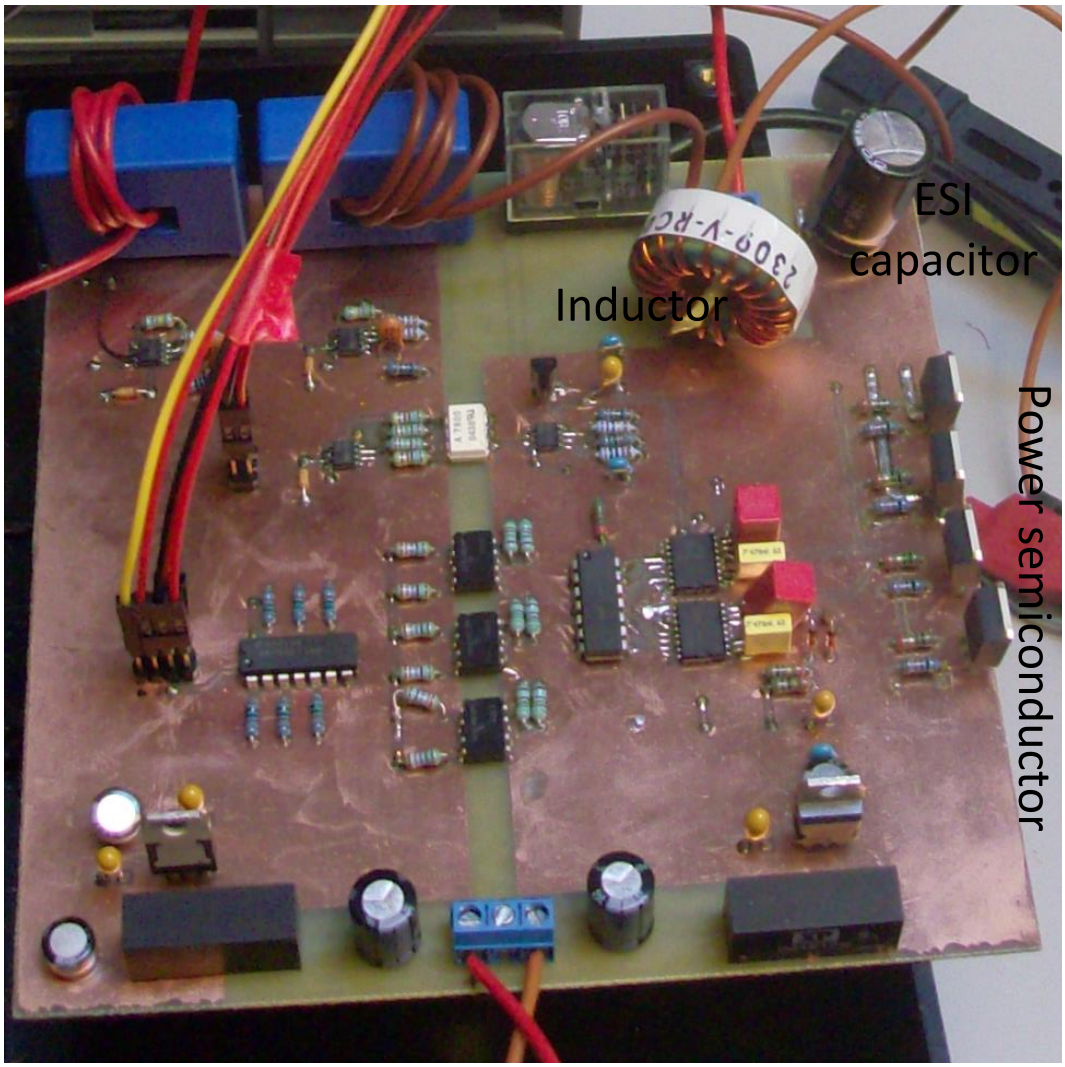

Figure 111. ESI and its sensing and control board.

Practical realization of the ESI and its other accessories are shown in Figure 111. In this figure inductor of 40 *uH* is connected in the negative rail of the three phase diode bridge rectifier. Size of this inductor is very small and in figure it can be compared against the LEM current sensor placed of the circuit PCB. The

ESI capacitor of 200 uF is connected along with the asymmetrical H-bridge formed by the power semiconductor. A relay was introduced in this circuit to bypaseed the ESI arrangement and to operate circuit only with the passive rectifier. Two current sensors are placed to measure inductor and load current individually. Voltage sensing of the ESI capacitor performed and processed through optically isolated OP-amp.

Control scheme was implemented in a floating point digital signal controller F28335 provided by *TI*. Voltage of ESI capacitor, inductor current and load current signal were given to ADC port of the DSP after required signal conditioning. DSP also generated the PWM signals for the ESI bridge, and these signals processed to gate drive circuit having opto-isolator in between the low voltage signals and high voltage power stage.

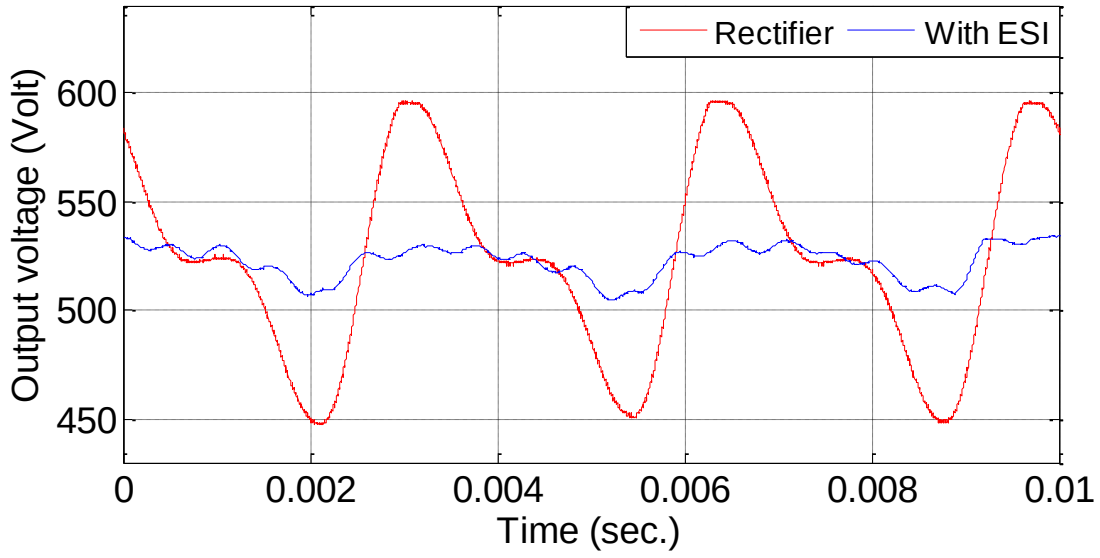

Figure 112. Steady state output voltage with ESI (in blue) and without ESI (in red).

Steady state waveform of output voltage is shown Figure 112. In this figure red colour waveform is obtain when ESI circuit is bypassed, i.e. only standard rectifier is in operation. The applied load was resistance of 127 Ω, i.e. load corresponding to 2.25 kW. It can be seen that peak to peak voltage ripple is

140V. Once ESI circuit is plugged in it controlled output voltage to a dc value, ripple voltage falls to around 20V. A three phase 400V line to line voltage source was used in non-linear simulation model and experimental test set-up. An external three phase inductor of 3mH per phase has been inserted between the grid and the front end of the system. These additional inductors are inserted to minimize the effect of grid impedance, as this impedance value is much higher than the grid impedance and therefore front end dynamics will be determined mainly by these inductors. Experimental test results are stored in data format and reproduced with the help of MATLAB.

Steady state waveform of input phase current is shown Figure 113. In this figure red colour waveform is obtain when ESI circuit is bypassed, i.e. only standard rectifier is in operation. It can be seen that peak value of current ripple 7.5A. Once ESI circuit is plugged in, peak value of current falls to 5A. Only half cycle of mains is shown in figure.

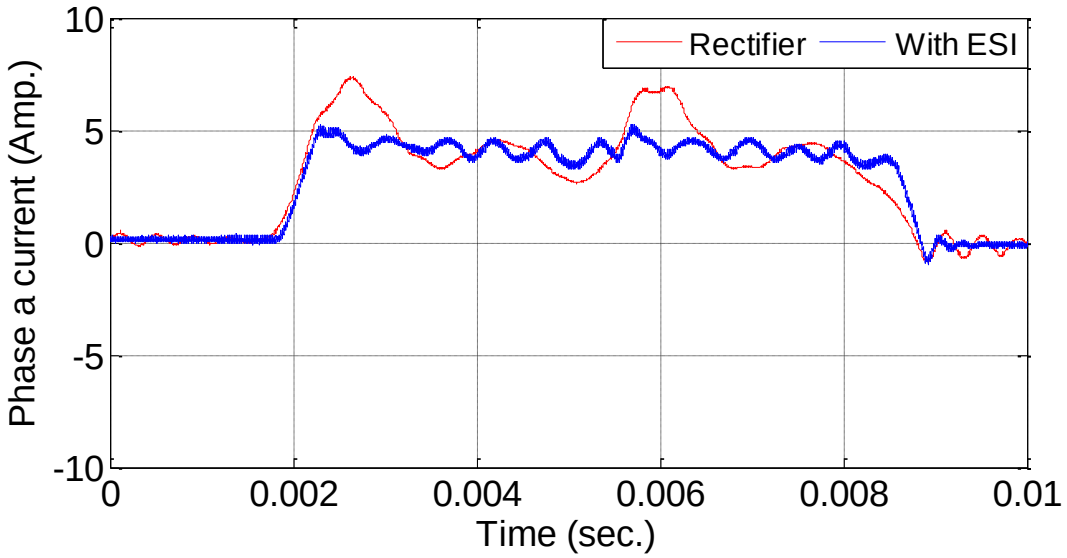

Figure 113. Steady state input phase current with ESI (in blue) and without ESI (in red).

Experimental results confirm the reduction of the ripple in output voltage corresponding to six times of mains frequency and THDs level at mains currents

to acceptable level. In practical circuit peak to peak ripple reduction in the output voltage is not as small as it is in simulation but it is reduced from 140V to 20V, to reduce this value further gain of the current controller should be increased and it will lead to instability during transient operation. There is some high-frequency oscillations present in the output voltage and in the mains current, these ripple do exist because of interaction of grid impedance with output capacitor.

7.4 Summary and conclusion

In this chapter control schemes of the ESI based three-phase rectifier are derived from the transfer functions based linear mathematical model. This linear model was very useful to develop a control scheme in order to achieve control objective. Two different control schemes were presented in this chapter. Comparison of these two different control schemes has been carried out in this chapter. PD type controller offers stable control for different type of loads connected at the output of the ESI based three-phase rectifier.

Practical realization and implementation of the ESI based converter have been done. Performance improvement is significant as compared to traditional diode bridge based rectifier. Weight and volume reduction is very significant in ESI based power converter as compared to traditional power converters. If Front end of the power converter in motor integrated variable speed drive will be used, then integration will be easier and improved performance at the grid side as well as motor side will be achieved, because it decouples the grid side to load side disturbances and dynamics.

Chapter 8. Modified Electronic Smoothing Inductor based drive

8.1 Background

Although ESI offers reduced size of DC chock, but average load current has to pass through two more power semiconductor devices and therefore conduction losses in classical ESI based drive are slightly higher than traditional three phase drive. The placement of circuit can be in series with the main dc-link capacitor and then only high frequency ac current will flow through additional the power semiconductors.

8.2 Circuit topology of Modified ESI

A modified ESI topology is shown in Figure 114. In this circuit arrangement MESI is connected to an inverter that drives a motor. In this case average load current will not flow through active switches of the MESI.

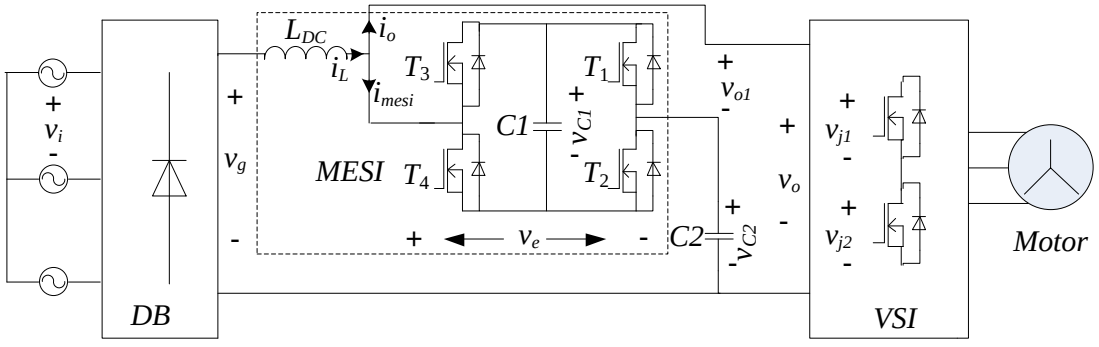

Figure 114. Circuit topology of the three phase electric drive with the MESI.

The MESI is a hybrid filter, it supplies only high frequency currents. In order to charge and discharge the DC-link capacitor *C*, the bidirectional current (i_{mesi}=

$i_o - i_L$) must be controlled. Therefore, four switches are employed. Three-level voltage modulation ($vc_2 - vc_1$, vc_2, or $vc_2 + vc_1$,) is then present at the inverter input voltage v_o . The DC current i_L, which can be controlled by the MESI, is increased at $v_o = vc_2 - vc_1$ and decreased at $vc_2 + vc_1$. There exists a current path to bypass C [7]. Current flowing into positive rail of inverter, i_o, is discontinuous and also having stepped waveform. Current flowing in full bridge of MESI, i_{mesi}, is difference of inverter current, i_o, and inductor current, i_o. Charging and discharging of capacitor of MESI is determined by the sign of i_{mesi}. The 3-level output voltage modulation would benefit the inverter. For instance, switching voltage of the IGBTs can be reduced by synchronizing an operational frequency of the MESI to an inverter switching timing.

When Inverter is operating without MESI, voltage in front of inverter v_O is equal to vc_2 as shown in Figure 115. In the case that the MESI is bypassed, v_o is always equal to vc_2, neglecting the voltage drops on the MOSFETs, and the IGBT voltage stress is also vc_2. However, the IGBT voltage can be reduced to $vc_2 - vc_1$, which is lower than vc_2, at the switching timings if the MESI operation is synchronized to the IGBT switching behavior. These 3 levels of voltage are shown in Figure 115., is possible because an operational frequency of the MESI can be much higher than that of the inverter e.g. the switching frequency of an inverter is normally set around 5 kHz and the switching frequency of the MESI could be in the range of 50 kHz to 100 kHz [7].

The lower switching voltage would bring some advantages. For instance, since switching loss depends on the switching voltage, switching losses of IGBTs and diodes in the inverter would be reduced. The peak of the spike voltage of IGBTs or diodes at a switching transition can also be reduced e.g. a sufficient voltage margin would be obtained. Therefore, a high switching speed could be realized by using a lower gate resistor without an overvoltage, which will also result in reduced switching losses.

Integration of MESI into main DC-link is a difficult task as in traditional VSI, DC link capacitors are directly connected to either bus-bar or two different plates corresponding to positive and negative DC rails. In order to integrate MESI, Main DC-link capacitor cannot be connected directly and MESI will be in series with that capacitor. Introduction of MESI will increase the inductance of high frequency current path of VSI. It will introduce high ringing and peak voltage stress across the IGBTs of the VSI.

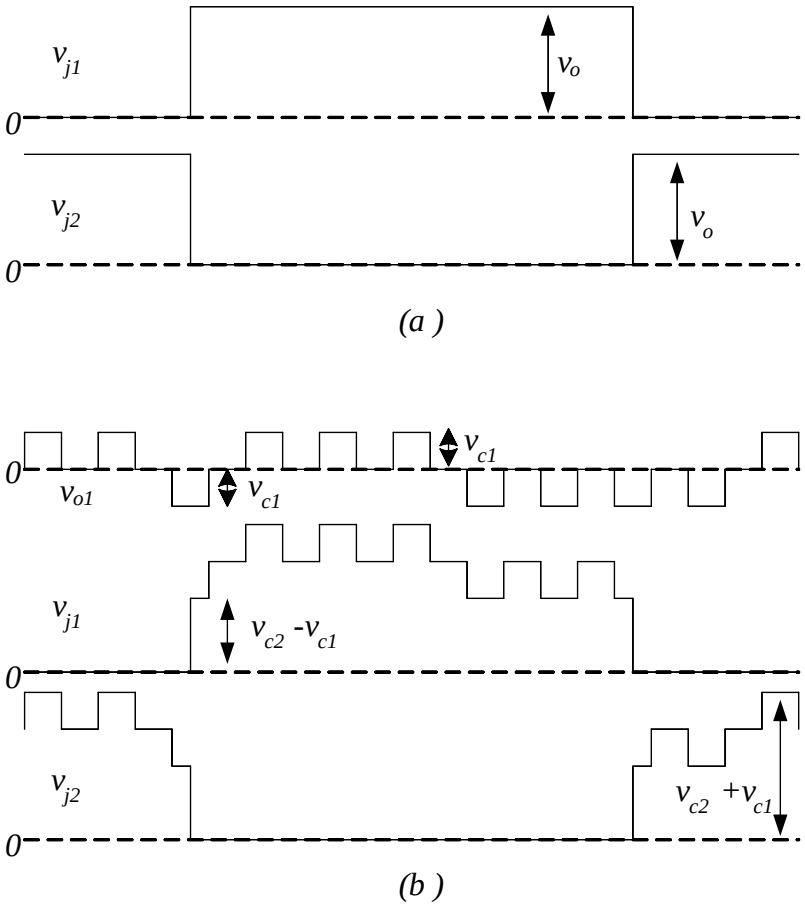

Figure 115. Three level operation of MESI converter.

8.3 Control scheme for MESI based electric drive

MESI has to support high frequency current demand of inverter, average current flowing from positive rail of DC bus to inverter will not flow through MESI. Current flowing in MESI is bidirectional. In this case also, a two-stage control is

applied where the duty-cycle of the switch is determined by an inner current control loop and the constant dc output voltage is defined by a superimposed voltage control of voltage of capacitor of MESI.

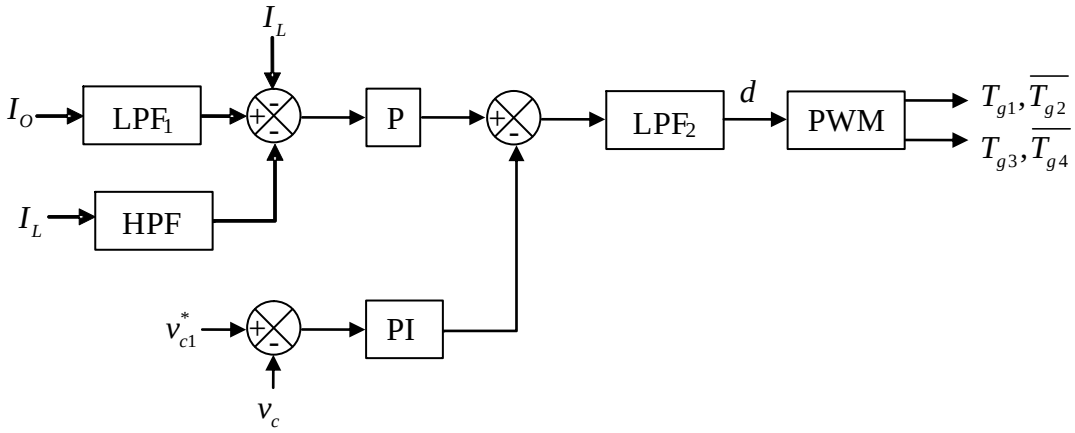

Figure 116. control block diagram of MESI.

The inductor current i_L is controlled to a constant value (DC current with super-imposed switching frequency current ripple) by operating four MOSFETs T_1, T_2, T_3 and T_4. T_1 and T_2 operate by complementary gate signals, T_3 and T_4 also operate by complementary gate signals. In the turn-on period of both T_1 and T_4, inverter voltage v_o is $vc_2 - vc_1$. When both T_1 and T_4 are turned off inverter voltage v_o is $vc_2 + vc_1$. When only one out of T_1 and T_4 is on, then MESI capacitor is bypassed. It has to be noticed that one out of T_2 and T_3 will be on during this time. Control scheme is similar to ESI control, schematic of control is shown in Figure 116. Instead of two gate signals, it PWM block has to generate four signals. Gate signals T_{g1} and T_{g4} are determined by comparing the control signal d and a triangular carrier waveform. Gate signals T_{g2} and T_{g3} are complementary to T_{g1} and T_{g4} respectively [66].

The simulated DC-link capacitor voltage of the MESI and input phase currents of drive in steady state, are presented in Figure 117. Input currents are very well controlled. Capacitor voltage of MESI contains 300Hz ripple in this case also, but as power flowing in MESI is very low, so ripple peak is not high. Total harmonic

distortion of input currents are close to 31% as 120 degree conduction occurred in three phase balanced mains.

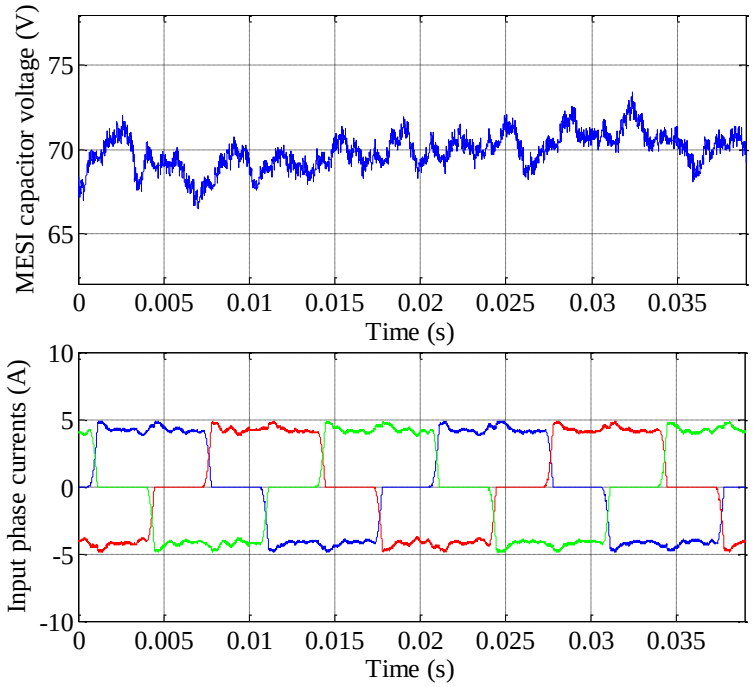

Figure 117. MESI capacitor voltage and input currents in simulation during steady state operation.

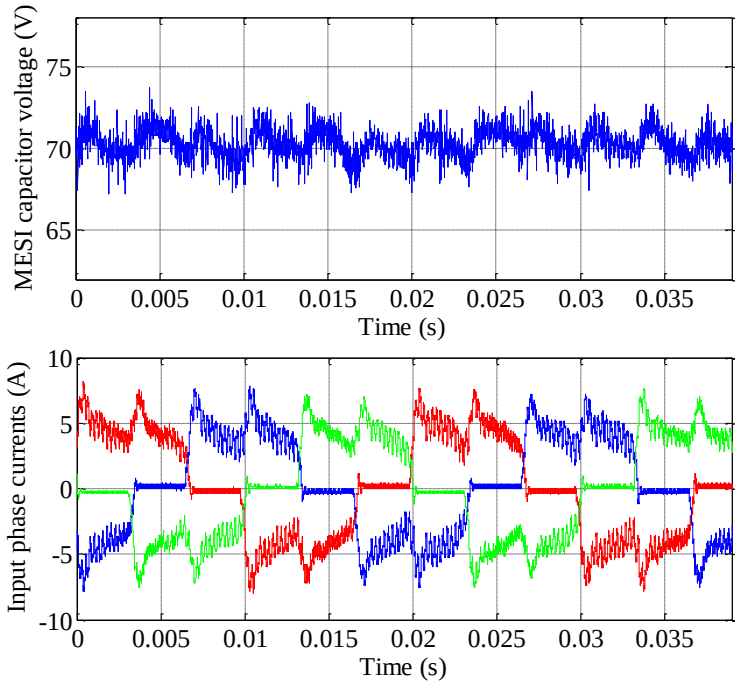

Figure 118. MESI capacitor voltage and input currents in experiment during steady state operation.

The experimental results of modified ESI based three phase electric drive are shown in Figure 118.

Capacitor voltage of MESI has 300Hz ripple. The waveforms of input phase currents are not very close to the simulation result, but THD is less than 40%. High frequency ripple in input currents are higher as compare to ESI, these ripple are because of inverter switching.

The MESI contains four MOSFETs 10A/200V, one small inductor of 40µH and a capacitor of 150µF/200V. The Control implementation of MESI has been carried out with a digital signal controller. Current sensing of inductor current and load current and voltage sensing of MESI capacitor is required to control inductor current. Inverter current is discontinuous and stepped as it depends on the state of inverter switches. Low pass filter is necessary to get average value of load current in such cases.

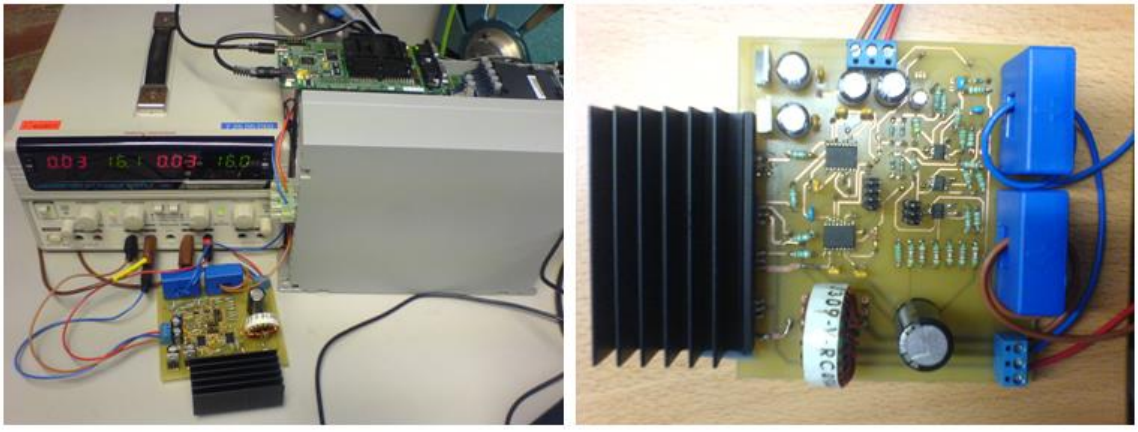

Figure 119. Experimental setup for MESI based drive.

Experimental setup of modified ESI based converter is shown in Figure 119. In this figure left half is showing PCB of modified ESI plugged into a traditional drive and auxiliary power is supplied by a separate DC power supply. MESI converter requires two current sensors and one voltage sensing. One controller is required to control four active switches based full bridge converter.

8.4 Summary and conclusion

In this chapter a modified ESI based three-phase rectifier for an electric drive was presented. This modified ESI is a full-bridge based converter instead of an asymmetrical H-bridge based ESI. Average load current does not pass through the full bridge which is connected in series with main dc-link capacitor. This topology has many advantages over traditional ESI, but control of this type converter involves difficulties. This converter also introduces an additional bus inductance in the series with dc-link capacitor to capacitor connected in the full bridge of modified ESI converter. Because of this inductance high frequency ringing takes place, and introduces high voltage stresses on the IGBTs connected to the main inverter.

Chapter 9. Conclusions

Motor integrated variable speed drive is very attractive choice some of the industrial and consumer applications. It gives freedom to consumer plug and play with drive, and also enables efficient and simplified way to utilize available electrical energy.

Motor and power converter, are two main components in any adjustable speed drive. Permanent magnet based motors have higher power density and improved efficiency as compared to induction machine and switched reluctance motors. Flux switching permanent magnet motor is one such machine in which magnets are placed on the stator side and because of this property cooling of the machine becomes relatively simple. Flux switching permanent magnet is one of the most suitable candidates for motor integrated VSD and it also offers the brushless ac operation and motion control of such machine is very simple and straight forward.

Many times VSD does not operate at full load condition, in such cases these topologies provides efficient performances of power processing unit. In motor integrated VSD, care need to be taken in selection of power converter and machine both and one need to optimize both for specific application. Integration of passive elements is possible in stator core of machine and value of passive components can be optimized. Because of vibration of the stator of machine passive component integration faces tough challenges, but by proper mechanical design it is possible without affecting the cost of overall system.

Three phase electric drive are used in different variable speed drive application. Efficiency of drive and quality of input currents drawn from grid are two major issues with these drives. Diode bridge based rectifier fed drives are usually choice as they can offer very high efficiency and comply with standards with the

help of filter. By considering cost and efficiency of the drive together with such filter, Electronic smoothing inductor based drives appeared to be better choice. Volume and weight of these drives with the ESI is smaller and it is suitable for integration with electrical motor. By proper control of the inductor current of the ESI based converter it is possible to operate with large variation in grid impedance and to minimize the effect of voltage variation of the grid on the performance of the motor integrated VSD. It is possible to use film capacitor for the main dc-link and it will have low ESR and high operating life. ESI capacitor will still be an electrolytic capacitor and one film capacitor with small capacitance can be connected in parallel to that to handle high frequency ripple.

Modified ESI based converter is an attractive option as losses associated with power semiconductors are reduced, but current control of such a filter and practical realization of the circuit is not simple. It also brings up issues by having high frequency oscillation with dc bus inductance. To limit these oscillation an auxiliary circuit or further modification will be required and then attractiveness of this filter will be faded.

Electronic smoothing inductor is a technique to reduce passive component size and therefore overall size of the power converter, and that works as an enabler to integration of motor and power converter. Performance of VSD having ESI is much better than the standard drive and it can handle small unbalance of the grid voltage.

-References

[1] M. A. Rahman, "Advances in interior permanent magnet (IPM) motor drives," in *Power Engineering Society Inaugural Conference and Exposition in Africa, 2005 IEEE,* 2005, pp. 372-377.

[2] De Almeida, A.T.; Ferreira, F.J.T.E.; Both, D., "Technical and economical considerations in the application of variable-speed drives with electric motor systems," Industry Applications, IEEE Transactions on , vol.41, no.1, pp.188,199, Jan.-Feb. 2005.

[3] J. Chang, "Design tradeoffs and technology outlook of highly compact integrated AC motors," in *Power Conversion Conference - Nagaoka 1997., Proceedings of the,* 1997, pp. 637-642 vol.2.

[4] Z. Q. Zhu, Y. Pang, J. T. Chen, Z. P. Xia and D. Howe, "Influence of design parameters on output torque of flux-switching permanent magnet machines," in *Vehicle Power and Propulsion Conference, 2008. VPPC '08. IEEE,* 2008, pp. 1-6.

[5] J. Luomi, C. Zwyssig, A. Looser and J. W. Kolar, "Efficiency optimization of a 100-W, 500 000-rpm permanent-magnet machine including air friction losses," in *Industry Applications Conference, 2007. 42nd IAS Annual Meeting. Conference Record of the 2007 IEEE*, 2007, pp. 861-868.

[6] M. Naidu,Thomas W.Nehl and S.Gopalakrishnan, "Electric Compressor Drive with Integrated Electronics for 42 V Automotive HVAC Systems," 2005.

[7] K. Mino, M. L. Heldwein and J. W. Kolar, "Ultra compact three-phase rectifier with electronic smoothing inductor," in *Applied Power Electronics Conference and Exposition, 2005. APEC 2005. Twentieth Annual IEEE,* 2005, pp. 522-528 Vol. 1.

[8] Mino, K., Novel Hybrid Unidirectional Three-Phase AC-DC Converter Systems, *PhD Thesis*, 2008, Swiss Federal Institute of Technology (ETH) Zurich: Zurich.

[9] C. Klumpner, F. Blaabjerg and P. Thogersen, "Converter topologies with low passive components usage for the next generation of integrated motor drives," in *Power Electronics Specialist Conference, 2003. PESC '03. 2003 IEEE 34th Annual,* 2003, pp. 568-573 vol.2.

[10] K. Mino, M. L. Heldwein and J. W. Kolar, "Ultra compact three-phase rectifier with electronic smoothing inductor," in *Applied Power Electronics Conference and Exposition, 2005. APEC 2005. Twentieth Annual IEEE,* 2005, pp. 522-528 Vol. 1.

[11] P. Thelin, "Design and Evaluation of a Compact 15 kW PM Integral Motor," PhD Thesis, 2002, KTH Royal Institute of Technology, Sweden.

[12] P. Thelin and H. P. Nee, "Development and efficiency measurements of a compact 15 kW 1500 r/min integral permanent magnet synchronous motor," in *Industry Applications Conference, 2000. Conference Record of the 2000 IEEE,* 2000, pp. 155-162 vol.1.

[13] Nussbaumer, T.; Raggl, K.; Boesch, P.; Kolar, J.W.; , "Trends in Integration for Magnetically Levitated Pump Systems," Power Conversion Conference - Nagoya, 2007. PCC '07 , vol., no., pp.1551-1558, 2-5 April 2007

[14] N. R. Brown, T. M. Jahns and R. D. Lorenz, "Power converter design for an integrated modular motor drive," in *Industry Applications Conference, 2007. 42nd IAS Annual Meeting. Conference Record of the 2007 IEEE,* 2007, pp. 1322-1328.

[15] Maldonado, M.A.; Shah, N.M.; Cleek, K.J.; Walia, P.S.; Korba, G.J., "Power Management and Distribution System for a More-Electric Aircraft (MADMEL)-program status," *Energy Conversion Engineering Conference*, 1997. IECEC-97., Proceedings of the 32nd Intersociety , vol.1, no., pp.274,279 vol.1, 27 Jul-1 Aug 1997.

[16] Ektesabi, M., Felic, H.. Newswood Limited for the International Association of Engineers; 2007. Motor management and energy saving by integration of motor drive system.

[17] Jie Chang; Wang, A., "New VF-power system architecture and evaluation for future aircraft," Aerospace and Electronic Systems, IEEE Transactions on , vol.42, no.2, pp.527,539, April 2006.

[18] Jie Chang; Changming Liao, "Novel DSC-IPM for Compact Converters at Elevated Temperatures," Aerospace and Electronic Systems, IEEE Transactions on , vol.43, no.3, pp.1052,1058, July 2007.

[19] C. Pollock and A. Michaelides, "Switched reluctance drives: a comparative evaluation," *Power Engineering Journal [See also Power Engineer]*, vol. 9, pp. 257-266, 1995.

[20] H. Hayashi, A. Chiba and T. Fukao, "Efficiency comparison of switched reluctance motors with low loss materials," in *Power Engineering Society General Meeting, 2007. IEEE*, 2007, pp. 1-6.

[21] A. Cavagnino, M. Lazzari, F. Profumo and A. Tenconi, "A comparison between the axial flux and the radial flux structures for PM synchronous motors," *Industry Applications, IEEE Transactions on*, vol. 38, pp. 1517-1524, 2002.

[22] K. Kyung-Tae, K. Kwang-Suk, H. Sang-Moon, K. Tae-Jong and J. Yoong-Ho, "Comparison of magnetic forces for IPM and SPM motor with rotor eccentricity," *Magnetics, IEEE Transactions on*, vol. 37, pp. 3448-3451, 2001.

[23] T. M. Jahns and W. L. Soong, "Pulsating torque minimization techniques for permanent magnet AC motor drives-a review," *Industrial Electronics, IEEE Transactions on*, vol. 43, pp. 321-330, 1996.

[24] K. Yamazaki, Y. Fukushima and M. Sato, "Loss analysis of permanent magnet motors with concentrated windings - variation of magnet eddy current loss due to stator and rotor shapes," in *Industry Applications Society Annual Meeting, 2008. IAS '08. IEEE*, 2008, pp. 1-8.

[25] H. Wei, C. Ming, Z. Q. Zhu and D. Howe, "Analysis and Optimization of Back EMF Waveform of a Flux-Switching Permanent Magnet Motor," *Energy Conversion, Ieee Transactions on*, vol. 23, pp. 727-733, 2008.

[26] H. Wei, C. Ming, J. Hongyun and F. Xiaofan, "Comparative study of flux-switching and doubly-salient PM machines particularly on torque capability," in *Industry Applications Society Annual Meeting, 2008. IAS '08. IEEE*, 2008, pp. 1-8.

[27] W. Hua, Z. Q. Zhu, M. Cheng, Y. Pang and D. Howe, "Comparison of flux-switching and doubly-salient permanent magnet brushless machines," in *Electrical Machines and Systems, 2005. ICEMS 2005. Proceedings of the Eighth International Conference on*, 2005, pp. 165-170 Vol. 1.

[28] C. X. Wang, I. Boldea and S. A. Nasar, "Characterization of three phase flux reversal machine as an automotive generator," *Energy Conversion, Ieee Transactions on*, vol. 16, pp. 74-80, 2001.

[29] C. Pollock and M. Brackley, "Comparison of the acoustic noise of a flux switching and a switched reluctance drive," in *Industry Applications Conference, 2001. Thirty-Sixth IAS Annual Meeting. Conference Record of the 2001 IEEE*, 2001, pp. 2089-2096 vol.3.

[30] A. Thomas, Z. Q. Zhu, G. W. Jewell and D. Howe, "Flux-switching PM brushless machines with alternative stator and rotor pole combinations," in *Electrical Machines and Systems, 2008. ICEMS 2008. International Conference on*, 2008, pp. 2986-2991.

[31] N. C. Harris, T. M. Jahns and H. Surong, "Design of an integrated motor/controller drive for an automotive water pump application," in *Industry Applications Conference, 2002. 37th IAS Annual Meeting. Conference Record of the*, 2002, pp. 2028-2035 vol.3.

[32] K. Kretschmar and H. P. Nee, "An AC converter with a small DC link capacitor for a 15 kW permanent magnet synchronous integral motor," in *Power Electronics and Variable Speed Drives, 1998. Seventh International Conference on (Conf. Publ. no. 456)*, 1998, pp. 622-625.

[33] C. Klumpner, P. Nielsen, I. Boldea and F. Blaabjerg, "A new matrix converter motor (MCM) for industry applications," *Industrial Electronics, IEEE Transactions on*, vol. 49, pp. 325-335, 2002.

[34] C. Klumper, F. Blaabjerg and P. Thoegersen, "Alternate ASDs: evaluation of the converter topologies suited for integrated motor drives," *Industry Applications Magazine, IEEE*, vol. 12, pp. 71-83, 2006.

[35] J. W. Kolar and H. Ertl, "Status of the techniques of three-phase rectifier systems with low effects on the mains," in *Telecommunications Energy Conference, 1999. INTELEC '99. the 21st International*, 1999, pp. 16 pp.

[36] C. Klumpner and F. Blaabjerg, "Using reverse blocking IGBTs in power converters for adjustable speed drives," in *Industry Applications Conference, 2003. 38th IAS Annual Meeting. Conference Record of the*, 2003, pp. 1516-1523 vol.3.

[37] J. W. Kolar, M. Baumann, F. Schafmeister and H. Ertl, "Novel three-phase AC-DC-AC sparse matrix converter," in *Applied Power Electronics Conference and Exposition, 2002. APEC 2002. Seventeenth Annual IEEE*, 2002, pp. 777-791 vol.2.

[38] J. Salmon and D. Koval, "Improving the operation of 3-phase diode rectifiers using an asymmetrical half-bridge DC-link active filter," in *Industry Applications Conference, 2000. Conference Record of the 2000 IEEE*, 2000, pp. 2115-2122 vol.4.

[39] M. Hengchun, C. Y. Lee, D. Boroyevich and S. Hiti, "Review of high-performance three-phase power-factor correction circuits," *Industrial Electronics, IEEE Transactions on*, vol. 44, pp. 437-446, 1997.

[40] J. S. Kim and S. K. Sul, "New control scheme for AC-DC-AC converter without DC link electrolytic capacitor," in Proc. IEEE PESC'93, vol. 1, Seattle, WA, June 1993, pp. 300–306.

[41] Siemens Building Technologies Inc., "Harmonics White Paper," 2002. http://www.sbt.siemens.com/HVP/Components/Documentation/SI033WhitePaper.pdf

[42] H. Sar´en, O. Pyrh¨onen, K. Rauma, and O. Laakkonen, "Overmodulation in voltage source inverter with small dc-link capacitor," in Proc. IEEE PESC'05, Recife, Brazil, June 2005.

[43] H. Sar´en, O. Pyrh¨onen, J. Luukko, O. Laakkonen, and K. Rauma, "Verification of frequency converter with small dc-link capacitor," in Proc. EPE'05, Dresden, Germany, Sept. 2005.

[44] M. Hinkkanen and J. Luomi, "Induction motor drives equipped with diode rectifier and small dc-link capacitance," in Proc. IEEE IECON'05, Raleigh, NC, Nov. 2005, pp. 1498–1503.

[45] S. D. Sudhoff, K. A. Corzine, S. F. Glover, H. J. Hegner, and H. N. Robey, Jr., “DC link stabilized field oriented control of electric propulsion systems,” IEEE Trans. Energy Convers., vol. 13, no. 1, pp. 27–33, Mar. 1998.

[46] H.Mosskull, “Stabilization of an induction motor drive with resonant input filter,” in Proc. EPE’05, Dresden, Germany, Sept. 2005.

[47] J. He, G. Liang and S. Wang, "The design of a switched reluctance motor drive system," in *Informatics in Control, Automation and Robotics, 2009. CAR '09. International Asia Conference on*, 2009, pp. 445-449.

[48] H. R. Andersen, T. Ruimin and K. Cai, "3-phase AC-drives with passive front-ends with focus on the slim DC-link topology," in *Power Electronics Specialists Conference, 2008. PESC 2008. IEEE*, 2008, pp. 3248-3254.

[49] A. Emadi , J. L. Young and K. Rajashekara "Power electronics and motor drives in electric, hybrid electric, and plug-in hybrid electric vehicles", IEEE Trans. Ind. Electron., vol. 55, no. 6, pp.2237 -2245 2008.

[50] http://www.pwrx.com/FullSicHybridDesign.aspx.

[51] ABB. Guide to harmonics with AC drives, http://www05.abb.com/global/scot/scot201.nsf/veritydisplay/518a84b65bb2ff40c1256d280083acbd/$file/technical_guide6_en.pdf
. *Techniicall Guiide no.. 6* .

[52] Ostroznik, S.; Bajec, P.; Zajec, P., "A Study of a Hybrid Filter," *Industrial Electronics, IEEE Transactions on* , vol.57, no.3, pp.935,942, March 2010.

[53] L. Asiminoaei , E. Aeloiza , P. N. Enjeti and F. Blaabjerg *"Shunt active-power-filter topology based on parallel interleaved inverters", IEEE Trans. Ind. Electron., vol. 55, no. 3, pp.1175 -1189 2008*

[54] H. Ertl and J. W. Kolar, "A constant output current three-phase diode bridge rectifier employing a novel "Electronic Smoothing Inductor"," *Industrial Electronics, IEEE Transactions on*, vol. 52, pp. 454-461, 2005.

[55] M. Rastogi, R. Naik, and N. Mohan, "A comparative evaluation of harmonic reduction techniques in three-phase utility interface of power electronic loads", *IEEE Trans. Ind. Appl..*, vol. 30, no. 5, pp.1149 -
1155 1994

[56] T. C. Neugebauer , J. W. Phinney and D. J. Perreault "Filters and components with inductanccancellation",
Conf. Rec. Ind. Appl. Soc. Annu. Meet., vol. 2, pp.939 -947 2002

[57] H. Mao, F. C. Y. Lee, D. Boroyevich, and S. Hiti, "Review of high-performance three-phase power-factor correction circuits", *IEEE Trans. Ind. Electron.*, vol. 44, no. 4, pp.437 -446 1997

[58] Hansen, S., Nielsen, P., Thoegersen, P., Blaabjerg F., Line side harmonic reduction techniques of pwm adjustable speed drives - a cost-benefit analysis, Proc. of PCIM'01, 2001, pp. 39-46.

[59] Salmon, J.; Koval, D., "Improving the operation of 3-phase diode rectifiers using an asymmetrical half-bridge DC-link active filter," Industry Applications Conference, 2000. Conference Record of the 2000 IEEE , vol.4, no., pp.2115,2122 vol.4, Oct 2000

[60] W. B. Lawrance and W. Mielczarski, "Harmonic current reduction in a three-phase diode bridge rectifier", IEEE Trans. Ind. Electron., vol. 39, no. 6, pp.571 -576 1992

[61] Galea, C.; Asiminoaei, L., "New topology of electronic smoothing inductor used in three phase electric drives," Electrical Power Quality and Utilisation (EPQU), 2011 11th International Conference on , vol., no., pp.1,6, 17-19 Oct. 2011

[62] A. R. Prasad, P. D. Ziogas, and S. Manias, "Passive input current wave shaping method for three-phase diode rectifiers", Proc Inst. Elect. Eng., vol. 139, no. 6, pp.512 -520 1992

[63] N. Mohan, T. M. Undeland and W. P. Robbins, Power Electronics: Converters, Applications, and Design. John Wiley & Sons, Inc., 2003.

[64] R. W. Erickson, D. Maksimović, Fundamentals of Power Electronics. 2 ed. 2001: Kluwer Acadenic Publishers 0-7923-7270-0.

[65] G. Gong, M. L. Heldwein, U. Drofenik, K. Mino, and J. W. Kolar, "Comparative evaluation of three-phase high power factor AC-DC converter concepts for application in future more electric aircraft", Proc. IEEE APEC',04, vol. 2, pp.1152 -1159 2004

[66] Singh,Y.V. ; Rasmussen,P.O.; Anderson,T.O., Three-phase electric drive with modified electronic smoothing inductor, Energy Conversion Congress and Expo, 2010 IEEE, pp. 4199-4203.

[67] Singh, Y.V.; Rasmussen, P.O.; Andersen, T.O.; Shaker, H., "Modeling and control of three phase rectifier with electronic smoothing inductor," IECON 2011 - 37th Annual Conference on IEEE Industrial Electronics Society , vol., no., pp.1450,1455, 7-10 Nov. 2011